NASA CONTRACTOR REPORT

NASA CR-1081

GENETIC STATES OF SIMULATED LUNAR ROCKS

by E. Azmon

Prepared by
NORTHROP CORPORATE LABORATORIES
Hawthorne, Calif.
for

NATIONAL AERONAUTICS AND SPACE ADMINISTRATION • WASHINGTON, D. C. • JUNE 1968

NASA CR-1081

GENETIC STATES OF SIMULATED LUNAR ROCKS

By E. Azmon

Issued by Originator as Report No. NCL 67-44R

Prepared under Contract No. NAS 7-358 by
NORTHROP CORPORATE LABORATORIES
Hawthorne, Calif.

for

NATIONAL AERONAUTICS AND SPACE ADMINISTRATION

For sale by the Clearinghouse for Federal Scientific and Technical Information
Springfield, Virginia 22151 – CFSTI price $3.00

TABLE OF CONTENTS

LIST OF ILLUSTRATIONS

LIST OF ILLUSTRATIONS (Cont)

LIST OF TABLES

ABSTRACT

The purpose of this study was to develop concepts leading to beneficial uses of rocks on the moon (while not blinding ourselves to terrestrial uses). This purpose did not encompass determination and refinement of melting curves for some rocks or even the establishment of equations of state for complex substances, although these could well be found as by-products. This implied that the accuracy and the reproducibility of an experiment were essential even when and where the precision of the measurements was less than desirable. It implied that non-equilibrium processes and contamination of the samples could be acceptable and/or desirable, as long as the final product was reproducible and had some potential value. It implied that textures developed during a process could be many times more characteristic and meaningful than the mineralogical identity. Most of the raw materials used are commonly and abundantly available silicate rocks. It is hoped that similar silicates will be found to be common and abundant on the lunar surface, but it is not necessary that all the processes tried and products obtained will also be found in nature.

The concept developed in this study is that of a genetic state which is the state from which a rock of distinct characteristics is born. This state is a function of the pressure and temperature conditions that a rock material is exposed to, as well as of the history (time and rate of changes) of pressures and temperature. Specific genetic states of several rocks are shown as genetic diagrams in this report. Most of the phases that are shown in the diagrams to coexist are not in equilibrium with their system, but were "frozen" into existance by quenching prior to attainment of equilibrium.

The experiments described in this report can be expanded and refined and continued for several years to bring full understanding of the kinetics as well as of the thermodynamics of the

reactions. However, since concepts leading to beneficial uses of rocks are the prime target, it is suggested that the next step be concentrated on one basaltic composition, trying to convert the new data and concepts into processes and prototype products.

INTRODUCTION AND SUMMARY

Since the lunar surface is undoubtedly composed of silicate minerals, it is important to understand the physical properties of those naturally occuring aggregates of silicate minerals which could exist on the moon. With such knowledge, one could:

1. Evaluate common rocks as a raw material for extracting supplies or for casting and forming into required objects.
2. Decipher the environmental history of the moon by an analysis of the petrographic-petrologic appearance of lunar rocks.
3. Explore for naturally concentrated lunar materials.

Two parallel benefits can be derived from the knowledge of the processes and conditions under which various igneous rocks are formed. One is the ability to generate rock end products at will, and the other is the ability to determine the provenance of antural rocks. These benefits correspond, respectively, to (a) production of mineral concentrates of defined properties in desired shapes, and (b) means of exploration for source rock. Here, knowledge regarding two different aspects of economic geology is gained simultaneously through experiments designed (1) to determine the processes that natural silicate mixtures must go through to generate specific rocks, and (2) to define the four parameters controlling these processes: composition-temperature-pressure-history. The parameters which determine the genetic state of a rock can be obtained either by inferences drawn from the observed characteristics of the rock as found in its natural environment, or from laboratory determinations of the conditions that lead to its formation.

The genetic state of many rocks is not necessarily an equilibrium or steady state. It is attained even in a large system, such as

a mountain or a portion of a continent, where it is possible for one end of the system to be far enough physically from the other end to appear independent. It is also attained in an open system, where a true equilibrium may never be reached because there is a continuous incorporation of rock mineral into the system. Amazing is the fact that such a heterogenous reaction may still achieve a distinct genetic state and result in a rock-type end product.

More extraordinary is the fact that in spite of the complex combination of variables required to obtain a genetic state, such combinations are found repeated geographically around the earth and stratigraphically down the geologic column.

The investigation of the properties of silicate minerals leads to experiments with real rocks which are compositionally complex metal oxides and to a study of the time dependence effects of the environmental system. Such a study is to be correlated with large, open, multicomponent systems, which allow ever increasing incorporation of more and new materials into the process.

The complex combination of parameters and events is governed by a multitude of known thermodynamic and kinetic processes, the interactions of which appear to be governed by unknown universal rules. An understanding of these rules can lead to the two benefits mentioned above: (1) ability to generate rock end products at will, and (2) ability to determine provenance of a natural rock.

The long term objectives of this investigation were (1) to determine the special characteristics of magma which may be unique to the lunar environment, (2) to develop technological concepts and know-how required to make use of magma products, (3) to correlate the rocks from laboratory experiments with rocks in natural environments in order to examine critical differences between the closed-small systems (in the laboratory) and the open-large systems (in nature), and (4) to determine the petrographic properties

of prototype casts and suggest their possible use in lunar and planetary logistics.

Tests were designed to control simultaneously the four variables which are crucial for magma generation and crystallization: pressure, temperature, time and composition. Several research tools were employed in this technological study. These tools included a high temperature press and a high temperature furnace. The test samples were analyzed by an x-ray diffractometer, a petrographic microscope and a hand lens in order to facilitate the correlation of laboratory data with field geology.

The philosophy behind this study was founded on the observation that natural processes, which could be simulated, can and do separate and segregate the mineral components of a rock through a combination of igneous processes such as differentiation and sedimentation (weathering and selective persistence). Understanding of these natural processes in real rocks might offer methods of artificial segregation should the benefication of any specific mineral prove desirable.

Selection of the range of the four variables mentioned above was guided by the interpretation of volcanic and high velocity impact processes. A range of rocks from acidic aluminum silicates to basic iron-magnesium silicates was used in the experiments to cover the several possible theories of composition of the lunar surface. The facilities allowed temperature control from 20°C up to at least 2,000°C; pressure from 1 atm to higher than 50 kb; and time from 1 sec to several days.

Since the beginning of this contract, approximately 700 experiments have been performed or solid-liquid transformations of seven rocks (a) Bruderheim meteorite, (b) tholeiitic basalt, (c) granodiorite, (d) serpentine, (e) obsidian, and (g) gabbro.

Three additional basalts were studied extensively over a range of temperature and range of time at one atmosphere pressure. These basalts will be identified in this report by the locality from which they were colled as (h) Hokook basalt; (i) Giva'at Hamoren basalt; and (j) Hazor basalt.

Bruderheim Meteorite

Solid-liquid transformation of the Bruderheim meteorite has been investigated from pressures of 1 atm to 45 kb and at 5-min duration of stay at temperature. The data were tentatively fitted to a straight line with a slope of $4.5^{\circ}C/kb$, from approximately $1300^{\circ}C$ near 1 atm to approximately $1500^{\circ}C$ near 45 kb. Preliminary determination of the time dependence shows a lowering of melting of approximately $50^{\circ}C$ with increase in duration of stay temperature from 5-min to 1 hour.

Tholeiitic Basalt

Solid-liquid phase transformation of tholeiitic basalt has been investigated from pressures of 1 atm to 40 kb and at temperatures from $920^{\circ}C$ to $1400^{\circ}C$ and 5-min stay at the highest temperature, using petrographic techniques. The data were tentatively fitted to a straight line with a slope of $4^{\circ}C/kb$ from approximately $1200^{\circ}C$, near 40 kb. Several indications of a high pressure phase (garnet) were recorded using x-ray techniques, and the detailed field of genesis of the garnet in this rock was examined.

Granodiorite

Solid-liquid phase transformation of granodiorite has been investigated from pressures of 1 atm to 30 kb and at temperatures from $1100^{\circ}C$ to $1450^{\circ}C$ with 5-min stay at the highest temperature. The data were tentatively fitted to a straight line from approximately $1230^{\circ}C$, near 1 atm, to $1300^{\circ}C$ near 30 kb.

Serpentine

Determinations of the solid-liquid phase transformation of serpentine have been made in the pressure range of 10 to 40 kb, and at temperatures of 1200°C to 1400°C with 5-min stay at the highest temperature. The data was tentatively fitted to a straight line from approximately 1200°C at 10 kb to 1280°C at 20 kb. Above 20 kb, the rate of change of temperature versus pressure seems to drop markedly. The range is being reexamined for verification. It has been seen already that this rock tends to melt in pockets much more than any of the other rocks that were duscussed above. This could be related to the water content.

Obsidian

All experiments with the obsidian were discontinued as soon as it became obvious that the existing analysis facilities at hand were not sufficient to differentiate between the original unaltered phases of the rock (mostly glass) and the quench products (mostly glass).

Olivine

Synthetic samples of forsterite 100, 80, 60, 40, 20 fayalite 100 have been prepared for examination of the shifting of the eutectic temperature and the effect of Al_2O_3 traces on the fructionation of iron magnesium silicate magma. The preliminary experimentation with pure forsterite ($2\ M_gO \cdot SiO_2$) at pressures of 20 kb and temperature of 2,000°C was kept at conditions for about 10 min each. It was found necessary to modify the sample-capsule arrangement to make it easier to locate the sample after a very high temperature run. These were first attempts to stay at such a high temperature for longer than 1 sec and the results are encouraging. It appears that the pistons and core survived the experiments with minimum degradation.

Gabbro

Pressure-temperature experiments with gabbro showed that exposing the sample to proper P-T combinations prior to quenching produces one of five quench phases; (1) unaltered original rock; (2) recrystallization of original crystals; (3) quench crystallization from melt; (4) glass; (5) any of the above in a vesicular matrix. It was assumed that if a single sample is prepared so that a thermal gradient would exist from end to end, it might be possible to obtain all five phases in one experiment on the one sample. Such an experiment would have served to examine the phase transitions. The actual determination showed that due to pressure dependence, there were P-T combinations at which one phase or another could not exist. Figure 1 shows these relations on a genetic diagram on a pressure-temperature scale. The genetic diagram shows the end products of the process. This is different from a phase diagram that shows the phases that coexist while a set of P-T conditions prevail.

Hokook basalt Giva'at Hamoreh basalt Hazor basalt

Solid-liquid transformations of three basalts have been investigated at a pressure of 1 atm, from 900°C to 1200°C, and at a duration of stay at temperatures of 1 hour, 2 hours, 6 hours, 24 hours and 72 hours.

This contract on the beneficial use of lunar magma is obviously moon oriented. However, the data derived from it are of equal interest to the studies of terrestrial complex metal oxides. Hence the research which was conducted at the Northrop Space Laboratories under NASA OART contract NAS-7-358 is being continued in essence at the Northrop Corporate Laboratories with the emphasis on the terrestrial applications as an integral portion of the study of complex metal oxides. Data thus developed on heat treatment of rocks will be applicable to lunar problems as well.

The concept of "Cost Effectiveness" is exemplified by this double utility of a basic research contract. Additional effectiveness was achieved by employing graduate students and doctoral candidates on a part-time basis to perform some tasks, thus helping train additional high level personnel.

STARTING MATERIALS

Bruderheim Meteorite

The Bruderheim meteorite is composed of approximately 41% olivine (chrysolite), 42% pyroxene (hypersthene), troilite, iron and other minerals. A significant resemblance in chemical and mineralogical composition is observed between the Bruderheim Meteorite and an average terrestrial periodotite. This observation is supported by a comparable similarity in petroligical textures. The meteorite differs, however, from periodotite in possessing the following: (1) a higher ratio of Fe oxides to the sum of Al and Si oxides, (2) metallic iron and nickel, (3) chondrules and chondritic textures, and (4) troilite (FeS) rather than pyrite (FeS_2) which contains less iron. Although both rocks are fundamentally igneous in nature, the possibility of their having an identical genesis is remote. To assume the melting range of a typical peridotite as an indication of the temperatures of origin that existed in the body from which the Bruderheim meteorite was detached may possibly be erroneous.

The Bruderheim meteorite fell (near Bruderheim, North-East of Edmonton, Alberta, Canada) at 1:06 a.m., MST, on March 1960. H. Baadsgaard, et al (1961) describes it as follows:

> The fireball traveled on an azimuth of N 100°, at a slope of 40°, with an initial atmospheric velocity of 8 to 10 miles per second. More than 300 kilograms have been recovered from the fall area, a well-defined ellipse centered about latitude 53° 54'N, longitude 112° 53'W. This ellipse is 3-1/2 miles long and 2-1/4 miles wide (5.6 by 3.6 km), with its long axis N80W and the larger individuals located near its southeast apex. Falling onto frozen ground at terminal velocity, most individuals rebounded onto the snow, facilitating recovery. The largest individual weighs 31 kilograms, and the catalogued collection of individuals weighing more than 100 grams now totals 188.

The stone selected for investigation was a large individual from the southeast apex of the fall. This stone originally weighed about 60 pounds, but was divided by the finders into a number of fragments. Twenty-five kilograms of these were subsequently acquired by the University of Alberta, and since the specimen was of little value for museum purposes, and had been recovered within a day of the fall, it has to date been used as the source of all Bruderheim investigation material.

By means of a combination of gravity and magnetic methods a number of mineral separates have been obtained from the stone: olivine, hypersthene (bronzite), a pigeonitic pyroxene, plagioclase, kamacite, taenite, troilite, and chromite. These minerals are being analized. Some of the plagioclase is in the glassy form, maskelynite. Apatite or merrillite, carbon or hydrocarbons, ilmenite and lawrencite, though not separable, are probably present in small amounts.

Bruderheim appears to be a typical gray chondrite. Density of the meteorite, as determined with a quartz glass pycnometer, is 3.75, higher than the average for chondrites (Urey and Craig, 1953).

The chemical composition and normative mineral composition calculated from this analysis are given in Table 1.

Tholeiitic Basalt

Tholeiitic basalt samples were collected from NE Madras, Oregon (SSL No. 669), by Dr. J. Green (1964) and were intended to be used as one of several lunar standards. The tholeiitic basalt of approximately 39% plagioclase (Labradorite), 14% olivine, 14% augite, 11% magnetite, chlorite, glass and other minerals.

TABLE I

CHEMICAL AND MINERAL COMPOSITION OF THE BRUDERHEIM METEORITE

SiO_2	39.94**	SiO_2	39.84*
TiO_2	0.12	TiO_2	0.12
Al_2O_3	1.86	Al_2O_2	2.19
Fe^o	8.59	Met Fe	6.97
FeO	12.94	FeO + Fe_2O_3(as FeO)	13.87
FeS	6.38	MnO	0.31
MnO	0.33	CaO	1.80
MgO	24.95	MgO	24.71
CaO	1.74	Na_2O	0.94
Na_2O	1.01	K_2O	0.10
K_2O	0.13	H_2O+	0.16
P_2O_5	0.29	H_2O-	0.01
H_2O-	0.01	P_2O_5	0.26
H_2O+	0.10	FeS	6.63
Ni^o	1.30	Ni(as metal)	1.28
Co^o	0.05	Cr_2O_3	0.54
Cr_2O_3	0.60		
C	0.04	TOTAL	99.73
TOTAL	100.38	TOTAL Fe	22.04
TOTAL Fe	21.53		

Mineral	Mode* Volume, %	Assumed Specific Gravity	Mode* Weight, %	Norm** Mol %
Pyroxene	45.83	3.35	42.26	31.24
Olivine	42.83	3.45	40.67	41.65
Feldspar	0.50	2.6	0.36	9.47
Apatite & merrillite	0.43	3.0	0.35	0.74
Metallic	3.54	7.8	7.60	9.94
Troilite	5.08	4.8	6.71	6.38
Chromite	0.54	5.7***	0.85	0.92
Holes	1.25	3.5***	1.21	

* Duke, Maynes, Brown (1961)
** Baadsgaard, Campbell, Falinsbee, Cummings (1961)
*** Holes weighed as average density of meteorite

As indicated, both glass and crystals are present in the original sample; hence, an indication of melting, as defined above, was considered valid when an increase in the glass percentage was verified.

The basalts form a continuation of the series rhyolite through dacite and andesite, to which it is related by the decreasing content of SiO_2. These rocks represent cooling and consolidation under pressures and temperatures which prevail in the shallow depth near the surface of the earth. They are similar in composition to that in the plutonic rocks ranging from granite to gabbro.

Textures are mirocrystalline, both glass and crystals are present. However, the interstitial glass is charged with microlites of magnetite and plagioclase. There are definitely two generations of plagioclase present. Most of the crystals are subhedral in form with the exception of the older generation plagioclase which has reentrants and rounded corners indicating partial resorbtion. The spectrum of grain size is not wide exclusive of the microlites found in the matrix glass. The older generation plagioclase are the largest crystals, averaging 0.15mm in length and 0.03mm in width. The augite and olivine grains are approximately the same size with the former averaging 0.05mm in diameter and the latter 0.04mm in diameter and the smaller microlites are less than 0.008mm in diameter. The chlorite grains are variable with some being marginal alterations of the pyroxenes and some occuring as discrete entities. The chemical composition, observed modal mineral composition, and normative mineral composition calculated from the chemical analysis in Table II.

Granodiorite

Granodiorite samples were collected from Bates Station, California (SSL No. 672), by Dr. J. Green (1964) and were intended to be used

TABLE II

CHEMICAL AND MINERAL COMPOSITION OF THOLEIITIC BASALT, OREGON

SiO_2	51.0
TiO_2	2.7
Al_2O_3	14.0
Fe_2O_3	3.4
FeO	8.8
MnO	0.25
MgO	4.4
CaO	8.0
Na_2O	3.4
K_2O	1.7
P_2O_5	1.4
H_2O+	0.76
H_2O-	0.1
Total H_2O	0.86
CO_2	0.03
S	0.004
TOTAL	100.0
TOTAL Fe	12.2

Mineral	Mode Weight %	Norm Mol %
Quartz	1	3.6
Orthoclase Glass	12	10.0
Plagioclase An_{67}+An_{54}	51	47.2
Olivine	13.5	
Pyroxene	10.5	25.7
Magnetite + Femetite	8	10.1
Chlorite	4	
Apatite	1	3.4
Epidote	1	

*Green (1964)

as one of several lunar standards. The granodiorite is composed of approximately 40% plagioclase (oligoclase to andesine), 39% quartz, 8% orthoclase, and other minerals. The rock has a wide range of grain size with many inclusions (e.g., zircon in the feldspars).

There are all gradations from granite to granodiorite through quartz monzonite. The division on the basis of the relative amounts of potash feldspar and plagioclase is arbitrary and convenient. Chemically, CaO and Na_2O increase and K_2O decreases from one end to the other. SiO_2 decreases from granite to granodiorite though there are irregularities. Many granodiorites have no higher content of dark minerals than granites.

Textures are poikilitic where a number of randomly oriented grains are completely enclosed in optically continuous crystals of different compositions. Some finger-like intergrowths of quartz are found penetrating plagioclase crystals (myrmekitic intergrowths). However, this condition is rare rather than being a general characteristic. There is a wide spectrum of grain size, but in general, the rock is medium-grained with hypidiomorphic structure. Small grain or crystal inclusions in the larger grains consist of zircon, sphene, apatite, and opaque ore minerals.

The chemical composition, observed model composition, and normative mineral composition calculated from the chemical analysis are given in Table III.

Serpentine

Serpentine samples were collected from Rogue River, Oregon (SSL No. 667), by Dr. J. Green (1964) were intended to be used as one of several lunar standards. The serpentine is composed of approximately 70% hydrated magnesium silicates (antigorite, chrysolite), 7% olivine, pyroxenes, and other minerals. It

consists of a typical mesh mixture of antigorite with flakes of fibrous chrysotile scattered at random. The total water content of this rock is 12.8% which adds a unique interest to the study of this rock in relation to lunar logistic minerals.

The apple green lineation seen in the hand specimen are aggregates of crystals consisting of olivine, pyroxene and amphibole. Grains as discrete entities are not evident except in the crystalline veinlets, where amphibole dominates with some crystals up to 0.4mm in diameter. Chain-like lineation of the ore minerals (magnetite and chromite) and also in elongated masses in common. In some sections of the slide, especially in the massive antigorite regions, a poorly developed bastite structure is recognized.

Untreated samples of this serpentine gave an x-ray diffraction pattern indicating the presence of antigorite ($Mg_6Si_4O_{16}$) only.

The great bulk of the ultra basic rocks are periodotites and dunite. These are associated in the field with lesser amounts of diallage gabbro, diallage olivine gabbro, and pyroxenites. Hornblende and mica periodotites are rare and unimportant rocks.

The periodotites and dunite are mostly represented by the serpentine rocks, derived from them by alteration of olivine and rhombic pyroxene. The alteration occurs immediately after consolidation; the water is of magmatic origin.

Olivine is converted to a submicroscopically fibrous mass of chrysotile.

Rhombic pyroxene is usually pseudomorphed by the micaceous variety of serpentine: antigorite. This pseudomorph is known as bastite. Serpentine rocks containing bastite are bastite serpentines. These large crystals of antigorite, with a perfect,

TABLE III

CHEMICAL AND MINERAL COMPOSITION OF THE GRANODIORITE, CALIFORNIA*

SiO_2	70.0	Na_2O	4.4
TiO_2	0.34	K_2O	2.2
Al_2O_3	16.0	P_2O_5	0.1
Fe_2O_3	0.07	H_2O+	0.47
FeO	2.1	H_2O-	0.2
MnO	0.04	Total H_2O	0.67
MgO	0.64	CO_2	0.05
CaO	3.2	S	Nil
		TOTAL	99.8
		TOTAL Fe	2.17

Mineral	Mode Weight %	Norm Mol %
Quartz	39	26.9
Orthoclase	8	13.4
Microline	2	
Biotite	7	
Muscovite		
Zircon	1	
Apatite		
S	1	
Ore minerals		
Chlorite	1	
Epidote	1	
Corundum		0.6
Pyroxene		5.0
Silmenite		0.6

*Green (1964)

but usually bent cleavage are embedded in fine fibrous and dull chrysotile derived from olivine. The texture thus resembles the prophyritic, and has been called pseudoporphyritic.

The serpentine rocks vary widely in color, being gray, greenish gray to green, blackish green, bluish gray to bluish green, purple. They are often mottled. Veins of chrysotile, carbonates, opal, quartz and chalcedony are common.

Shearing of the serpentine rocks due to expansion on serpentinization is widespread.

The chemical composition, observed model mineral composition, and normative mineral composition calculated from the chemical analysis are given in Table IV.

Obsidian

Obsidian samples were collected from Newberry Caldera, Oregon (SSL No. 671), by Dr. J. Green (1964) and were intended to be used as one of several lunar standards. The obsidian is composed of silica glass with several percent of plagioclase, augite and chlorite. Its texture is primarily glass matrix charged with glass shards, microlites and crystallites. The microlites are of the longulite and belonite varieties. The glass shards have rounded resorption boundaries and some are cloudy under cross nicols indicating devitrification. A few widely scattered plagioclass grains are also present. The glass shards and microlites show a general preferred orientation with their long dimension parallel to the splinter fracture pattern. Microlite density is variable occurring in streaks nearly parallel to the splinter fracture system. Relic plagioclase laths occur as scattered unoriented grains.

The chemical composition, observed model composition, and normative mineral composition calculated from the chemical analysis are given in Table V.

TABLE IV

CHEMICAL AND MINERAL COMPOSITION OF SERPENTINE, OREGON*

SiO_2	40.0		Na_2O	0.08
TiO_2	0.04		K_2O	0.04
Al_2O_3	1.8		P_2O_5	0.02
Fe_2O_3	6.4		H_2O+	12.5
FeO	1.8		H_2O-	0.3
MnO	0.11	Total	H_2O	12.8
MgO	37.2		CO_2	0.04
CaO	0.9		S	0.022
			TOTAL	101.2

Mineral	Mode Weight %	Norm Mol %
Antigorite	50	
Chrysotile	20	
Magnetite or chromite	7	9.5
Olivine	7	46.7
Pyroxane	6	38.8
Chlorite	2	
Talc	1	
Dolomite or Manganese	1	
Corundum		0.1
Albite		0.5
Anorthite		5.0

*Green (1964)

TABLE V

CHEMICAL AND MINERAL COMPOSITION OF OBSIDIAN, OREGON*

	SiO_2	72.8
	TiO_2	0.23
	Al_2O_3	14.4
	Fe_2O_3	0.54
	FeO	1.5
	MnO	0.07
	MgO	0.04
	CaO	0.84
	Na_2O	4.9
	K_2O	4.0
	P_2O_5	0.03
	H_2O+	0.2
	H_2O-	0.1
TOTAL	H_2O	0.3
	CO_2	0.0
	S	Nil
	TOTALS	99.7

Mineral	Mode Weight %	Norm Mol %
Quartz		27.2
Glass	60	
Orthoclase		23.9
Microlites	30	
Corindum		1.2
Plagioclase	5	43.6
Pyroxene	3	2.2
Magnetite and Ilmenite	2	1.2
Apatite		

*Green (1964)

Fayalite

The fayalite used in the present work was synthesized hydrothermally from a reagent-grade mixture of α - cristobalite and iron powder combined in stoichiometric properties. The conditions of synthesis were: temperature around 900°C, fluid pressure at 500 bars, and run duration about six days. Each sample was ground and rerun at the above temperature and pressure to assure complete reaction. Microscopic observation of the run product indicated that over 99.5% fayalite was obtained. Any remaining iron and/or quartz appeared only in trace amounts. The synthetic crystals so produced were anhedral and equant with diameters of around 5 microns or less.

The mineral fayalite $2FeO \cdot SiO_2$ is orthorhomtic, yellow to brown and black mineral. It is 6.5 on Mohs hardness scale. Fayalite and forsterite are rare in nature by themselves, but are very common in isomorphous mixture. The usual mixture, in which the magnesium salt predominates, is known as olivine, chrysolite or periodot.

Olivine is an essential pyrogenic constituent of many eruptive rocks, such as periodiotite, norite, basalt, diabase and gabbro. Dunite is a rock consisting of olivine alone, or at most accompanied by trivial amounts of accessories. Since olivine, fused with silica, yields enstatite, it can occur normally only in rocks low in silica. As the latter increases in amount, pyroxenes take takes its place. Olivine, however, sometimes appears abnormally, as a minor accessory, in highly siliceous rocks like trachyte and andesite. Fayalite was found by J.P. Iddings (1885) to be associated with tridymite in rhyolite and obsidian, in the Yellowstone Park. At Rockport, Massachusetts, fayalite has been found in granite (Penfield - 1896). Olivine is also a common constituent of meteorites and is often conspicuously associated with metallic iron.

The members of the olivine group all undergo alteration with extreme facility. The typical alteration of peridotite rocks is into serpentine.

Gabbro

The gabbro used for this study was collected from Horton County, Quebec and is one in a whole range of rock composition that would qualify as gabbro. The petrological composition of the gabbro is as follows: LABRADORITE, 45%, well twinned, $AB_{35}An_{65}$, N (index of refraction) = 1.562 in (001) cleavage plane, rod-like inclusions of opaque and nonopaque minerals; PYROXENE, 50% irregular grains of augite (diallage) with inclusions of opaque minerals, mixed with green serpentinized OLIVINE and with clear highly fractured olivine grains filled with magnetite; ACCESSORIES, 5%, coronas of pleachroic hypersthene, pale green amphibole, brown hornblende, calcite in veinlets cutting the labradorite.

The gabbro group of important and diversified hypabyssal and plutonic rocks forms a continuation of the series granite-diorite, to which it is related by the decreasing content of SiO_2, increase in content of dark minerals and the appearance of olivines as important constituents. These rocks represent cooling and consolidation under pressures and temperatures which prevail in the depth of the earth. Textures are typically xenomorphic granular where the minerals are not bounded by their own crystal faces but have their outline impressed on them by adjacent minerals.

The study of melting of a crystaline gabbro rather than that of a glass of gabbroic composition was intended to determine conditions under which this gabbro is stable and conditions under which this gabbro would transform into other rocks.

Hokook Basalt, Giva'at Hamoreh Basalt, Hazor Basalt

Basalt from three locations in Israel was used for comparison with the Oregon tholeiitic basalt and the Quebec gabbro. These locations are identified as Hokook, Giva'at Hamoreh and Hazor.

APPARATUS

The experiments with the melting of rocks at high pressures and temperatures were conducted with a Transis-tronics Kiloton Hydraulic Press of the piston-cylinder type (Figure 1) related in design to the devices described by Coes (1962), Hall (1958), and Boyd and England (1960) and is most similar to that used by Kennedy and LaMori (1961). This apparatus was used by Sterrett (1962) for the study of transformation in iron at high pressures. The total uncertainty in pressure determination is, according to him, $\pm$ 1 kb. The presence of a temperature gradient in the graphite furnace and along the sample, and temperature fluctuation during experiments combine to give a temperature uncertainty of $\pm$ 10°C. The temperature gradient along the graphite furnace is almost symmetrical with the hottest spot close to the center.

The experimental arrangement for single-stage operation of the press is shown in Figure 2. The data on the rocks presented here extend to 55,000 bars, the upper pressure limit of single-stage operation. The high pressure platen shown in Figure 2 is made up of a cemented tungsten carbide core (Carboloy 55A) with a 1/2-inch experimental chamber, inserted into a prestressed assembly of 4340 steel binding rings. These hardened steel binding rings were previously pressed together with interference fits, thus providing lateral support for the central carbide pressure vessel. A 240 ton load is applied to the ends of the carbide core through the use of a separate ram and appropriate shims. No end load is placed upon the 4340 hardened steel binding rings.

The experimental chamber is pressurized by advancing a tungsten carbide piston into the core and binding ring assembly, known as a "platen". The pistons are ground to a fit of about 0.0005 in to the lapped bore, and the ends and sides are coated with molybdenum disulfide grease to reduce friction. The sample assembly

is wrapped with several thicknesses of lead foil also for this purpose. A 16 inch Heise Bourdon gauge is used to measure master ram oil pressure. This gauge was calibrated by the manufacturer against a free piston to an accuracy of better than one part per thousand.

The safe loading range on the core is shown in Figure 3. Ideally, one should increase the pressure and temperature simultaneously for maximum loading safety. In reality, however, the experiments may dictate a procedure which requires operating close to or slightly outside of the safe loading range. Hence, the press is facilitated with a hinged steel gate 1/2 inch thick which should be enough to protect the operator from any danger due to the failing of the core during an experiment.

The experiments with the melting of rocks at one atmosphere pressure and high temperatures were conducted with a Lindberg 1650°C Muffle Furnace. This furnace has been operated up to 1400°C on a continuous basis. Above this temperature the furnace can be operated only for 1/2 hour at a time.

PROCEDURES

The procedures involve preparation of the "run", selection of thermocouples, conduction of the experiment, measurements during the experiment and post experiment analysis. The "run" is assembled (around the sample) of steel top plugs, pyrophyllite, talc, boron-nitride or glass, in several different combinations. The thermocouples are Pt-Pt 10% Rh for temperatures up to 1500 to 1600°C, and W-W 26% Re for higher temperatures. The experiment is made of the following steps:

a. Assembling the tool stack and end loading

b. Soaking; raising the pressure approximately 1/2 kb to make electrical contacts and raising the temperature approximately 300°C to check the thermocouples; raising the pressure to several kilobars below the desired final pressure; raising the temperature to 500 to 600°C to fire the talc; raising the temperature to the desired heat

c. Quenching and quench rates (Figure 4)

d. Recovery of the sample; dissecting the run; dissecting the sample

The measurements were conducted on

1. Pressure

2. Temperature; single point; two points; differential thermal analysis

3. Rate of heating; stay at a temperature; cooling

The reaction capsules containing the sample and the rest of the above gabbro assembly were kept in a drying oven at 110°C prior to each experiment to prevent lowering of the "dry" melting temperatures by absorbed water. The platinum capsules when used were left unsealed to permit any trapped moisture to escape soon after the temperature of the furnace exceeded 100°C.

Quenching was attained by cutting off the power supply to the furnace. Figure 4 shows the temperature drop as a function of time using three different setups for insultation. The 1/2 inch diameter talc sleeve was adopted as outer sleeves for all the experiments since it allowed the most effective quench. Temperatures dropped to below 500°C in 6 to 10 sec. The capsule was removed from the assembly and cut longitudinally into two parts, one part for x-ray work and the other for thin section petrography study. For correlation of the petrographic observations with the temperature readings only the area immediately next to the thermocouples was considered (the area which fell within an imaginary circle about the thermocouple tip as a center, and the distance from the tip to the capsule sidewall as a radius).

Three experimental assemblies were used as shown in Figures 5,6 and 7. The first assembly consists of the parts listed in Figure 5, with a DTA arrangement of the thermocouples (Figure 8). It was hoped that phase changes occurring near the upper tip of the platinum capsule would show on the DTA curve and would be correlated with the petrographic identification. However, the great detail and number of fluctuations in the curve made it very difficult to correlate these data with specific change in the complex samples. A distinct thermal gradient developed in the capsules from top to bottom where the hot end was on top. This gradient permitted phase changes to occur in portions of the samples and the transition into unchanged sample would be examined petrographically. The transition temperature was then estimated on the basis of distance from the thermocouple and the experiment was repeated using a second assembly and the estimated temperature as a guideline. The second assembly consists of parts listed in Figure 6, using a very small sample to minimize the thermal gradient, and thermocouples on both upper and lower ends of the sample. The third type assembly consists of parts listed in Figure 7 using an iron capsule to maintain an excess of iron in the reaction during the experiment.

TEMPERATURE OF MELTING OF COMPLEX SILICATES

The common and most abundant rock-forming minerals are found in their native geological environments as complex aluminum and Fe-Mg silicate systems. Pure monomineralic rocks are scarce, and it is to be expected that minor accessory minerals will always be associated with the major constituents. For example, a dunite rock which is composed primarily of a chrysolite member of the olivine group ($Fo_{80}Fa_{20}$), was found to contain as much as 1.9 % Al_2O_3, 1.1 % Fe_2O_3, 0.49 % CaO, and traces of other oxides. Diffusional processes in such a system have two significant consequences: (1) they influence the melting temperatures of the system directly allowing the development of new uetectic compositions, (2) they affect the textural characteristics of the final products indirectly by allowing the formation of new minerals of slow rates of crystallization from these eutectic compositions. This compositional complexity of the natural silicate rocks is further increased by the fact that the natural igneous phenomena differ from each other not only in their temperature-composition-time variables, but also in their pressure-composition history. Magma formation and solidification in the hydrospheric-atmospheric low pressures in the presence of water and excess oxygen could not generate characteristic high pressure plutonic rocks or even characteristic low pressure lunar rocks (which are formed and solidified in the absence of hydrosphere-atmosphere). Omitting any one or two of the variables in the laboratory experiments and using pure synthetic rocks may help to understand the geologic history of the simulated events. For example, a study of rapid heating and rapid cooling with short stay at temperatures in the order of 1 sec, along with rapid rise and drop in pressure up to 40 kb and down to one atmosphere yields data on impact melting of rocks, whereas a study of slow heating long stay at temperature and pressure in the order of several days, followed by simultaneous quenching of temperature and relaxation of pressure clarifies volcanic melting of the rocks. In comparing a dunite with a gabbro, it appears that the time dependence of the melting temperature of the former is much more

significant than that of the latter. Increasing the duration of heating, at 1 atm pressure, from 1 sec to 6 days, the initial melting temperature of dunite drops from 1700°C ± 50° to 1200°C ± 50°. The initial melting temperature of gabbro, which at several seconds culminates at 1200°C ± 50°, does not seem to drop with increased duration of heating. Hence, both volcanic and impact melting of the gabbro may be expected to occur at the same temperature, whereas volcanic melting of dunite may be expected to occur several hundred degrees Centigrade below impact melting.

The petrological expression of time is the texture of the rock, the degree of segregation of the minerals, and the range of end products from total fusion to partial melting. The rate of heating, time of stay, and rate of cooling, discussed in previous paragraphs, are only means to simulate such conditions which are likely to have operated on the moon.

A major observation of the products of melting of complex silicates in a search for understanding geological phenomena is that the origin of rocks usually takes place in open systems, in many cases at non-equilibrium and often at dynamic equilibrium (Azmon, 1963), or at mosaic equilibrium (Korzhinskiy, 1962). The thermodynamics of magmatism and metamorphism in general is discussed by Barth in his second edition of Theoretical Petrology (1962). It may be necessary only to reemphasize that the state of lowest free energy cannot be determined once for all rocks; it changes with temperature, pressure, and composition, and requires time to reach equilibrium. Therefore, each combination of these variables must be taken into consideration. Also, the rock systems in nature (for example: mantle, crust, batholith, or mountain ranges) are "big things," not hand speciments, and experimental petrology and physicochemical experiments with combinations of the above variables must be conducted against the background of field geology and systematically correlated with it.

Direct correlation of the physical processes can be accomplished only where such processes are still active and accessible. Mostly, one has to be content with the correlation of the physical properties of the products which are all that have remained of a multitude of events that took place in the geologic realm. However, rocks should be studied in reference to both the physicochemical laws which govern their genesis anywhere in the universe and to the geologic forces and processes that work in the body of a specific planet. Natural processes can be simulated in the laboratory due to the fact that the governing physicochemical laws are universal, but exploration must be conducted out in the natural environment, because the working geologic forces and processes do differ from place to place. This division holds regardless of whether one studies the earth, the moon, or another planet.

The fundamental method of approaching problems of rock formation was outlined by Korzhinskiy (1962) as:

a) a systematic analysis of a wide range of natural occurrences
b) a search for any regularities in physicochemical circumstances
c) subsequent experimental verification, and
d) theoretical substantiation of any hypotheses that evolve.

In this report the field geology data, the ideas summarized, the experiments described, and the curves plotted, are all part of a search for regularities and for experimental verification.

DETERMINATION OF GENETIC STATES OF ROCKS

Genetic State Concept

The history (time and rates of changes) of pressure and temperature conditions that a rock material is exposed to defines a genetic state from which a rock of distinct characteristics is born. When a genetic state is a state of final equilibrium, the phase diagram of that rock is also its genetic diagram. However, many rocks of distinct characteristics are found in nature, or may be produced in the laboratory under conditions far from equilibrium; hence, their genetic states represent interception of the path of the reaction and may bear no similarity to the phase diagram. The genesis of these rocks is no more a function of the composition, temperature and pressure alone; it depends on the path of the reaction (and where it was intercepted), grain size, presence of gases, rate of diffusion, degree of mixing, and other properties. The following discussion deals primarily with this type of genetic state.

Bruderheim Meteorite

"Melting" was arbitrarily defined to be "the first evidence of quenched glass or new microcrystallites as determined with a petrographic microscope". However, x-ray examination indicates that with this rock this definition corresponds closer to 50% melting rather than to initial melting.

Semiquantitative x-ray analysis (see Appendix) of those samples that were quenched at 10 kb indicates a very peculiar melting pattern (Figure 9). The highest concentration of hypersthene remaining crystalline, when 58% of the sample has melted, is found to be 34% (plus 8% remaining olivine). This concentration can be obtained at two different temperatures, 1220°C and 1350°C.

A possible explanation is that between these two temperatures the rate of recrystallization of hypersthene increases until it is equal to the rate of melting of the same.

Experimental observations of melting temperatures for the Bruderheim meteorite as a function of pressure up to 40 kb (Table VI) indicate that melting occurs at several hundred degrees Centigrade below the melting of the equivalent pure olivines and pyroxenes (if they are assumed to be in equilibrium within a closed system). It has also been determined that under certain pressure-temperature conditions most of the olivines will disappear from the solid state before the pyroxenes contrary to what has been observed in a simple FeO-MgO-SiO_2 system.

New and old experiments on the phase transformation were reexamined in terms of 10 genetic states and a genetic diagram was prepared (Figure 10). This diagram shows the existence of four areas: solidus area, liquid transition area, glass quench area (the quench product is only glass with no recrystallization) and a crystal quench area (the quench product is only crystalline with no glass).

Tholetiitic Basalt

Many researchers in several well known laboratories have been studying the origin of various basalts. Their prime interest concentrates around equilibrium behaviour of the basalts. Three typical studies are cited: Tilley, Yoder and Schairer (1964); Green and Ringwood (1964); Jamieson (1966). In this study under NASA contract, emphasis has been on nonequilibrium conditions.

Petrographic analyses of tholeiitic basalts were run to determine the changes in percentages of glass and crystals after the specimens had been subjected to various temperature-pressure combinations for durations of 5 min (Table VII). The results of

TABLE VI

GENETIC STATE DATA FOR THE BRUDERHEIM METEORITE

Samples are core; all times were 5 minutes except runs 103 (4.5 min) and 137 (1.5 min)

Run	P,kb	T,°C	PETROGRAPHY	Hypersthene to olivine in crystalline phase	Percent glass phase	Notes
101 top	10.0	1230 ± 30	Glass and crystals	48/52	62	a, b
bot	10.0	1325 ± 25	Glass	77/23	57	g, h
102 top	10.0	1200 ± 20	Glass and crystals	86/14	40	a, b
bot	10.0	1270 ± 20	Glass and crystals	72/28	69	a, b
103 top	4.0	1120 ± 30		72/28	29	a
bot	4.0	1190 ± 40				a, b
104 top	5.0	1210 ± 20	Traces of glass			a, b
bot	5.0	1275 ± 15	Glass and relics O	81/19	37	
105 top	10.4	1260 ± 10				a
bot	10.4	1325 ± 15	Traces of glass			a, b
106 top	15	1450	Quench crystals all over, relics O & C			i
bot	15	1475				i
107 top	14.8	1330 ± 30	Relics O + glass			c
bot	14.8	1400 ± 25	Quench crystals + glass			h
108 top	10.2	1340 ± 25	Glass & quench crystals	82/18	57	g, h
bot	10.2	1365 ± 20	Glass quench crystals			
109-1 top	5	1265 ± 35	Glass & quench crystals	70/30	38.5	h
bot	5	1360 ± 25	Glass			g
110 top	5	1240 ± 10	Original crystals and trace of glass	82/18	38	h
bot	5	1310 ± 15				g
111 top	22.8	1165 ± 5	Trace of glass			a, b
bot	22.8	1185 ± 5	Trace of glass			a, b
112 top	23	1405 ± 10	Original crystals, glass			a, b
bot	23	1420 ± 10	Quench crystals, glass			g, h
114A top	12	1400 ± 15	No glass, no quench crystals			a
bot	12	1470 ± 10				a
115 top	30	1485 ± 50	Quench crystals & relic crystals			i
bot	30	1570 ± 40	Quench crystals			i
122 top	40	1475 ± 5	Original crystals and trace of glass			a, b
bot	40	1485 ± 5				a, b
124 top	40	1485 ± 5	Quench crystals			b, i
bot	40	1540 ± 15	Original crystals			a, b
125 top	40	1555 ± 15	Quench crystals			i
bot	40	Lost thermocouple				
126 top	39	1375 ± 15	Original crystals			a
bot	39	1430 ± 10	Original crystals			a
127 top	41	Lost thermocouple				
bot	41	1425 ± 15	Original crystals			a
128 top	23	1215 ± 35	Original crystals			a
bot	23	1300 ± 30	Original crystals			a
129 top	18	1200 ± 30	Original crystals			a
bot	18	1250 ± 30	Original crystals			a
130 top	11	1410 ± 40	Glass			g
bot	11	Lost thermocouple				
131 top	25	1455 ± 20	Some quench crystals			h
bot	25	1510 ± 10	Quench crystals			i
132 top	20	1245 ± 5	Original crystals and trace of glass			a, b
bot	20	1405 ± 15	Glass			g
133 top	22	1505 ± 5	Quench crystals			i
bot	22	Lost thermocouple				
134 top	15	1400 ± 10	Quench crystals and glass			h
bot	15	1525 ± 15	Quench crystals			i
135 top	18	1415 ± 10	Quench crystals and glass			h
bot	18	1510 ± 10	Quench crystals			i
136 top	12	1455 ± 35	Glass			g
bot	12	1555 ± 35	Glass, vesicle (probably developed during drop in pressure)			g
137 top & bot	12	1415 ± 25	Quench crystals and glass			h
	12	1525 ± 15				

[a]original rock [b]50% melt [c]relic O [d]vesicular [e]scoriaceous [f]pumiceous [g]glassy
[h]50% quench crystals [i]relic C [j]quench crystals

TABLE VII

GENETIC STATE DATA FOR THOLEIITIC BASALT FROM OREGON

Samples are core; all times were 5 min except run 102 (1 min)

Run	Capsule	P, kb	T, °C	% Glass near Tip	Petrography of Half the Sample
101 top	BN	11	1240		brown glass and opaque metallic globules (magnetic?)
bot	BN	11	1280		brown glass and opaque metallic globules (magnetic?)
102 top	BN	4	850		Original crystals
bot	BN	4	920		
102-1 top	BN	10	1060	60	Original crystals
bot	BN	10	1110	85	Glass and relic crystals
103 top	BN	5	1020	20	Original crystals
bot	BN	5	1040	95	Glass
104 top	BN	15	1055	5	Mixed original crystals - glass
bot	BN	15	1120	75	Glass + relic crystals
105 top	BN	15	990	45	Original crystals
bot	BN	15	1020	70	Original crystals
106 top	BN	10	990	80	Original crystals
bot	BN	10	1025	100	Glass
107 top	BN	20	1025	10	Original crystals
bot	BN	20	1080	95	Original crystals and glass
108 top	BN	20	1040	97	Original crystals
bot	BN	20	1105	97	Original crystals
109 top	BN	20	1205	100	Glass
bot	BN	20	1260	100	Glass
110 top	BN	27	1100	90	Original crystals + glass
bot	BN	27	1310	98	Glass
111 top	BN	27	1040	60	Original crystals
bot	BN	27	1140	80	Quench crystals
112 top	BN	37½	1215	80	Recrystallized
bot	BN	37½	1265	98	Recrystallized
113 top	BN	33	1285 ± 45	100	Glass
bot	BN	33	1405 ± 45	100	Glass
114 top	BN	35	1015 ± 15		Recrystallized feldspar
bot	BN	35	1050 ± 35		Recrystallized feldspar
115 top	BN	32½	Lost Thermocouple		
bot	BN	32½	1055 ± 25	95	Recrystallized feldspar
116 top	BN	6	785 ± 5	80	Original crystals
bot	BN	6	920 ± 10	86	Original crystals
117 top	BN	5	1220 ± 15	100	Glass
bot	BN	5	1365 ± 15	100	Glass
118 top	BN	44	1300	100	Glass
bot	BN	44	1370	100	Glass
119 top	BN	39	1150 ± 20		Original crystals, recrystallized, garnet?
bot	BN	39	1230 ± 20		Glass
BAx1	BN	1	1000	0.5	Trace of glass on periphery
BAx2	BN	1	1000	2	50% glass
BAx3	BN	1	1000	6	Vesicular, no recrystallization
BAx4	BN	1	1000	24	Glass, no vesicles, 25% recrystallization
BAx5	BN	1	1000	144	75% recrystallized
BAxx1	Pt	1	1000	0.5	Original crystals
BAxx2	Pt	1	1000	2	Original (plastic flow-took shape of capsule)
BAxx3	Pt	1	1000	6	Lost sample
BAxx4	Pt	1	1000	24	Lost sample
BAxx5	Pt	1	1000	144	Original crystals
BAx1-3	BN	1	1100	0.5	50% vesicular
BAx2-3	BN	1	1100	2	Vesicular, no relics
BAx3-3	BN	1	1100	6	All glass, no vesicles, no crystals
BAx4-3	BN	1	1100	24	Glass, some new crystals on periphery, no vesicles
BAx5-3	BN	1	1100	144	50% glass, no vesicles, 50% new crystals
BAxx1-3	Pt	1	1100	0.5	
BAxx2-3	Pt	1	1100	2	
BAxx3-3	Pt	1	1100	6	
BAxx4-3	Pt	1	1100	24	
BAxx5-3	Pt	1	1100	144	

these data are plotted in Figure 11 showing pressure versus percent glass divided by the corresponding pressure, and temperature versus percent glass divided by corresponding temperature. The temperature plot shows no definite pattern whereas the pressure plot shows a definite trend. This indicates that pressure is the dominant factor controlling the percent glass in the samples in the pressure temperature range covered by the experiments.

When plotting the data as percent crystals versus the ratio of temperature to pressure all the points fall along the sides of a triangle (Figure 12). It is interesting to compare this figure with Figure 13 and search for correlations between physical properties measured as seismological data and the petrological identities measured as genetic states in the rocks at high temperatures and pressures. It is convenient to use T-P rather than specific volume as a common denominator for comparison of petrological and seismological properties because both T and P can be easily measured in the laboratory on a routine basis. The P and T estimates for the earth are shown in Figure 14.

It is interesting to note that when a basalt sample was kept at 1 atm and 1,000°C for 6 hours, it developed a rock froth with cavities that are not interlocking (high porosity, low permeability) with indications of partial melting. When an equivalent sample was kept under the same conditions for 24 hours, it de developed glass plus abundant new crystallites. The 6 hour data seem to support our theory that the presence or absence of the atmosphere is not critical for the formation of rock froth since the hot silicate rock supplies its own gas phase and since the frothing depends on the pressure differential more than its absolute value.

The "24-hour" data are in general agreement with Kopecky's observations (oral communication) of recrystallization of molten basalt (in Czechoslovakia's Cast Basalt Industries). However, our sample

is deficient in olivines; hence, we did not premelt the sample before heat treating it. In contrast, we obtained the results in one simple heating procedure.

A time dependence curve showing the development of ten genetic states was derived for a set of conditions and compared with a curve of the same nature derived for gabbro (see Figure 15). It is important to note that although the genetic states from one to ten do not have numerical values, they develop in a successive order. Each genetic state can be described as a physicochemical phase, such as liquid (glass) or solid (crystalline); it can be described as a mineralogical phase (no example in this figure); or it can be described as a textural distinction, such as vesicular or pumiceous. The genetic states are descriptive and all have one common denominator--they describe distinct rocks. In attempting to relate features which are found in the natural environment, basalt samples taken at various depths from the Malpar's Flow of east-central New Mexico were examined. The examination indicated that:

1. More glass occurred near and at the margins of the flow, e.g., top, sides and bottom.
2. No significant mineralogical changes occurred in the traverse.
3. Vesiculation studies indicated that the vesicles occur in greater number near the top of the flow than the sides and bottom.
4. Vesicles are more ellipsoidal at the top and bottom of the flow.
5. The largest and most spherical vesicles occur about midway between the top and bottom of the flow.
6. The greatest concentration of zeolites also occur where the largest vesicles are found.

7. Flow lineation only gave a two-dimensional orientation and the source direction could not be picked.
8. Imbrication of Pc laths was inconclusive as to the source direction of the flow.
9. Mega-features such as bent vesicles and streaming indicates directional vector; however, these only indicated the last flow direction.

The evaluation of the Malpar's basalt in terms of the genetic states which existed during its genesis must wait until we complete the laboratory experiments on the equivalent rocks.

Granodiorite

Run data for the melting of granodiorite are listed in Table VIII. Melting of a complex substance like granodiorite is not a simple transformation of a solid into a liquid. It occurs over a range of temperatures and it is gradual. The major components, plagioclase feldspar and quartz may melt as individual minerals or the feldspar may melt and dissolve some of the quartz. The criteria for recognizing melting after the temperature quench is a problem since the high temperature solution of one silicate by another silicate melt may result in a product that looks no different from that of mutual melting of these silicates.

Petrographic and x-ray examinations of granodiorite were run to determine phase transformations, including changes in percentages of glass and crystals after the specimens had been modified by various temperature pressure combinations for durations of 1, 5 and 10 min. The original phases of plagioclase feldspar and quartz mostly disappear near 35 kb and new minerals, coesite and jadeite, appear. It seems that the amount of glass increases with the time maintained at temperature, but no drop in apparent melting temperature was observed. A drop in the "percent glass"

TABLE VIII

GENETIC STATE DATA FOR GRANODIORITE FROM CALIFORNIA

Abbreviations are coesite (coes), crystalline phase (cp), feldspar (f), glass (gl), jadoite (jad), new phase (np), original phase (op), plagioclose (pl), and quartz (q).

Run	P, kb	T, °C Top	T, °C Bot	Time (min)	% Glass	Microscopy	X-ray	Plag. comp.	Remarks
GD 101	11	1190	1195	5	10	q ore	q, f		
102	11	1210	1110	5	15	pl, q	q, f	An [illegible]	
103	10	1215	1155	5	55	q, pl	f, q	An [illegible]	
104	[illegible]	1240	1190	5	90	q, pl, biot	q, f	An [illegible]	[illegible]
105	5	1180	1150	5	15	q, pl	q, f	An [illegible]	
106	15	1245	1220	5	15	q, f (Sanid)	q, f		
107	14.6	1260	1110	5	75	q, pl (Sanid)	q, f	An [illegible]	
108	20	1355	1415	5	65	q, Sanid, biot	q, f		
109	10	1300	1185	5	20	q, f (Sanid)	q, f		
110	15		1420	5	95	q	q		
111	22.5	1340	1445	5	95	q	q, f		
112	10	1100?	1345	5			q, f		Thin section damaged
113	5	1100	1380	5		q	q		Thin section damaged
114	35	1150	1220	5	70	np	coes, jad, q, garnet		
115	25	1240	1170	5	20	q, pl, biot	q, f		
116	42	1265	1360	5	95		coes, garnet		
117	41	(lost)	1400	5	70		coes, jad		
118	45	1? 0	1100	1	70	cl, px, np	coes, jad		
118-I	47	1400	1450	5	75	Sanidine, cl, px	coes, jad, garnet		
GD 119	30	1215	1250	5	30	q, pl	q, f		
120	34	1115	1145	5			q, f		Thin section not made
121	18	1185	1200	5	85	pl, coes, cl, px	coes, q, jad		
122	26	1140	1180	5	20	q, pl, Sanid	q, f		
123	30	1035	1120	5	15	q, pl, Biot	q, f		
124	26.5	910	960	10	10	q, pl, Biot, cp	q, f, jad?		
125	11.5	760-820	850-900		10	q, Sanid, Biot	q, f	DTA	DTA
126	15	875	945		20	q, pl, cp	q, f	DTA	DTA
127	11.5	(lost)	800		5	pl, Biot	q, f		DTA
128	20	350	450						DTA - thin section not made
129	9.2	800	900	50	20	q, pl, Biot	q, f	An 30-45	DTA
130	14	715	810		tr	q, pl, Biot, cp	q, f		DTA
131	5	700	(lost)	10	10	q, pl, Biot	q, f		
132	35	950	1015	10	20	q, f, Biot	q, f		
133	35	960	1020	60	25	pl, q, Biot	q, f		
134	40	(lost)	1010	10	40	q, Sanid	a, coes (jad)		
135	40		1000	60	50	cl, px, Biot	coes, jad		
136	30	760	815	10	0	pl, q, mica	q, f		
137	30	925	(lost)	10	5	pl, q, Biot	q, f		
138	25	770	830	10	tr	q, pl, Biot	q, f		
139	21	950	1005	10	10	Biot, q, Sani	q, pl, Biot?	An 45-50	
140	15	780	860	5	tr	q, pl, Biot			
141	25	925	1040	10	tr	q, pl	q, f		
142	40	780	815	10	5	cl, px, co, mica	q, coes, jad, f		

curve (Figure 16) between 30 and 35 kb corresponds with the transformation of the quartz and feldspar into coesite and jadeite and garnet. These transformation probably take place as follows:

$$3(CaO \cdot Al_2O_3 \cdot 2SiO_2) \rightarrow 3CaO \cdot Al_2O_3 \cdot 2SiO_2 + 2(Al_2O_3 \cdot SiO_2) + 2SiO_2$$

Anorthite — Garnet — Kyanite — Quartz coesite

$$Na_2O \cdot Al_2O_3 \cdot 6SiO_2 \rightarrow Na_2O \cdot Al_2O_3 \cdot 4SiO_2 + 2SiO_2$$

Albite — Jadeite — Quartz Coesite

Figure 17, which displays the percent glass as function of temperature at 10 kb pressure shows an abrupt rise in the amount of glass between 1150 and 1250°C. suggesting substantial melting of the sample.

As to the formation of coesite, more experiments will be necessary to evaluate the significance of its high rate of formation.

Based on the data that were collected thus far, a hypothetical genetic diagram (Figure 18) has been prepared which shows the rock type that would quench out of a system having the granodiorite composition and exposed to different pressure-temperature conditions. Three rock types are displayed by this genetic diagram: (1) granodiorite, which is the unaltered sample material; (2) dacite, which is primarily aphanitic composed of both microcrystalline and cryptocrystalline material, but including some glassy material; (3) dacite vitrophyre, which is primarily glassy; and (4) eclogite equivalent, which would be a true eclogite if its pyroxene percentage was significantly higher.

Serpentine

Examination of the ratio of glass to crystalline material as a function of temperature and pressure suggests that the ratio increases with pressure up to a point and then decreases, a phenomenon observed in reference to the Bruderheim meteorite.

An examination of crystalline stability regions of serpentine after treatment at various temperatures and pressures was conducted by means of x-ray diffraction analysis. These analyses were conducted on small core samples which were powdered and mounted on specially cut quartz plates. The weight of sample used in the analysis varied from 1.0mg to 6.0mg. Samples of this serpentine were analyzed after treatment at temperatures ranging up to 1400°C and pressures up to 30 kb.

Preliminary results of these analyses (Figure 19) indicate four general regions of crystalline stability at various temperatures and pressures. These stability fields have been identified from the peak positions and intensities of the x-ray diffractograms. Antigorite was the stable mineral phase at temperatures as high as 300°C and pressures up to 20 kb. Forsterite (Mg_2SiO_4) appeared to be the only mineral phase present at temperatures between 780°C and 1250°C when the pressure was generally below 12 kb. Combinations of forsterite and enstatite ($MgSiO_3$) became stable at temperatures over 1200°C and pressures over 14 kb. Enstatite was the only mineral phase identified in a few samples after treatment at temperatures greater than 1260°C and pressures greater than 16 kb. These stability regions have been identified in samples that have been maintained at the indicated temperatures for 5 min in most cases. In the few cases when the temperatures were maintained for longer periods of time or when the rate of heating varied, there appeared to be a corresponding shift in the stable crystal phase.

Petrographic and x-ray diffraction examination of the experiment products reconfirm the previous observation that with increased pressure and temperature the original mineral antigorite loses water and transforms into forsterite; then, at still higher pressure and temperature the forsterite gains silica and gains and breaks into enstatite plus some enriched iron-magnesium oxides. The x-ray diffraction analysis gives a fairly accurate estimate of the ratio of the crystalline phases. As to our attempt to make quantitative determinations based on x-ray diffraction it appears that the absolute peak heights are too sensitive to even traces of pyrophyllite, and the error in intensity reading is as much as 1 to 4 times their correct height. Comparing stay time at pressure and temperature for 5 min versus stay time for 15 min shows coarser recrystallization at 15 min, as expected.

Study of the serpentine phases under pressure at temperatures from 300°C to 1500°C was continued, using DTA techniques to determine changes in situ, and petrographic and x-ray diffraction techniques for examination of the samples after quenching. Four phases were defined:

1. Serpentine antigorite
2. Olivine forsterite
3. Pyroxene enstatite
4. Glass

The antigorite-to-forsterite transformation is obviously a loss of water which evaporates into the boron nitride and talc sleeves.

The forsterite to pyroxene transformation involves loss of metal oxide; however, the final glass should regain the composition of the forsterite.

Two minor problems were encountered during the examination and are being evaluated: (1) at around 900°C, some Fe and Mg migrate

along the platinum thermocouple wires; (2) several x-ray diffraction patterns show evidence of a magnesium borate which is a definite evidence that the boron nitride capsule occasionally reacts with the Fe-Mg silicate.

Antigorite, which is the major constituent of the serpentine, persists at temperatures up to 650°C even at 45 kb. At lower pressures, however, it seems to persist at temperatures 50 to 75°C higher than that.

At the higher temperature, olivine (forsterite) is dominant and pyroxene (enstatite) is abundant. The upper temperature limits for this zone rise from 800°C at 10 kb to 900°C at 35 kb to 1100°C at 45 kb.

At still higher temperatures, pyroxene is dominant. Olivine is abundant up to at least 35 kb, but between 35 and 45 kb it disappears completely and pyroxene is the only crystalline component in the zone.

Above this, a 100% glass zone persists. The liquidus curve which is at 1350°C at 10 kb rises to 1450°C at 35 kb and to 1475°C at 45 kb.

As a matter of record it is important to note two contaminants. One, boron phlogopite in the region of approximately 600 to 900°C noted at pressures of 10 and 35 kb but not at 45 kb; two, boron magnesium oxide noted at 1450°C at 35 kb. The significance of the data is clear. A quick examination of the data indicates that the temperature dependence of the deserpentinization (dehydration of the serpentine) is far greater than the pressure dependence. Should serpentine be found on the moon, then a water extracting process would probably be carried through temperature manipulation rather than pressure manipulation.

Another very important significance is that the zones of stability of olivine versus pyroxene measured in terms of pressure and temperature can be expressed also in terms of depth versus temperature in models of the moon and the earth.

Obsidian

It became obvious in the process of experimentation that the existing analysis facilities at hand were not sufficient to differentiate between the original unaltered phases of the bock (mostly glass) and the quench products (mostly glass). At this point the experimentation with obsidian was terminated. Data at 1 atm are listed in Table IX.

Fayalite

Run data for the melting of fayalite are listed in Table 5. Melting was detected by noting a conspicuous difference in texture between samples which had recrystallized from liquid during quenching and those that had recrystallized in the solid state or remained intact below the melting temperature (Figure 20). Fayalite recrystallized in the solid state (Figure 21) occurs as anhedral equant grains attaining sizes of several tens or even hundreds of microns. The quench crystals, in contrast, occur as sheaves of coarse lamellae arranged in radia, interlocking or subparallel patterns (Figure 22). Some show a typically graphic texture (Figure 23). The maximum length of these lamellae may reach 600 microns or more. Interstices between these quench crystals are invariably filled with a dark brown to black, nearly opaque material very likely consisting of glass and finely divided iron. This iron appears to represent incongruent melting of fayalite.

Liquid fayalite could be quenched to glass only at temperatures far above the determined melting curve. Within about 120°C of the curve quench crystals were invariably obtained. When boron nitride was used as sample container, this interval dropped to less than 20°C and the melting temperature was lowered about 50°C at 25 kb pressure (Table X). Boron nitride has a binder of boric acid ($B_2O_3 \cdot xH_2O$) of 3 to 5 wt percent. Thus the "fluxing effect" caused by the boron nitride is probably due to a solution

TABLE IX

DATA AT 1 ATM ON CASTING OBSIDIAN

Run	Mold	T,°C	Time	Remarks
7	Graphite	1100	1.5	Crushed obsidian, mold burned away, good cast, many air bubbles (no slide).
8	Graphite	1100	1.5	Crushed obsidian, mold burned away, good cast, many air bubbles (no slide).
9	Graphite	1000	1.25	Partial melting only (no slide)
10	Graphite	1100	1.50	Nice cast, graphite burned (no slide)
11	Graphite	1050	15	L Tube, 2 hours at temp then raise to 1075°C and left for 11 hours, smooth cast, mold burned (no slide)
12	Graphite	1050	15	U Tube, 2 hours at temp then raise to 1075°C and left for 13 hours, smooth cast, mold burned (no slide)
13	Graphite	1050	3	A try to determine the melting point 1 hr at 1050°C, 1 hr at 1060°C, 1 hr at 1070°C (no slide)
14	Pyrophyllite	1150	1/2 to 2	4 samples (different time) half an hour intervals
			1/2	-1. Looks powdery
			1	-2. Still powdery
			1 to 1/2	-3. Smoother surface
				-4. Smoother than 3
15	Pyrophyllite	1200	1/2 to 2	-1. Smooth and shiny surface, melted all the way through
				-2. Smooth and shiny surface, large air bubbles
				-3. Rounded corners, less bubbles, glassy surface
				-4. (very) glassy and shiny; small bubbles, round corners
16	Phrophyllite	1300	1/2 to 2	4 samples:
				-1, -2, -3, -4 all have same outside appearance, ball shape, huge air bubbles, very brittle
17	Pyrophyllite Impreg. w/ Graphite	1300		Mold cracked
18	Pyrophyllite	1175	24 to 96	4 samples (were left in) 24 hr intervals
			24	-1. Rounded, glassy, full of bubbles
			48,72,96	-2, -3, -4 Look the same as -1
19	Pyrophyllite Graphite Tubing	1200	1	(T shape) very porous and brittle, nice cast (no slides)
20	Cured Talc	1200	1	One mold impregnated with graphite (one pure talc) very fine and smooth cast, almost no sticking (no slide)
21	Cured Talc	1200	1	(H shape) mold broke, sample stuck to the mold, nice finish on top, bubbly (no slide)
22	Cured Talc	1200	1	Shape, same as No. 21
23	Uncured Talc	1200	11	(6 holes in a block) block cracked, obsidian stuck to the walls, large bubbles in the cast (no slide)
SE66-1	Uncured Talc	1100	4	Mold covered with Aquadag as a parting film, nice separation of the sample, rough surface
SE66-2	Uncured Talc	1100	2/3	Same as SE66-1, but no signs of melting, looks like sand pressed together
SE66-3	Cured Talc	1100	5	Moily powder was used as a film, complete melting, glassy appearance, stuck to mold
SE66-4	Phyrop. Uncured	1150	3 to 5	Brushed with Aquadag, half hour intervals
			3	-5. Smooth sample, some bubbles, stuck to the bottom
			3-1/2	-6. Larger bubbles than No. 5
			4	-7. Bubbles raised the surface
			4½ to 5	-8,-9. Bubbles raised the surface

TABLE X

GENETIC STATE DATA FOR SYNTHETIC FAYALITE

Run	Capsule	P,kb	T, °C	Result		Remarks
G127	Fe	40	1425	Quench crystal Matrix	95% 5%	Melting
G167	Fe	40	1405	Quench crystal Matrix	95% 5%	Melting
G170	Fe	40	1390	Crystal Quench crystal Matrix	50% 43% 2%	Partial melting due to trace H_2O
G124	Fe	40	1370	Crystal	100%	No melting
G145	Fe	35	1500	Glass	100%	Melting
G156	Fe	35	1470	Quench crystal Matrix	95% 5%	Melting
G144	Fe	35	1400	Quench crystal Matrix	95% 5%	Melting
G171	Fe	35	1380	Quench crystal Matrix	95% 5%	Melting
G143	Fe	35	1370	Crystal	100%	No melting
G142	Fe	35	1345	Crystal	100%	No melting
G150	Fe	30	1500	Glass	100%	Melting
G157	Fe	30	1450	Quench crystal Matrix	95% 5%	Melting
G120	Fe	30	1405	Quench crystal Matrix	95% 5%	Melting
G125	Fe	30	1375	Quench crystal Matrix	95% 5%	Melting
G121	Fe	30	1350	Quench crystal Crystal Matrix	15% 80% 5%	Partial melting due to thermal gradient
G122	Fe	30	1340	Crystal Quench crystal Matrix	80% 10% 10%	Partial melting due to trace H_2O
G123	Fe	30	1305	Crystal	100%	No melting
G140	Fe	25	1480	Quench crystal Matrix	95% 5%	Melting
G139	Fe	25	1455	Quench crystal Matrix	95% 5%	Melting
G138	Fe	25	1410	Quench crystal Crystal Matrix	70 28 2	Partial melting due to thermal gradient
G137	Fe	25	1400	Crystal	100%	No melting
G111	Fe	20	1460	Glass Quench crystal	98 2	Melting
G112	Fe	20	1400	Quench crystal Matrix	95 5	Melting
G113	Fe	20	1375	Quench crystal Matrix	95 5	Melting
G114	Fe	20	1340	Quench crystal Matrix	95 5	Melting
G115	Fe	20	1308	Quench crystal Matrix	95 5	Melting
G116	Fe	20	1300	Quench crystal Matrix	95 5	Melting
G117	Fe	20	1250	Crystal	100%	No melting
G118	Fe	15	1355	Quench crystal Matrix	95 5	Melting
G119	Fe	15	1295	Quench crystal Matrix	95 5	Melting
G158	Fe	15	1270	Crystal	100	No melting
G159	Fe	15	1250	Crystal	100	No melting
G161	Fe	10	1430	Glass	100	Melting
G131	Fe	10	1400	Quench crystal Matrix	95 5	Melting
G133	Fe	10	1280	Quench crystal Matrix	95 5	Melting
G134	Fe	10	1250	Crystal	100%	No melting
G135	MM	25	1420	Glass Spherules	93% 7%	Melting
G136	MM	25	1400	Glass Spherules	93% 7%	Melting
G162	MM	25	1290	Glass Spherules	93% 7%	Melting
G181	MM	25	1270	Crystal Quench crystal	90% 10%	No melting
G151	MM	25	1260	Crystal Quench crystal	90% 10%	No melting
G152	MM	25	1230	Crystal Quench crystal	90% 10	No melting
G128	C	35	1395	Quench crystal Matrix	95% 5%	Melting
G129	C	30	1375	Quench crystal Matrix	95% 5%	Melting

of B_2O_3 in the melt or due to H_2O from $B_2O_3 \cdot H_2O$ in the melt (personal communication with L. H. Cohen). The fayalite glass obtained at 10 kb (Run G131) has an index of refraction n_D = 1.772 $\pm$ 0.002.

The melting curve constructed from the data in Table 5 is shown in Figure 24. Some runs quenched from temperatures near the solidus showed partial melting. If patches of quench crystals occupied an irregular position in the capsule (Figure 21), the partial melting is interpreted as due to the presence of a trace amount of H_2O. If there was a gradual change from quench crystals to intact crystals in compliance with the thermal gradient of the furnace, the melting is explained as a result of the gradient.

By calculating all iron in each mixture as FeO, Bowen and Schairer (1932) and later Allen and Snow (1955) showed that fayalite bears an eutectic relation with wustite, FeO. The two investigations obtained the same eutectic temperature of 1177°C but different eutectic compositions. The oxidation state of the sample is not known; however, in view of the short run duration, conversion of appreciable iron in the capsule to wustite is unlikely and the eutectic effect on the melting of fayalite is probably negligible. To check this effect graphite capsules were used in several runs. The data, although inconclusive, seem to support the proposed melting curve.

The melting curve in Figure 24 is not "reversed", yet it is drawn from consistent data. The curve approaches a straight line defined by the equation, T = 1205 + 4.85P, where T is temperature in degree Celsius and P is pressure in kilobars. This curve has a slope only slightly steeper than the corresponding curve for forsterite determined by Davis and England (1964). The broken curve above the melting curve in Figure 24 indicates the upper temperature limit for the formation of quench crystals in those experiments when iron capsules were used.

In their study of the $FeO-SiO_2$ system at atmospheric pressure, Bowen and Schairer (1932, pp 196) demonstrated that incongruent melting with separation of metallic iron is characteristic not only of ferrous oxide but of all mixtures along the $FeO-SiO_2$ join. They showed that both synthetic and natural fayalites melt incongruently with separation of about 3/4 wt % Fe. The equilibrium diagrams in the system $FeO-Fe_2O_3-SiO_2$ prepared by them and later by Muan (1955) all showed the iron encroaching upon the $FeO-Fe_2O_3-SiO_2$ triangle.

To confirm the incongruent melting of fayalite at high pressure, a series of runs using boron nitride capsules were made at a pressure of 25 kb (Table 5). The melting temperature thus obtained was about $50^{\circ}C$ lower than that using iron capsules as previously described. When fayalite did not melt, the periphery of the sample in contact with the boron nitride capsule was stained to reddish pink and gave rise to minute acicular crystals similar to quench crystals obtained from the iron capsules. Once melted in boron nitride capsules, fayalite liquid quenched to a glass, clear yellowish-green in color with $n_D = 1.773 \pm 0.002$ and with inclusions of black and opaque spherules showing metallic luster (Figure 25). The size of the spherules ranged from several to tens of microns in diameter. These spherules were separated from the fayalite glass; x-ray diffraction indicated that they are mostly iron with a very small proportion of wustite. Their precipation of copper from a copper sulphate solution and their strong attraction to a magnet further demonstrated that the spherules were essentially metallic iron. The presence of such iron spherules in fayalite glass demonstrates the incongruent melting of fayalite up to at least 25 kb.

All the iron silicate melts, as demonstrated by Bowen and Schairer (1932), have some amount of Fe_2O_3 which cannot be reduced by any strong reducing agent at their respective liquidus temperatures.

This peculiar behavior of iron silicate melts may be responsible for incongruent melting of fayalite probably through the following process without involving the redox reaction:

$3FeO$ (in melt) = Fe_2O_3 (in melt) + Fe (separated metallic iron)

This reaction takes place at strong reducing conditions probably with oxygen fugacity at or lower than that defined by the iron-wustite buffer. Using FeKα radiation and Si (d_{111} = 3.1351 A) as an internal standard, d_{130} of fayalite quench crystals obtained from three runs using iron capsules was determined to be 2.828 ± 0.001 A which is essentially the same as for the original crystals.

Unlike many other silicate minerals such as diopside, albite (Boyd and England, 1963), and enstatite (Boyd et al, 1964), fayalite appears to have an almost linear melting curve with the slope only slightly steeper than for forsterite. The incongruent melting of fayalite with separation of metallic iron persists up to at least 25 kb at strong reducing conditions. Thus the nature of the solid solution relation for the olivine series at high pressures does not seem to differ appreciably from that at atmospheric condition.

Gabbro

Run data for the melting of gabbro are listed in Table XI. Melting of a complex substance like gabbro is not a simple transformation of a solid into a liquid. It occurs over a range of temperatures and it is gradual. Some of the components, like the feldspars, may melt first as individual minerals or eutectically. Others, like the pyroxenes and olivines, may melt next as individual minerals, or eutectically, or they may dissolve in the feldspar melt below their own melting temperatures. The criteria for recognizing melting after the temperature quench is a problem by itself, since several characteristics can develop in the sample

during the process. The application of pressure to a core sample may crush the granules into fine grain, uniform-looking material. This pulverization depends on the mechanical characteristics of the sample and the applied pressure and involves no melting. At elevated temperature below the melting range, recrystallization can take place in the solid state. The recrystals are coarser grained than the original crystals and distinctly different (Figure 26) but they should not be taken as a criterion for melting. Three criteria were used to recognize evidence of melting in the quench product, the presence of glass, vesiculation (Figure 27) and the presence of needle-like quench crystals (Figure 28). The glass forms when a molten rock is quenched since the kinetics of recrystallization are too slow to allow orderly arrangement of crystals. The needle-like crystals form out of the same melt but at higher temperatures or pressures. Their maximum length is approximately 600 microns and their width approximately 15 microns. Vesiculation forms at one atmosphere pressure when trapped gases in quenched magma support the structure of the cavity in which trapped. The vesicles range in diameter from several microns up to 375 microns. It is conceivable that their upper limit is controlled primarily by the dimensions of the sample.

Liquid gabbro can be quenched to vesicular matter over the entire range of melting at 1 atm pressure. Above 1 atm and below approximately 25 kb (25,000 atm) there are three temperature regions (Figure 29): one, where liquid gabbro quenched into glass coexists with original unaltered crystals; two, at higher temperatures the glass coexists with recrystallized material forming a vitrophyric porphyry; three, at still higher temperatures only the glass exists as obsidian. Above 25 kb, the region of glass and unaltered crystals does not exist; the vitrophyric porphyry changes into quench crystals with recrystallized original crystals forming a porphyry; and the obsidian glass gives way to quench crystals, forming basalt.

A qualitative reconfirmation of the existence of these temperature and pressure regions can be observed in the analyses of those capsules which display a thermal gradient. For example, sample number 123 (Table 6) was run at 30 kb with the thermocouple recording 1450°C at the hot end where the original crystalline material had all transformed into glass. On the "cold" end the temperature is not known, however, the presence of relics of the original crystals indicates a temperature lower than 1360°C (Figure 29). Between the ends, the analysis shows quench crystals. Examination of areas in Figure 29 which are intersected by a line at 20 kb extending from 1450°C to 1360°C, suggests that sample 123 should contain: glass, quench crystals, recrystals or more glass, and original crystals. Another example is sample 129 (Table 6) which was run at 40 kb with the thermocouple recording 1550°C at the hot end where the original crystalline material had all transformed into quench crystals. The transition towards the cold end in this sample is first into recrystals and second into original crystals, with no glass at all. This is in agreement with what would be indicated by examination of Figure 29.

Normally, when conducting experiments at high-temperature-high-pressure, one should expect the capsule material to participate in the reaction and contaminate the sample, causing a change in its melting behavior. Contamination was expected more in the use of boron nitride capsules than in the use of platinum capsules because for the large scale manufacturing of boron nitride, the process requires boric oxide, calcium phosphate, water, ammonia and other compounds (Ingles and Popper, 1960). As a result, the end product "pure" boron nitride has a binder of boric acid ($B_2O_3 \cdot H_2O$) of 3 to 5 wt % (Hsu, 1967). Thus "fluxing effect" may be caused by boron nitride. However, in comparing the data obtained from the platinum capsules with that obtained from the boron nitride capsules, it was not possible to isolate the suggested effect of the latter.

The melting range constructed from the data in Table 6 is shown in Figure 29 as the area between the solidus and the liquidus curves. At 1 atm this range spans over 275°C from 1095°C up to 1370°C. At 45 kb the range is only 65° C, from 1445°C to 1510°C. These curves approach straight lines defined by the equations, $T_{solidus} = 1095 + 7.82P$ and $T_{liquidus} = 1370 + 3.06P$, where T is temperature in degree Celcius and P is presure in kilobars. Extrapolating the solidus and liquidus to higher pressures, the two curves join at 58 kb and 1550°C forming a single melting curve. The only indication of the expected plagioclase high pressure transformation (Green and Lambert, 1965) is the presence of garnet in two samples (Table 6).

Although a melting point of a rock like gabbro does not exist in the true physico-chemical sense, a melting range can be defined and delineated with a solidus and a liquidus curves. The processes that take place between these two curves at elevated temperatures and pressures are multiple and complicated. However, below the solidus, the rock complex is a true solid and above the liquidus it is a true liquid. The type of rock that will be generated by quenching is determined by the genetic state of the system prior to quenching.

TABLE XI

GENETIC STATE DATA FOR GABBRO FROM QUEBEC

Run	Sample	Capsule	P, kb	T, °C	Time, sec	Comments
148	powder	Pt	0.001	1100	60	Unaltered crystal, trace of glass
149	powder	Pt	0.001	1200	60	Glass relic crystals; vesicular
150	powder	Pt	0.001	1300	60	Glass, trace of re-crystals
133	powder	Pt	0.001-2	1370	60	Glass, relic crystals
266 top	core	BN	10	1100	300	Original crystals
266 bot	core	BN	11	1310	300	Glass, relic crystals
265 top	core	BN	11	1185	300	Mixed glass and original crystals
265 bot	core	BN	11	1210	300	Glass around original crystals
143	powder	Pt	10	1200	50	Mixed glass and original crystals
277	core	BN	10	1250	90	Glassy periphery around original crystals
262	core	BN	10	1290	300	Glass
274 top	core	BN	10	1295	300	Glass and relic crystals
274 bot	core	BN	10	1410	300	Glass (quench crystals between top and bottom)
264	core	BN	10	1333	300	Glass, + relic crystals
270	core	BN	10	1350	300	Glass + relic (less glass toward cold end)
142	powder	Pt	10	1370	90	Glass + re-crystals
269 top	core	BN	10	1375	300	Glass
269 bot	core	BN	10	1500	300	Glass
272	core	BN	10	1525	210	Glass
152 top	core	BN	16½	1393	300	Glass (relic crystals away from hot end)
152 bot	core	BN	16½	1455	300	Glass
111	powder	Pt	20	1345	540	Glass; re-crystals
132	powder	Pt	20	1395	45	Glass; re-crystals
136	powder	Pt	20	1430	19	Quench crystals, glass + re-crystals
123	powder	Pt	20	1450	7	Glass (toward cold end: quench crystals, glass, relic crystals)
141	powder	Pt	32	1430	45	Quench crystals, recrystals
126	powder	Pt	30	1470	60	Quench crystals
125	powder	Pt	30	1475	53	Quench crystals (relic crystals toward cold end)
137	powder	Pt	35	1480	25	Quench crystals (relic crystals toward cold end)
134	powder	Pt	40	1350	~ 1	Original crystals
128	powder	Pt	40	1430	~ 1	Quench crystals transition into re-crystals. Garnet
138	powder	Pt	40	1480	16	Quench crystals (+ recrystals?)
129	powder	Pt	40	1550	79	Quench crystals (recrystals and relic crystals on cold end)
151 top	core	BN	48	1280	10	Original crystals
151 bot	core	BN	48	1350	10	Original crystals
130	powder	Pt	45	1430	63	Original crystals. Garnet(?)
147	powder	Pt	45	1500	38	Quench crystals in matrix of re-crystals
131	powder	Pt	45	1590	3.5	Quench crystals (Original crystals on cold end)
GA1-7	core	BN	1	900	1	Original crystals
GA2-7	core	BN	1	900	2	Original crystals
GA3-7	core	BN	1	900	6	25% glass, balance original crystals
GA4-7	core	BN	1	900	24	25% glass, balance original crystals
GA5-7	core	BN	1	900	48	25% glass, with vesicles around periphery, balance original crystals
GA6-7	core	BN	1	900	132	Glass, relic crystals
GA1-7	core	Pyrophyllite	1	900	1	Original crystals
GA1-7b	core	Pyrophyllite	1	900	1	Original crystals, 15% vesicles, 50% glass
GA1-7c	core	Pyrophyllite	1	900	1	100% glass along the pyrophyllite several vesicles
GA2-7	core	Pyrophyllite	1	900	2	Original crystals
GA3-7	core	Pyrophyllite	1	900	6	Glass, several vesicles
GA4-7	core	Pyrophyllite	1	900	24	Original crystals
GA5-7	core	Pyrophyllite	1	900	48	Original crystals
GA6-7	core	Pyrophyllite	0	900	132	Original crystals

TABLE XI (Cont)

GENETIC STATE DATA FOR GABBRO FROM QUEBEC

Run	Sample	Capsule	P, kb	T, °C	Time, sec	Comments
GA1-1	core	BN	1	1000	0.5	25% glass, rest original crystals
GA1-2	core	BN	1	1000	0.5	25% glass, rest original crystals
GA2-1	core	BN	1	1000	2	Glass, relic crystals
GA2-2	core	BN	1	1000	2	Glass, relic crystals
GA3-1	core	BN	1	1000	6	Glass, glass psuedomorphs of feldspar, vesicular filled with glass, relic crystals
GA3-2	core	BN	1	1000	6	Glass, glass psuedomorphs of feldspar, vesicular filled with glass, relic crystals
GA4-1	core	BN	1	1000	24	Glass
GA4-2	core	BN	1	1000	24	Glass
GA5-1	core	BN	1	1000	132	Glass, 25% quench crystal needles
GA5-2	core	BN	1	1000	132	Glass, 25% quench crystal needles
GA1-1	core	Pt	1	1000	0.5	Lost sample
GA1-2	core	Pt	1	1000	0.5	Original crystals
GA2-1	core	Pt	1	1000	2	Original crystals, took shape of capsule
GA2-2	core	Pt	1	1000	2	Original crystals, took shape of capsule
GA3-1	core	Pt	1	1000	6	Lost sample
GA3-2	core	Pt	1	1000	6	Original crystals
GA4-1	core	Pt	1	1000	24	Lost sample
GA4-2	core	Pt	1	1000	24	Traces of glass
GA5-1	core	Pt	1	1000	132	Lost sample
GA5-2	core	Pt	1	1000	132	Traces of glass
GA1-3	core	BN	1	1100	0.5	50% glass, original crystals large, 5% vesicles, relic crystals
GA2-3	core	BN	1	1100	2	Climbed out of the capsule (vesicle & relic - repeat)
GA3-3	core	BN	1	1100	6	Rough glass, peripheral vesicles
GA4-3	core	BN	1	1100	24	Glass, vesicles 25%
GA5-3	core	BN	1	1100	132	Glass, few vesicles on periphery, 50% quench crystal needles
GA1-3	core	Pt	1	1100	0.5	Rough glass, 5% vesicles?
GA2-3	core	Pt	1	1100	2	Top and bottom missing, middle original crystals
GA3-3	core	Pt	1	1100	6	Top and bottom missing, middle original crystals
GA4-3	core	Pt	1	1100	24	Glass, relic crystals, 1 or 2 vesicles
GA5-3	core	Pt	1	1100	132	Glass, relic crystals
GA1-6a	core	BN	1	1200	2	Glass, no relics, 2 to 3 vesicles along edges
GA2-6b	core	BN	1	1200	2	Rough glass, no relics, 20 to 30 vesicles
GA3-6a	core	BN	1	1200	6	Rough glass, 25% vesicles
GA3-6b	core	BN	1	1200	5	Rough glass, 25% vesicles
GA4-6a	core	BN	1	1200	24	Rough glass, a few vesicles
GA4-6b	core	BN	1	1200	24	Rough glass, 25% vesicles, 50% quench crystal needles
GA5-6a	core	BN	1	1200	48	Glass, 75% quench crystal needles, no vesicles
GA5-6b	core	BN	1	1200	48	Glass, 75% quench crystal needles, no vesicles
GA6-6a	core	BN	1	1200	132	Glass, 75% quench crystal needles
GA6-6b	core	BN	1	1200	132	Glass, 75% quench needles, several vesicles
GA2-6c	core	Pyrophyllite	1	1200	2	Glass, 2-3 vesicles, relic crystals
GA2-6d	core	Pyrophyllite	1	1200	2	Glass, 2-3 vesicles, relic crystals
GA3-6c	core	Pyrophyllite	1	1200	5	Rough glass, no vesicles
GA3-6d	core	Pyrophyllite	1	1200	6	Rough glass, no vesicles
GA4-6c	core	Pyrophyllite	1	1200	24	Glass, long prismatic quench crystals along pyrophyllite
GA5-6d	core	Pyrophyllite	1	1200	24	Glass and rough glass, long prismatic quench crystals along pyrophyllite
GA5-6c	core	Pyrophyllite	1	1200	48	Glass, long prismatic quench crystals along pyrophyllite
GA5-6d	core	Pyrophyllite	1	1200	48	Glass, long prismatic quench crystals along pyrophyllite

Hokook, Giva'at Hamoreh and Hazor Basalts

Run data for the melting of Hokook, Giva'at Hamoreh and Hazor basalts are listed in Table XII. The complexity of silicate rock oxide systems makes it difficult to analyze the involved processes quantitatively; therefore, a descriptive treatment is required. The descriptive terms define eight sets of rocks. Each set represents all the igneous rocks that can achieve a certain definite genetic state when heat treated. Several of these sets may be null under certain conditions of composition, pressure and temperature; however, the order of genesis of the sets remains unchanged. The null position of these particular sets is by itself a characteristic of certain genetic states. The eight genetic states were selected on the basis of a hypothetical succession of events experienced by a complex metal silicate oxide during a prolonged heat treatment. This succession can be described as follows: Beginning with the ORIGINAL rock, the complex oxides gradually melt until the substance is 50% MELT. As the melting proceeds, a point is reached where only 5 or 10% RELICS are left of the original. The melt may then begin to degas leading to the formation of 50% VESICULAR state and then as degassing continues, establishing the VESICULAR state. It is possible that the original rock will begin degassing as soon as it starts melting. Under such circumstances, the "50% melt" and "relics" states will be skipped and the original rock will transform directly into the "50% vesicular" state. If the degassing is completed while the rock is still molten, the cooled product may be GLASSY with no vesicles left in it. If crystallization sets in, the product may be 50% CRYSTALLIZED; when crystallization has ceased, the product may be completely CRYSTALLIZED.

The above treatment represents a frame of reference which enables us both to treat nonnumerical data in a seminumerical way and to plot genetic diagrams showing the pressure, temperature and/or

TABLE XII

GENETIC STATE DATA FOR BASALT FROM ISRAEL

All samples are core; capsules are BN; pressure is 1 ATM

Run	T, °C	Time, hrs	Comments
AZ67-8	900	1	Original crystals
AZ67-9	900	2	Original crystals + 5% glass
AZ67-10	900	6	Original crystals + 25% glass
AZ67-11	900	24	50% original crystals, 50% glass, around periphery glass is vesicular
AZ67-12	900	48	25% original crystals, 75% vesicular glass
AZ67-13	900	72	Relic crystals, vesicular glass
AZ67-1	1000	1	25% glass (plagioclase?), several vesicles
AZ67-2	1000	2	50% glass, several vesicles
AZ67-3	1000	6	50% glass (molten rim), vesicles along rim, original crystals core
AZ67-4	1000	24	75% glass, 2 to 3 vesicles
AZ67-4b	1000	24	(same spl as AZ67-4, but taken from material spilled over the pyrophyllite holding the BN) 95% glass, 1 to 2 vesicles, 5% quench crystals
AZ67-5	1000	48	90% glass, 10% quench crystals
AZ67-6	1000	72	50% quench crystals, relic crystals 5%, 12 vesicles, glass matrix
AZ67-26	1100	1	25% glass, 75% original crystals, few vesicles on periphery
AZ67-27	1100	2	Melted to a kidney, stayed in BN 75% glass, peripheral vesicles
AZ67-28	1100	6	All glass and 10% vesicles, sample floved out of BN on top of pyrophyllite
AZ67-29	1100	24	Melted to a globule, 75% quartz crystals, no vesicles, BN partly dissolved, sample run on pyrophyllite
AZ67-30	1100	48	90% quartz crystals, balance glass, no vesicles, most of BN dissolved, sample run on pyrophyllite
AZ67-31	1100	72	90% quartz crystals, no vesicles
AZ67-68	1200	1	Vesicular (in glassy matrix)
AZ67-69	1200	2	50% vesicular in glassy matrix
AZ67-70	1200	6	Glassy
AZ67-71	1200	24	95% crystalline
AZ67-72	1200	48	95% crystalline
AZ67-73	1200	72	95% crystalline, smaller needles than AZ67-71 and 72.
AZ67-44	900	1	Original vesicles vanished, 5% glass, mostly original crystals
AZ67-45	900	2	Original vesicles vanished, 5% glass, mostly original crystals
AZ67-46	900	6	25% glass, balance original crystals
AZ67-47	900	24	25% new vesicles in glass, relics 75%
AZ67-48	900	48	50% new vesicles in glass, relics 50%, trace of new crystallization
AZ67-49	900	72	50% vesicles, 50% glass, trace of new crystallization
AZ67-47A	900	24	Original vesicles vanished, 5% glass, mostly original crystals
AZ67-38	1000	1	No change. Original vesicles
AZ67-39	1000	2	10% glass around periphery. Original vesicles disappeared
AZ67-40	1000	6	50% glass, 50% original crystals, 2 to 3 small vesicles
AZ67-41	1000	24	Vesicular in glass ground mass
AZ67-42	1000	48	25% recrystallization in glass, 25% vesicles
AZ67-43	1000	72	50% recrystallization, 15% vesicles
AZ67-14	1100	1	50% glass, 50% original crystals, the glass has irregular and ropey structure
AZ67-15	1100	2	75% smooth glass, 25% relic
AZ67-16	1100	6	Glass, smooth, no vesicles
AZ67-17	1100	24	25% new crystals
AZ67-18	1100	48	95% new crystals
AZ67-19	1100	72	95% new crystals
AZ67-62	1200	1	All glass, 2 to 3 vesicles
AZ67-63	1200	2	Glass, 25 to 50% vesicles
AZ67-64	1200	6	Glass, 5% vesicles, 10% new crystals
AZ67-65	1200	24	95% new crystals
AZ67-66	1200	48	95% new crystals
AZ67-67	1200	72	95% new crystals
AZ67-65A	1200	24	All glass. (This is material which stayed in the hole and may have been less hard)
AZ67-32	1000	1	Original minerals
AZ67-33	1000	2	75% original - 25% plus 3 to 4 vesicles
AZ67-34	1000	6	50% original, 50% glass, no vesicles
AZ67-35	1000	24	Relics 10 to 15%, glass plus 30% vesicles
AZ67-36	1000	48	Relics, vesicular 90%
AZ67-37	1000	72	Glass and relic, no vesicles
AZ67-20	1100	1	50% glass, 50% original crystals
AZ67-21	1100	2	One large vesicle, periphery: vesicular glass
AZ67-22	1100	6	Brown glass, several vesicles
AZ67-23	1100	24	50% crystalline, small needles in glass matrix
AZ67-24	1100	48	75% or more recrystallized; small needles
AZ67-25	1100	72	95% or more recrystallized; needles 2 or 3 times larger than AZ67-24
AZ67-56	1200	1	All glass, 2 to 3 vesicles on periphery
AZ67-57	1200	2	All glass, 2 to 3 vesicles on periphery
AZ67-58	1200	6	New crystals
AZ67-59	1200	24	New crystals — Size of crystals increase from AZ67-58 to AZ67-61. Brightness of slide suggests increase in percent from 30 to 95%.
AZ67-60	1200	48	New crystals
AZ67-61	1200	72	New crystals 95% larger than AZ67-58

time dependence of several sets of genetic states. For example, Figure 30 shows the genetic state of basalt from Hokook, Israel as a function of temperature. Each one of the seven curves displayed in this figure represents a different length of time for which the temperature of the furnace was held at the indicated temperatures. The results show that as the temperature rises from 900°C to 1100°C, the genetic states develop in the direction A to H, and the same direction A to H is held when the time maintained at any temperature is increaed from 1 hour to 75 hours. All the curves have slopes of the same sign, and no portion of any curve reverses its sign, which proves that the successive order of listing the genetic states from A to H is valid, at least for this basalt. It is obvious that the curves should bundle and merge at two temperatures. One temperature is at the solidus point, and the other temperature is above the liquidus point. The minimum and maximum temperature points at which the time curves intersect the "glassy" line (940°C - 1215°C) represent the melting range for this basalt.

Figure 30 is based on semiquantitative analysis; nevertheless, it can be used to derive valuable information regarding the Hokook basalt. Out of the four variables that control the genetic state of a rock two were fixed. Composition was fixed by using only the above basalt, and pressure was fixed by conducting all the experiments in a Lindberg furnace at one atmosphere pressure. The two free variables were, time (or the duration of exposure to heat) and heat (or the temperature maintained for the duration of exposure of the sample before quenching). Thus, the genetic conditions of the samples were made similar to certain volcanic conditions, so that the rock products of the experiments can be correlated with natural volcanic rocks, with the distinct advantage of knowing the temperature-time conditions under which they wer formed. Six time lines display the events that can take place between 1 hour duration of heating and 72 hours.

Observing that the genetic states A through H in the Hokook basalt develop substanially in the quenched sample after heat treatment of between 1 and 72 hours, it is assumed for the purpose of analysis that these time limits describe an envelope within which the total volcanic history of the rock takes place. If the temperature is fixed, for example, at 1100°C the rock will not melt immediately to any substantial degree. At 1 hour, it may be only 25% molten; at 2 hours it will be 75% molten; at approximately 4 hours degassing will cause a vesicular texture in the rock; between 5 and 10 hours the escaping gases would leave the rock and the vesicles collapse leaving a uniform glassy rock; the escape of the entrapped and dissolved gases make the system more viscous to a point where at 15 hours crystallization can take about 50% of the sample; by 72 hours crystallization will engulf the bulk of the sample.

If a definite product is desired, for example, a vesicular rock, then a set of temperature-time combination can be outlined to satisfy this requirement.

At 1200°C, the rock can be heated for no longer than one hour to develop the proper vesiculation, or the degassing will result in a glassy product; at 1080°C the rock should be heated for 5 hours to obtain the desired texture; at 900°C it requires 72 hours of heating to obtain the same; below 900°C, the solidus temperature is crossed and no melting will take place at all.

From a geologic point of view the above analysis can be used to establish a "rock thermometer" data for the Hokook basalt. Three genetic states A, B and C, represent the melting temperatures of the rock from initial melting to almost complete melting where only relics of the original crystals remained. The corresponding melting temperatures are from 840°C to 1180°C. Estimates of the temperatures of origin of a vesicular, glassy or crystalline rocks depend on estimates of time or duration of heating. For

example, a crystalline sample from the Hokook basalt collected from a lava flow is assumed to have had more than 72 hours heating prior to extrusion; hence, the temperature of the magma could have been as low as 1130°C.

A similar analysis to that of the Hokook basalt is repeated for the Giva'at Hamoreh basalt (Figure 31) assuming the same time envelope of 1 hour to 72 hours. The premise is that the dissimilarities reflect the peculiar composition of each basalt, whereas the similarities reflect the group properties of many basalts.

If the temperature is fixed, as above, at 1100°C, then at 1 hour the rock will be 50% molten; at 2 hours it will be completely molten and almost 100% vesicular; at 4 hours degassing would be followed by collapse of vesicles leaving an almost uniform glassy rock; between 5 and 10 hours the escape of gases will make the system more viscous and crystallization will begin to take place; at 15 hours crystallization will reach 50%, the same as for the Hokook basalt; and by 72 hours crystallization will engulf the bulk of the sample, the same as for the Hokook basalt.

It seems logical that the two basalts would tend to be more similar to each other in behavior at the higher temperatures (1100°C to 1200°C) and longer time (15 hours to 72 hours) since each rock has had a chance to melt into a uniform magma. If a definite product is desired to be made of the Giva'at Hamoreh basalt, a set of temperature-time combination can be outlined to satisfy the requirement in the same way discussed above for the Hokook basalt. Also, "rock thermometer" data can be established for this basalt too.

A similar analysis to that of the above two basalts was conducted for the Hazor basalt (Figure 32). It can be seen that the genetic events for this rock occur primarily within the same time and temperature envelope as the above.

SOME ROCK FORMING PROCESSES AT HIGH PRESSURES AND TEMPERATURES

Rock forming processes in nature takes place in open large systems, as indicated in the introduction, which may involve a mountain or a mountain range and where several reactions may take place simultaneously and yet be geographically remote from each other, thus resulting in a mosaic equilibrium in the system or a mosaic of nonequilibrium subsystems. Nevertheless, it is possible and common in the geologic realm that such a complex system with its range of compositions and textures would fit into a category of a specific rock, for example: obsidian, basalt, gabbro, or: porphyry, vitrophyric porphyry. Figure 24 displays a system of that complex nature. Superimposed on the phase diagram illustrating the solidus and liquidus curves in Figure 24 it was necessary to show additional curves separating between states of the system which quench into distinct rocks. These states can be referred to as genetic states, and the figure as a genetic diagram. The genetic diagram displayed in Figure 24 shows several temperature-pressure areas where the rock used as an initial sample would quench into new rocks.

A significant resemblance in chemical and mineralogical composition is observed between an average terrestrial peridotite and a chondritic meteorite, e.g., the Bruderheim meteorite. This observation is supported by a comparable similarity in petrological textures. The meteorite differs, however, from peridotite in possessing the following: (1) a higher ratio of Fe oxides to the sum of Al and Si oxides, (2) metallic iron and nickel, (3) chondrules and chondritic textures, and (4) troilite (FeS) rather than pyrite (FeS_2) which contains less iron. Although both rocks fundamentally igneous in nature, the possibility of their having an identical genesis is remote. To assume the melting range of a typical peridotite as an indication of the temperatures of origin that existed in the body from which the Bruderheim meteorite was detached may possibly be erroneous. Experimental observations

of melting temperatures for the Bruderheim metecrite as a function of pressure up to 40 kb indicate that melting occurs at several hundred degrees Centigrade below the melting of the equivalent pure olivines and pyroxenes (if they are assumed to be in equilibrium within a closed system). It has also been determined that under certain pressure-temperature conditions most of the olivines will disappear from the solid state before the pyroxenes. This is the reverse of what has been observed in a simple FeO-MgO-SiO_2 system.

The process of olivine and pyroxene disappearance during pressurization and heating is obviously not a simple melting. This suggests that the known meteorite composition may very well be only a portion of a more complex system whose character and identity is not yet known and is hence one of the puzzling problems of planetary exploration.

CASTING, FORMING, SINTERING AND PULLING OF ROCKS

As shown in the previous sections of this report, each of the silicate rocks which was examined does have its own characteristics, but many other characteristics are common to all the silicates. The genetic diagram prepared for each specific rock supplies the most elementary information necessary for planning casting, forming, sintering and fiber pulling of the rock. Figure 33 shows the result of bending a straight basalt bar into a circle at a temperature below the melting of the rock (Figure 34). The same figure shows also two forms cast of obsidian at one atmosphere pressure but at two different time-temperature combinations. Basalt fibers (glassy) were pulled off a viscous mass of basalt at several temperatures. It remains now to determine the specific properties required of these rock products and the economic value of producing them

The following is taken from Kopecky (1959), and from a summary by Dr. J. Green (1962) of his conversation with Dr. L. Kopecky during the former's visit to the cast basalt industry in Czechoslovakia in 1960. This is supplemented by the author's personal communication with Dr. L. Kopecky during the Lunar Geological Field Conference, Bend, Oregon in 1965.

Early work in France was based on the substituting melted basalt for glass and was not directed toward improving the product over the raw material. The Germans advanced another step by evolving the technology for recrystallizing the melt and casting it into simple shapes. The Soviet Union began experimentation with basalt in the 1930's, but was obliged to work with diabase, which is more difficult to cast because of its higher viscosity. More recently, work has been intensified at the Moscow Rock Foundry Works. A current development phase in the manufacture of cast basalt is operating in Czechoslovakia and Poland. Czechoslovak Ceramics distributes the products mostly to Sweden and England.

Many basic patents are held by Mr. H. L. Watson of the now dissolved Compagnie Generale du Basalte in France.

From laboratory studies and operational experience, the basalt should contain as much pyroxene as possible over 60% because this mineral imparts to the recrystallized mass such desirable qualities as resistance to abrasion, mechanical strength and chemical resistivity. The presence of magnetite and olivine is also important because these two minerals induce crystallization. However, the magnetite-olivine concentration should not exceed 10%. If it did, the SiO_2 content would be reduced, leading to the formulation of larger crystals and this, in turn, would tend to promote bursting on annealing.

Another reason why too much olivine is undesirable is its high melting point. Olivine, which is difficult to melt, would not dissolve in the short time available for melting, particularly if it were in large crystals. Feldspars influence the viscosity and regulate the rate of crystallization when present in optimum proportions. Nepheline and plagioclase should be present in a ratio of between 1:1 and 1:3, with a total content of about 20% (Voldan, 1956, p 53).

In addition, the material must be fine-grained, homogeneous, unweathered, nonporphyritic and uncontaminated. A melting temperature range of 1200°C to 1300°C must be associated with a relatively low viscosity (10^2 to 10^3 poises) for it to cast well. The casts must recrystallize easily in a fine-grained state and not crack after cooling.

The melting data obtained in the laboratory were applied to manufacturing operations. Raw material, 8 to 15 mesh basalt, was swelted at 1300°C to 1350°C in shaft furnaces similar to the open-hearth processing of steel; the molten material then was conducted into a homogenizer where, at carefully controlled temperatures and slightly reduced pressures, the melt began to

crystallize. The carting process following this was similar to conventional metallurgical processing except for differences imposed by the greater viscosity and cooling rates.

Static casting in the sand molds originally employed produced castings with rough surfaces having wide tolerances. Metal molds now supplant sand molds and are currently used in the production of tiles, plates and fittings. Recently, centrifugal casting of basalt in metal molds at speeds of 900 rpm has resulted in a product of superior quality. Pipes, milling balls and other materials of high density are made by centrifugal casting techniques.

Lehr or chamber furnaces are used to cool the castings from 800°C to room temperature over a 24 hour period. Careful control of temperature reduction is required to prevent bursting and other imperfections on annealing.

Most of the castings weigh between 3 and 80 kg (6.5 and 175 lb). The largest casting, representing the limit of present equipment, weighs 300 kg (660 lb); the smallest cast product, a 60mm diameter ball, weighs 0.34 kg. Tiles are usually made in thicknesses of 25 to 40 mm, and pipes are made with walls of 15 to 20 mm, to a maximum of 50 mm. The lower limit of thickness is determined by the rate of heat loss and danger of vitreous solidification.

The sintering process is similar to that used in power metallurgy. The basalt frit made from molten material is finely ground (1600 mesh), impregnated with a plasticizer, shaped under a pressure of 1000 kg per square centimeter (14,200 psi) and sintered in electric furnaces at 1120°C to 1140°C (2048°F to 2084°F). Sintered basalt is valuable in the manufacture of small articles such as nozzles, wire-drawing dies, spheres and special fabrications.

Fibres or basalt wool are produced by processes similar to those used for producing certain kinds of glass fibers. The thickness of the fibers ranges from 15 to 25 microns. This is thinner than

Pele's hair, a naturally occurring basalt wool which, at Kilauea, ranges from 25 to 200 microns and, for 80 measurements, averages 60 microns. Artificial basalt wool is used as a filler in asbestos-cement manufacture and for acoustic and thermal insulation.

ROCKS IN LUNAR LOGISTICS

The geologic aspect of lunar logistics is recognized as the utilization of the lunar natural resources (whatever they may be) for support of man's activities on the moon. This utilization may take four forms: (1) direct use of raw material as it is found on the surface of the moon, (2) direct use of raw material after processing, (3) use of information derived from surface material to determine the location of buried economic minerals, and (4) use of information derived from surface material to determine the geologic environmental history and to predict future environments. The importance of understanding the petrologic properties increases in the above order from direct use to the prediction of environments. Increased sophistication in the demand for specific minerals, which will no doubt follow the initial exploration of the moon, will increase the demand for understanding the petrologic processes even more.

We have accepted the general premise that the moon is within the group of "terrestrial planets", thus implying that it is made of igneous rocks, primarily silicates (Azmon, 1962). We also maintain that the typical atmospheric-hydrospheric minerals will be scarce or lacking in the lunar environment. Hence, our efforts are concentrated on the understanding of petrologic processes in igneous rocks, with an elaboration on processes that might be favored on the moon.

Igneous rocks are essentially aggregates of mineral grains which have solidified from molten magma into a single rock. The characteristic properties of the rock are bulk properties whose net effect is determined by the combination of the individual properties of the component minerals. Although these bulk properties may not be similar to the physical properties of the components, they are nevertheless characteristic of the rock. They can be defined in descriptive terms, and they can represent a set of igneous rocks which have reached a certain genetic state.

The genetic state of many rocks is not necessarily an equilibrium or steady state. It is attained even in a large system, such as a mountain or a portion of a continent, where it is possible for one end of the system to be far enough physically from the other end to appear independent. It is also attained in an open system, where a true equilibrium may never be reached because there is a continuous incorporation of rock material into the system. More surprising, however, is the fact that such a heterogeneous reaction may still achieve a distinct genetic state and result in a rock-type end product. Even more extraordinary is the fact that, in spite of the complex combination of variables required to obtain a genetic state, such combinations are found repeated geographically around the earth and stratigraphically down the geologic column. The complex combination of parameters and events that leads to the culmination of a genetic state appears to be too systematic to be accidental. One must admit that, although the parameters and events are governed by a multitude of known thermodynamic and kinetic processes, their interactions appear to be governed by unknown universal rules.

Four groups of variables go into the establishment of the bulk properties, namely, composition, temperature, pressure, and history (Azmon, 1965). The composition may vary with respect to essential minerals, accessory minerals, and minor constituents. The temperature may vary with respect to the rate of heating, power level, duration of stay, and rate of cooling. The pressure may vary with respect to the rate of application (shock vs. gradual) and duration of stay. The history may vary with respect to the order of application of the above variables and to changes in the variables while a rock-forming process is in action.

The complexity of such rock-forming systems makes it extremely difficult to analyze the involved processes quantitatively;

therefore, a descriptive treatment is required. To illustrate this, descriptive terms which define 10 sets of rocks are given below. Each set represents all the igneous rocks than can achieve a certain, definite genetic state. Several of the sets may be null under certain conditions of composition, pressure, and temperature. The null position of these particular sets is by itself a characteristic of certain genetic states.

The 10 sets are as follows:

Original rock = K_1 = (a/all granular igneous rocks which suffer no metamorphism)

50% melt = K_2 = (b/all "a" which show 50% melting $\pm$ 10%)

Relic, original = K_3 = (c/all rocks which show relics of "a" with the bulk molten)

Vesicular = K_4 = (d/all "a" or "b" which develop vesicular structure (crystalline groundmass))

Scoriaceous = K_5 = (e/all "d" which develop scoriaceous structure (crystalline groundmass))

Pumiceous = K_6 = (f/all "c" which develop pumiceous structure (hyaline groundmass))

Glassy = K_7 = (g/all "a, b, c, d, e, f" which form glass)

50% Recrystallized = K_8 = (h/all "g" which show 50% recrystallization $\pm$ 10%)

Relic, glass = K_9 = (i/all rocks which show relics of "g" with the bulk recrystallized)

Complete recrystallized = K_{10} = (j/all rocks which show complete recrystallization)

It is important to note that, as in typical Cartesian arithmetic, Set K_{11} will be identical with Set K_1. In the geologic sense, this means that, unless we can establish the relative ages of the rocks, we cannot recognize the difference between K_1 and K_{11}.

The above discussion represents a frame of reference which enables us both to treat nonnumerical data in a seminumerical way and to plot genetic diagrams showing the temperature, pressure, and/or time dependence of several sets of genetic states. Figure 15, for example, shows the time dependence of 10 genetic states for two rocks, gabbro and tholeiitic basalt. The temperature and pressure for these genetic states were maintained fixed at 1000°C and one atmospheric pressure. A close examination of these data reveals the following:

1) During the first 10 hours, both rocks went through six genetic states, which began and concluded their volcanic history (States 4, 5, and 6).
2) In the following days, the histories of the two rocks departed from each other. The gabbro reached the glassy state (7) and rose asymtotically and imperceptibly towards the crystalline states (8, 9, 10). The basalt reached the crystalline state (9), and from there it rose asymtotically to State 10.

In order to evaluate these data in terms of the forms of utilization discussed above, we can do one of two things: (1) use information of the type shown here to select the proper heat treatment needed to develop a desired genetic state, or (2) map observed petrologic features in the field and infer from the map the direction of shorter heat duration, which may also be the direction of the source of the rock. Obviously, this curve is only one example of the genetic states of two rocks at a specific temperature. To complete the picture, we then must consider similar curves for these rocks at other possible conditions.

Figure 35 shows a typical genetic diagram for gabbro (compare with Figure 29) where the pressure and temperature of formation of the 10 genetic states were plotted and then contoured. We

can derive the following information from this diagram:

a) Gabbro has a melting range of about 250°C (1000° to 1250°C) at one atmosphere.
b) As this range rises in temperature with increased pressure, it also narrows to about 50°C.
c) The peculiar shape of the upper curve may be related to the behavior of anorthite under pressure; that is, the melting point falls with rising pressure up to about 33 kb (Boyd, 1962).
d) Above the melting range, the quench product is either glassy or microcrystalline. It seems as if both the glassy material and the crystalline material can be recognized on the genesis diagram as two distinct genetic states (comparable to two phases in a typical phase diagram).
e) Line 9 represents a temperature region above which the quench product is never crystalline, always glassy. It also represents a pressure region beyond which the quench product is always crystalline regardless of the temperature.

Just as in Figure 15, these data permit evaluation in terms of the forms of utilization: (1) An optimum heat and pressure combination can be selected to develop a product of a certain genetic state; (2) a field map of observed features will probably be of the same nature as Figure 35; hence, it will indicate the direction of the source of high temperature and/or high pressure.

A striking example of the good correlation between the physical parameters (the variables) that define a genetic state and the recognized petrologic characteristics of the rock can be seen in Figure 36 which displays four photomicrographs of heat-treated basalt. Figure 36-1 shows the rock after a 2-hour heat treatment.

No change from the original crystalline rock could be observed under the petrographic microscope. Figure 36-2 shows the rock after a 6-hour heat treatment. The rock developed typical volcanic scoriaceous characteristics. (We are using the term scoriaceous to mean not only higher-percentage cavities than in a typical vesicular rock, but also partial conversion of the crystalline material into glass. If all the crystalline material around the cavities converted to glass, the rock would classify as pumiceous.) At 24 hours (Figure 36-3), all the cavities had disappeared completely, thus practically concluding the typically volcanic genetic states, and some recrystallization is clearly evident. Last, at $5\frac{1}{2}$ days (Figure 36-4), crystallization proceeds to replace the glassy material. Again, as in the above discussion, the utilization may take a production form, whereby these data can be used to manufacture rock of any of the above properties. Or, if used for field mapping, samples may be collected on a grid, as shown in Figure 37. (Elgin and Azmon, 1964), and examined in the laboratory for indicators of the genetic states.

We can see in the above examples how two parallel benefits can be derived from the knowledge of the processes and conditions under which various igneous rocks are formed. One is the ability to generate rock end products at will, and the other is the ability to determine the provenance of a natural rock. These benefits correspond, respectively, to (1) production of mineral concentrates of defined properties in desired shapes, and (2) means of exploration for source rock. Here, knowledge regarding two different aspects of economic geology is gained simultaneously through experiments designed to determine the processes that natural silicate mixtures must go through to generate specific rocks, and to define the four parameters controlling these processes: composition, temperature, pressure, and history. The parameters

which determine the genetic state of a rock can be obtained either by inferences drawn from the observed characteristics of the rock as found in its natural environment, or from laboratory determinations of the conditions that lead to its formation.

An understanding of these rules can lead to the two benefits mentioned above: (1) an ability to generate rock end products at will, and (2) an ability to determine the provenance of a natural rock.

TERRESTRIAL BENEFITS OF LUNAR RESEARCH

For more than six years Northrop Corporation and NASA OART have been supporting the study of complex rock materials under extreme pressures and temperatures, thus developing the technique and skill for handling and analysis of complex materials. The prime purpose of that study was to develop the basic knowledge needed for beneficial use of lunar rocks. Several results, which may have been incidental to that study, establish a better understanding of complex solids in three fields of terrestrial interests: (1) materials, or complex metal oxides; (2) high speed transportation, or reentry temperature systems; and (3) geophysics, or elastic wave propagation through rock media at elevated temperature and pressure. Each one of those fields will be discussed briefly in the following pages with an attempt to show the way in which the lunar study has yielded terrestrial byproduct of significance.

Complex Metal Oxides

With the prospects of landing man on the moon and the probability that the major raw material on the moon is one kind or another of common silicate rock, the need for common rock utilization came into focus. The new problem is not how to combine ceramic and metallic properties, but how to add some metallic properties to a common silicate rock. The products of such benefication could be a single phase, a multiphase, or composite of interlocking grains having properties not possessed by the original rock. A systematic study of the behavior and properties of common rocks under conditions of high pressure and temperature yielded much basic data which is needed to develop processes for melting, casting, heat treating, forming in the plastic state and sintering of rock powders. Figure 33 shows examples of two rocks cast into shape and one bent in the plastic state below the melting temperature of the rock.

The art of using natural rock material for production of useful utensils is one of the oldest human trades on earth. Beginning thousands of years ago with porous ceramics made from naturally occurring clay silicates, this art took a big jump forward as early as the seventh century A.D. with the invention of a dense white "china porcelain." The raw material for this new ceramic was primarily naturally occurring kaoline, feldspar, and quartz. When fired at high temperatures, this complex mixture formed a multiphase composite of crystals, glass and gas inclusions. It was not until after the beginning of the twentieth century that the next step forward was taken with the development of single phase sintered ceramics, made of pure oxides of metals such as aluminum, beryllium, hafnium, thorium and zirconium. These new products have high chemical and abrasion resistance, low density, and high refractory properties. In the past decade another step forward was taken to combine metal oxides with metal oxides or with their metals and develop end products having some properties of the constituents and some new properties of their own. The common, abundant and accessible raw material that was used for the earlier ceramics, gave way to more scarce material thus raising the price of the final products.

While considerable effort was invested by many laboratories to enhance the properties of metals and pure oxides, the naturally occurring common rock was gradually left behind as unsuitable for the requirements of modern metallurgy or ceramics. Current studies of beneficial uses of common rocks are directed toward the exploitation of the moon. One could however, outline beneficial terrestrial uses based on these studies. The following is a list of typical items that can be considered for manufacturing from common rocks for terrestrial use:

a) High temperature thermal insulators: flat plates and curved fixtures.
b) High temperature electrical insulators: flat plates and curved fixtures.

c) Wear resistant flat plates: chemical and mechanical abrasion.
d) Wear resistant conduits: chemical and mechanical abrasion.
e) Architectural surfaces: wall panels, floors, and table tops.
f) Ornamental objects: sculptures, bookends, etc.

In a sense, this is a ceramic line of products except for the "new" raw material, common-rock. The description of Kopecky and Voldan (1959) is an excellent example of the commercial utilization of common basalt rock products. It should be obvious to the reader that the beneficial use of rocks is by no way limited to lunar rocks and that new common rock complex ceramics may turn out to be just as useful on earth as on the moon.

Reentry Temperature Systems

One of the interesting characteristics of many rocks is that they retain in their texture and structure the evidence of the environments and processes to which they have been subjected. The temperature, pressure, and time history, and composition combine to give the rock its characteristics. A plutonic rock, for example, generated in the depths of the earth looks distinctly different from a volcanic rock of the same composition. In the same way a feldspar exposed to conditions exceeding 30 kb and 1400°C will develop garnets and kyanites which disclose the prevailing pressures and temperatures.

One of the problems studied in relation to lunar magma has been the correlation between the physical environmental conditions imposed on a variety of rocks, and the recognizable characteristics of the rock end-product. This requirement for correlation dictated the need to use a sample which is large enough for both x-ray and petrographic analyses to be conducted after exposure to the experimental conditions. Figure 38 shows a laboratory generated series of characteristics

induced by laboratory treatment of a basalt sample from Hokook, Israel, as function of temperature and of time sustained at that temperature. Of these three parameters, time, temperature, and induced characteristics, any two parameters approximate the third one. The characteristics of the rocks can thus be used as approximate indicators of the adjacent environmental conditions. The geologic interpretations of the history of the earth are partly based on such clues to the paleo-environments. Experiments such as those conducted on the Hokook basalt were repeated on a whole range of silicate rocks and similar experiments were conducted at elevated pressures. The correlation of the petrographic characteristics of the end products with the experimental conditions is being cataloged with the anticipation that as lunar rocks will be examined, their genetic history will be reconstructed on the basis of the acquired data.

This type of analysis can be applied to the study of meteorites and to the study of the reentry of bodies into the earth's atmosphere. A thorough understanding of the physical and chemical changes that occur during the entry of a body into the atmosphere requires data on the preentry size of the body, its precise path through the atmosphere versus time, the effect of the atmospheric composition on the hot body, and the time-temperature-composition correlation with the physical and chemical changes that take place during deceleration. Some reentry data should be obtained by using crystalline silicate rocks as artificial meteorites where every crystal that survives ablation can be utilized as a sensing device, thus recording the temperature history at each point during the fall.

Figure 39 shows the calculated temperature gradient that develops in a sphere made of dunite weighing one kilogram and having a specific gravity of 3.3, when dropped from an altitude of -50 km with an initial velocity of zero. Figure 40 shows the rate of heating of the same sphere. Both figures indicate that even a small meteorite

at free fall could develop high temperatures at least near its surface.

The characteristic of a crystalline rock as a multisensor device has been the essence in the study of lunar magma, but it is by no means unique or limited to the extraterrestrial realm.

Elastic Wave Propagation Through Rock Media at Elevated Pressures and Temperatures

One of the difficult problems in the determination of melting in a rock while it is under high pressure is the result of two characteristics of the experiments: (1) the bulk of material which surrounds the sample is essential to contain the pressure, but it also makes the sample inaccessible during the experiment and conceals it from direct observation; (2) the complex nature of most rock samples and the multiplicity of reactions that may take place in them during a run make the data obtained by conventional electric probing techniques to measure melting (such as differential thermal analysis, or resistivity changes) overwhelmingly detailed and too complicated to be simply correlated with the melting event. So, rather than determine melting in situ, one is forced to resort to a quench technique where a "post mortem" petrographic analysis of the sample determines whether or not melting had occurred.

One promising technique to provide an in situ indication of melting while under pressure is an ultrasonic probing of the elastic characteristics of the rock. Compressional waves and shear waves are dependent on the bulk properties of the medium. Shear waves, for example, attenuate more rapidly as the solid rock gradually becomes more plastic, and are completely absorbed when it melts. Figure 41 shows the geometry of the laboratory configuration and Figure 42 shows a basalt sample and heater arrangement used by Dr. R. D. Tooley (Northrop Corporation) in velocity measurements under high pressure and temperature.

The most extensive velocity measurements of rocks under pressure are those of Birch (1961) and Simmons (1964). These measurements were made in a hydrostatic pressure vessel. The measurements are very precise, but were only made to 10 kb. Hughes and Cross (1951) have worked at both high pressure and elevated temperatures. Their pressure and temperature limits are 5 kb and 300°C. Ahrens and Katz (1962) reached 40 kb and room temperature. There are no simultaneous high pressure and high temperature values in the literature above these values. All the work done by the above cited references was strictly directed towards geophysical research. Their published experience was relied on in the attempt to develop an in situ measurement of rock melting as part of a lunar magma study. Now let us redirect our attention to the earth and examine one example of application of the comtined petrographic-seismic studies to terrestrial interests.

Petrographic analyses of tholeiitic basalt were run by Dr. E. Azmon (Northrop) and Dr. R. Gaal (USC) to determine the changes in percentages of glass and crystals after the specimens had been subjected to various temperature-pressure combinations for a duration of 5 minutes. The results of these measurements were plotted (Figure 12) as percent crystals vs. the ratio of temperature to pressure. Figure 13 which follows shows that elastic wave velocities in the rocks can be plotted against the same temperature to pressure ratio. If a temperature-to-pressure ratio can represent conditions at some depth point below the surface of the earth, then the corresponding data on percent crystals, wave velocities, or many other physical parameters may be related to the rocks at that point. It is convenient to use temperature over pressure rather than specific volume as a common denominator for the above correlation since both temperatures and pressure can be easily measured in the laboratory on a routine basis. Conducting both petrologic and seismic experiments side by side on cuts of the same rocks makes the genetic state of the rock, at specific pressures

and temperatures, a known parameter which corresponds to measureable wave velocities. Conducting seismological exploration in the field gives us the wave velocities. The estimates of temperatures, pressure (depth), and identity (composition and genetic state) of the rock medium must agree then with the laboratory correlation.

This combination of petrology and seismology in laboratory studies is a byproduct of this study, but by no means is it unique or limited to the extraterrestrial realm.

APPENDIX

APPENDIX

Absorption Effects for a Pure Poly-Crystalline Sample on a Diffractometer

The diffracting volume of a layer of powder of thickness dt at depth t in a slab sample will diffract an incident x-ray beam I_o at a Bragg angle θ and the diffracted beam I will be affected by absorption according to:

$$dI = I_o e^{-\mu s} dV$$

where dV is the diffracting volume, μ is the linear absorption coefficient, and s is the path length of the beam through the sample.

If A is the cross-sectional area of the beam, then the area of the diffracting volume is

$$dV = \frac{A}{\sin \theta} dt,$$

and $t = 1/2\ s \sin \theta$ or $s = 2t/\sin \theta$.

Thus,

$$dI = \frac{A\ I_o}{\sin \theta} e^{-2\mu t/\sin \theta} dt$$

$$I = \frac{A\, I_o}{\sin\theta} \int_{t=0}^{t} e^{-2\mu t/\sin\theta}\, dt$$

$$I = \frac{-AI_o}{\sin\theta} \cdot \frac{\sin\theta}{2\mu} \left[e^{-2\mu t/\sin\theta} - 1 \right]$$

$$I = \frac{I_o A}{2\mu} \left[1 - e^{-2\mu t/\sin\theta} \right]$$

In the limit, as $\mu t \rightarrow \infty$

$$I = \frac{I_o A}{2\mu},$$

which is the usual formula for thick samples. This simplified expression is commonly used if $\mu t \geq 3.2 \sin\theta$ and

$$e^{-2\mu t/\sin\theta} < 0.0017$$

For this case then I is maximum and essentially constant with respect to sample thickness and Bragg angle.

On the other hand, intermediate values of μt will cause I to be less than the maximum value and to be an exponential function of $t/\sin\theta$.

Finally, as $\mu t \rightarrow 0$ then

$$e^{-2\mu t/\sin\theta} \rightarrow 1 - \frac{2\mu t}{\sin\theta}$$

and

$$I \cong \frac{I_o A t}{\sin\theta}$$

so that, at a given Bragg angle I is directly proportional to the thickness of the sample provided it is small.

Examples:

1. Chrysolite (Olivine): $2(Mg_{0.88}Fe_{0.12})O \cdot SiO_2$

Let us compute I as a function of t at $\theta = 16.12^{\circ}$ ($\sin\theta = 0.27759$):

Atom	Atomic Weight	Total Weight of Atom in Compound	Fraction of Total Weight
1.76 Mg	24.32	42.80	28.86
0.24 Fe	55.85	13.40	9.04
Si	28.09	28.09	18.94
4 O	16.00	64.00	43.16
		148.29	100.0

For Cu Kα radiation:

Atom	(μ/ρ)	$P\ (\mu/\rho)$
Mg	40.6 g^{-1}	11.7 g^{-1}
Fe	324	29.3
Si	60.3	11.4
O	12.7	5.5
	$\Sigma\ P(\mu/\rho) =$	57.9 g^{-1}

The density, ρ', of Chrysolite is 3.338 g/cm^3, thus,

$$\mu = \rho' \Sigma\rho\left(\frac{\mu}{\rho}\right) = 3.338 \times 57.9 = 193\ cm^{-1}$$

and

$$I = \frac{K}{386}\left[1-e^{-1.391 \times 10^{3}t}\right]$$

if we assume $\frac{K}{386} = 1$, then:

$$I = 1 - \exp - (1.391 \times 10^{3}t)$$

If the Chrysolite samples are prepared as thin slabs of dimensions 2 x 1 cm, then the thickness t is related to the weight of the sample, W according to

$$2t\rho = W\ (g)$$

$$t = \frac{W}{2\rho'}$$

and by substitution

$$I = 1 - \exp - (1.391 \times 10\ \frac{3W}{2\rho})$$

$$I = 1 - \exp - (2.084 \times 10^{2}W)$$

In order to determine the scale of the calculated I values, seven experimental intensity determinations were made with varying sample weights. Scale factors were computed to relate the observed to calculated intensities, and the factors were averaged with equal weights (the first two experimental points were thrown out). The results are shown in Table XIII and Figure 43.

From this curve, it is clear that if the sample weight is larger than 30.7 mg ($\mu t > 3.2 \sin \theta$), the intensity is constant and sample weights lower than 1 mg are necessary if it is desired to use the linear relationship between weight and intensity.

TABLE XIII

EXPERIMENTAL CHRYSOLITE (OLIVINE) DATA

W_{mg}	I_{obs}	I_{cal}	$\frac{I\ calc}{I\ obs} \times 10^2$	Remarks
1.4	7.5	0.253	3.36	rejected
2.0	15	0.341	2.27	rejected
4.0	35	0.566	1.62	
5.1	40	0.655	1.64	
5.8	42	0.702	1.67	
6.8	43	0.758	1.76	
7.5	50	0.791	1.58	

Av. $\frac{I_{calc}}{I_{obs}} = 1.654 \times 10^{-2}$ Av. $\frac{I_{obs}}{I_{calc}} = 60.5$

2. Hypersthene (Pyroxene) $(Mg_{0.88}Fe_{0.12})\ O.\ SiO_2$

Let us compute I as a function of t at $\theta = 15.52^{\circ}$ ($\sin\theta = 0.27424$):

Atom	Atomic Weight	Total Weight of Atom in Compound	Fraction of Total Weight P %
0.88 Mg	24.32	21.40	20.54
0.12 Fe	55.85	6.70	6.43
Si	28.09	28.09	26.96
3 O	16.00	48.00	46.07
		104.19	100.00

For Cu Kα.

Atom	(μ/ρ)	$P\ (\mu/\rho)$
Mg	$40.6\ g^{-1}$	8.3
Fe	324	20.8
Si	60.3	16.3
O	12.7	5.8
	$\Sigma\ P\ (\mu/\rho) = 51.28^{-1}$	

The density, ρ', of Hypersthene is 3.19 g/cm^3. Thus

$$\mu = \rho' \Sigma P (\mu/\rho) = 3.19 \times 51.2$$

$$\mu = 163 \text{ cm}^{-1}$$

and

$$I = \frac{K}{326} \left[1 - e^{-1.189 \times 10^3 t} \right] .$$

If we assume $\frac{K}{386} = 1$, then

$$I = 1 - \exp - (1.189 \times 10^3 t),$$

and for the same size sample slabs as for the Chrysolite case,

$$I = 1 - \exp - (1.864 \times 10^2 W).$$

This calculated curve was again fitted to seven experimental points in the same manner as previously (see Table XIV and Figure 43.)

TABLE XIV

EXPERIMENTAL HYPERSTHENE (PYROXENE) DATA

W_{mg}	I_{obs}	I_{calc}	$\frac{I_{calc} \times 10^2}{I_{obs}}$	Remarks
1.4	6	0.770	3.83	
1.8	7	0.715	4.07	
3.8	12	0.493	4.22	
5.1	14	0.386	4.39	
5.9	17	0.333	3.92	
6.9	14	0.276	5.17	
7.5	18	0.247	4.18	

Av. $\frac{I_{calc}}{I_{obs}} = 4.254 \times 10^{-2}$ Av. $\frac{I_{obs}}{I_{calc}} = 23.51$

Absorption Effects for One Phase in a Mixture on a Diffractometer

The absorption coefficient of a mixture as a whole affects the intensities of any given crystalline phase in the mixture. Thus,

$$I_i = \frac{(I_o)_i A}{2\mu} \left[1-e^{-2\mu t/\sin\theta}\right] f_i \quad .$$

where μ is the linear absorption coefficient of the mixture and f_i is the volume fraction of the ith component which can be expressed as a function of weight fraction, P_i, and the densities of the mixture, ρ_o, and that of the ith component, ρ_1,

$$f_i = \frac{P_i \rho}{\rho_i} \quad .$$

Thus, by substitution

$$I_i = \frac{(I_o)_i A \; P_i \rho}{2\mu\rho_i} \left[1-e^{-2\mu t/\sin\theta}\right] \quad .$$

Example: Chrysolite and Hypersthene in the Bruderheim Meteorite. Let us compute the intensity of a reflection at $\theta = 16.12^\circ$ ($\sin\theta = 0.27759$) for Chrysolite in the Bruderheim meteorite as a function of its percentage weight and the weight of the total sample. For this example, the overall elemental composition and, therefore, μ' remains constant, but, through various physical means the fraction of crystalline Chrysolite and Hypersthene may vary.

TABLE XV

LINEAR ABSORPTION COEFFICIENT FOR BRUDERHEIM

Atom	P_i, %	μ/ρ (Cu)
O	36.80	12.7
Fe	21.96	324.0
Si	18.62	60.3
Mg	14.90	40.6
S	2.42	91.3
Ca	1.29	172.0
Ni	1.28	49.2
A	1.16	48.7
Na	0.70	30.9
Cr	0.37	259.0
Mn	0.24	284.0
P	0.11	73.0
K	0.08	143.0
Ti	0.07	204.0
	100.00	

$\Sigma P_1 (\mu_1/\rho_1)' = 100.92$

$\mu = \rho' \, 100.92$

$\mu = 378.45 \text{ cm}^{-1}$

From the calibration curve of Chrysolite we know that

$$\frac{(I_o)_{chrys} A}{2\mu_{chrys}} = 60.5$$

or

$$(I_o)_{chrys} \; A = 60.5 \times 2 \times 193 = 23353.$$

We also know that the density of the Bruderheim meteorite and Chrysolite are 3.75 and 3.338 g/cm^3, respectively.

To simplify calculations, μ for the mixture was calculated from the elemental composition (see Table XV) and found to have a value of 378 cm^{-1}.

Thus,

$$\frac{I_{chrys} = 23353 \times 3.75 \; P_{chrys}}{2 \times 378 \times 3.338} \left[1-e^{-2 \times 378t/0.27759}\right]$$

$$I_{chrys} = 34.69 \; P_{chrys} \left[1-e^{-2.723 \times 10^3 t}\right]$$

Since

$$t = \frac{W}{2P} = \frac{W}{2 \times 3.75} = \frac{W}{7.50}$$

$$I_{chrys} = 34.69 \; P_{chrys} \left[1-e^{-3.631 \times 10^2 W}\right].$$

From this expression then, we can compute a family of curves for constant sample weight with I_{chrys} versus P_{chrys} (Figure 44).

The same curve may be plotted for Hypersthene in the Bruderheim meteorite (Figure 45). As seen earlier:

$$\sin\theta = 0.27424$$

$$\rho_{hyp} = 3.19 \text{ g/cm}^3$$

$$(I_o)_{hyp} \quad A = 7694$$

Thus,

$$I_{hyp} = \frac{7694 \times 3.75}{756 \times 3.19} \quad P_{hyp} \quad 1\text{-}4^{-756} \; / 7.5 \times 2.27424$$

$$I_{hyp} = 11.96 \quad P_{hyp} \quad 1\text{-}e^{-3.676 \times 10^{2} W}$$

REFERENCES

Ahrens, Thomas J.; and Katz, Samuel (1962). An Ultrasonic Interferometer for High-Pressure Research, Journ. Geoph. Res., Vol. 67, No. 7 pp. 2935-2944.

Allen, W. C.; and Snow, R. B. (1955). The Orthosilicate-rich Oxide Portion of the System CaO-"FeO"-SiO_2, Journ. Am. Ceram Soc., Vol. 38, pp. 264-280.

Azmon, Emanuel (1962). Lunar Soil Sampling and Testing, American Society for Testing and Materials, Symposium on Field Testing of Soils, Sp. TM. Pub. No. 322, pp. 303-318.

Azmon, Emanuel (1963). A Note on Multiple Equilibria in Melting of Natural Silicate Rocks, Northrop Space Laboratories, TM 63-181.

Azmon, Emanuel (1965). Melting Temperature of Complex Silicates, Annals of New York Academy of Science, Vol. 123, Art. 2, pp. 481-494, Geological Problems in Lunar Research.

Baadsgaard, H.; Campbell, F. A.; and Folinsbee, R. E.; Cumming, G. L. (1961). The Bruderheim Meteorite, J.G.R., Vol. 66, No. 10, pp. 3574-3577.

Barth, T. F. W. (1962). Thermodynamics as a Help to the Study of Rocks, Appendix to 2nd Ed., Theoretical Petrology, John Wiley and Sons, pp. 381-403.

Birch, F. (1961). The Velocity of Compressional Waves in Rocks to 10 Kilobars, Part I, J. Geoph. Res., Vol. 65, pp. 1083-1102.

Bowen, N. L.; and Schairer, J. F. (1932). The System FeO-SiO_2, Am. J. Sci., 5th Ser., Vol. 24, pp. 177-213.

Boyd, F. R.;and England, J. L. (1960). Apparatus for Phase Equilibrium Measurement at Pressure up to 50 Kilobars and Temperature up to 1750°C, Jour. Geoph. Res., Vol. 65, pp. 741-748.

Boyd, F. R.; England, J. L.; Davis, Brian T. C. (1964). Effects of Pressure on the Melting and Polymorphism of Enstatite, $MgSiO_3$, Jour. Geophys. Res., Vol. 69, No. 10, pp. 2101-2109.

Boyd, F. R.; and England, J. L. (1963). Effect of Pressure on the Melting of Diopside, $CaMgSi_2O_6$, and Albite, $NaAlSi_3O_8$, in the Range up to 50 Kilobars, Jour. Geophys. Res., Vol 68, pp. 311-323.

Coes, L. (1962). Synthesis of Minerals at High Pressure, Chpt. 7, Modern Very High Pressure Techniques, Butterworth, Washington, pp. 137-150.

Daly, R. A. (1943). Meteorites and an Earth Model, Bull., G.S.A., No. 54, pp. 401-456.

Davis, B. T. C.; and England, J. L. (1964). The Melting of Forsterite up to 50 Kilobars. J. Geophys. Res., Vol 69, pp. 1113-1116.

Duke, Michael; Maynes, Donald; and Brown, Harrison (1961). The Petrography and Chemical Composition of the Bruderheim Meteorite. J.G.R., Vol. 66, No. 10, pp. 3557-3563.

Elgin, J.; and Azmon, E. (1964). Apollo Experiment Support Mission, Lunar Surface Vehicle, Unpublished Report, Northrop Space Laboratories, LSV/S-MO-1.

Green, D. H.; Ringwood, A. E. (1964). Fractionation of Basalt Magmas at High Pressures, Nature, Vol. 201, No. 4926, pp. 1276-1279.

Green, D. H.; Lambert, I. B. (1965). Experimental Crystallization of Anhydrous Granite at High Pressures and Temperatures, Jour. Geophys. Res., Vol. 70, No. 20, pp. 5259-5268.

Green, Jack (1962). The Geology of the Lunar Base, Space Science Lab. North American Aviation, Space and Reference Center, SID-61-358.

Green, J. (1964). A Study of the Feasibility of Using Nuclear Versus Solar Power in Water Extruction from Rocks, Space Science Lab., Space and Inf. Systems Div., North American Aviation, Downey, California, Contract AF19(628)3292 Project 0000, Scientific Report No. 1, Prepared for AFCRL.

Hall, H. T. (1958). Some High Pressure Apparatus Design Considerations; Equipment for Use at 100,000 Atmospheres and 3000°C, Rev. Sci. Inst., No. 29, pp. 267-275.

Hsu, L. (1967). The Melting of Fayalite up to 40 Kilobars, Jour. Geoph. Res., Vol. 72, No. 16.

Hughes, D. S.; and Cross, J. H. (1951). Elastic Wave Velocities in Rocks at High Pressures and Temperatures, Geophysics, Vol. 16, pp. 577-593.

Iddings, J. P. (1885). Am. Bur. Sci., 3rd Ser., Vol. 30, p. 58.

Ingles, T. A.; and Popper, P. (1960). The Preparation and Properties of Boron Nitride, Academic Press, Special Ceramics, Chap. 8, pp. 144-167.

Jamieson, B. G. (1966). Evidence on the Evolution of Basaltic Magma at Elevated Pressures, Nature, Vol. 212, No. 5059, pp. 243-246.

Kennedy, G. C.; and LaMori, P. N. (1961). Some Fixed Points on the High Pressure Scale, Conf. of Very High P., Lage George, N. Y., June 1960, John Wiley and Sons.

Kopecky Lubomir, Voldan Jan (1959). Krystalisace Tavenych Hornin (Crystallization of Melted Rocks), Nakaladatelstvi Ceskoslovenske akademie ved, Praha English summary pp. 185-207.

Korzhinskiy, D. S. (1962). A Theory of the Processes of Mineral Formation. Translated from Teoriya Protsessov Mineraloobrazovaniya AN SSSR, Int. geokhim. i analiticheskoy khimii im. V. I. Vernadskogo, 24 pages, Izdvo AN SSSR, Moscow (Translation: Int. Geol. Rev. Vol. 6, No. 3)

Muan, A. (1955). Phase Equilibria in the System $FeO-Fe_2O_3-SiO_2$, Am. Inst. Mining and Metal. Engr. Transaction, Vol. 203, pp. 965-976.

Penfield, S. L.; and Forbes, E. H. (1896). A. Jour. Sci., 4th. Ser., Vol. 1, p. 129.

Simmons, G. (1964). Velocity of Compressional Waves in Various Minerals of Pressures to 10 Kilobars, J. Geoph. Res., Vol. 69, pp. 1117-1122.

Sterrett, K. F. (1962). The α-γ and γ-α Transformation in Iron at Ultra-High Pressures, Northrop Space Laboratories, TM 62-223.

Tilley, C. E.; Yoder, H. S., Jr.; Schairer, J. F. (1963). Melting Relations of Basalts, Carnegie Inst. Wash., Year Book 62, pp. 77-84.

Urey, H. C.; and Craig, H. (1953). The Composition of the Stone Meteorites and the Origin of Meteorites, Geochim. et Cosmochim. Acta No. 4, pp. 36-82.

Voldan, J. (1956). Selection of Rocks for Petrurgical Treatment, Silikattechnik. Glass. Res. Inst. Hradek Kralove, 7(2) pp. 48-53.

FIGURES

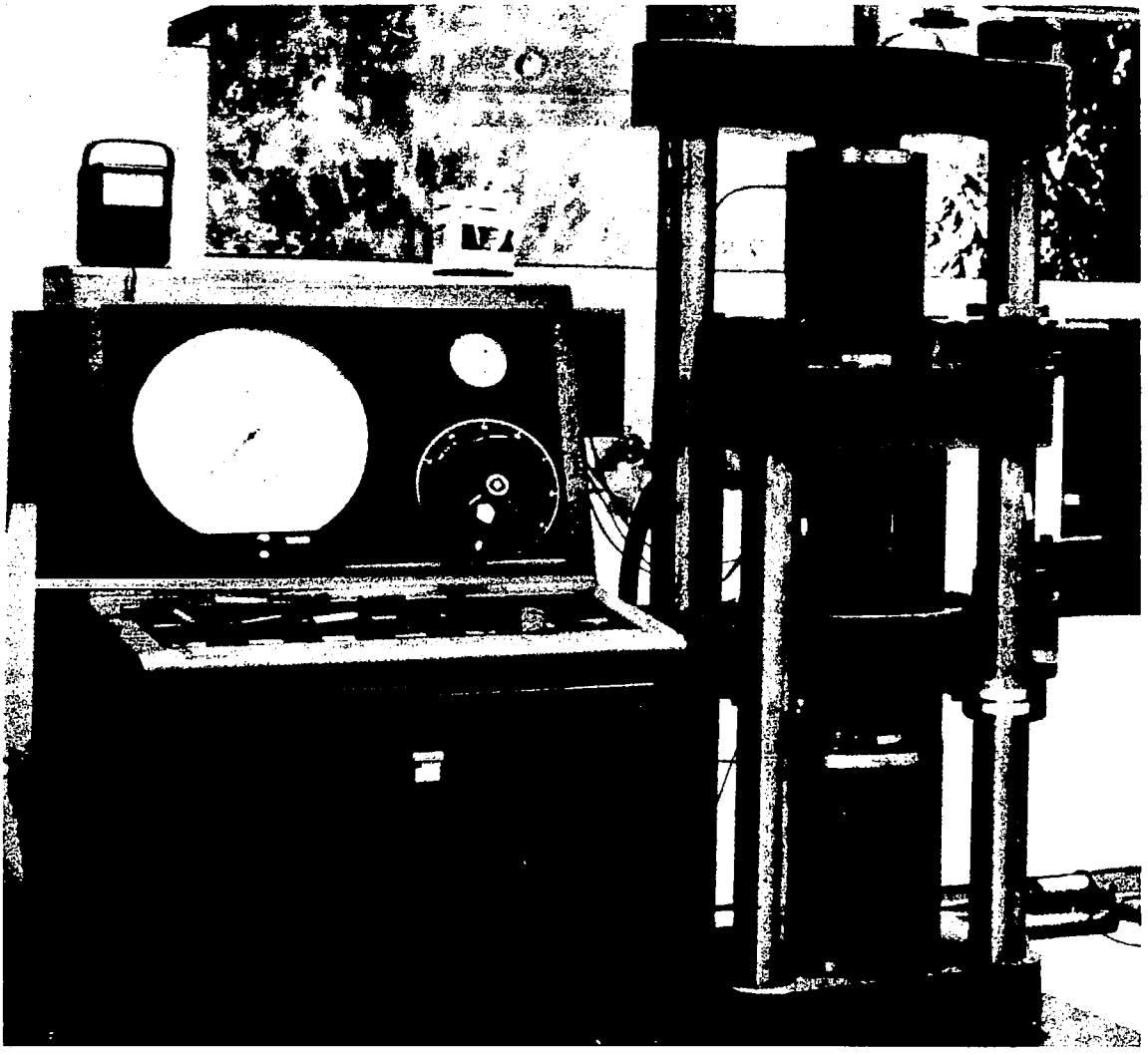

FIGURE 1. TRANSIS-TRONICS KILOTON HYDRAULIC PRESS

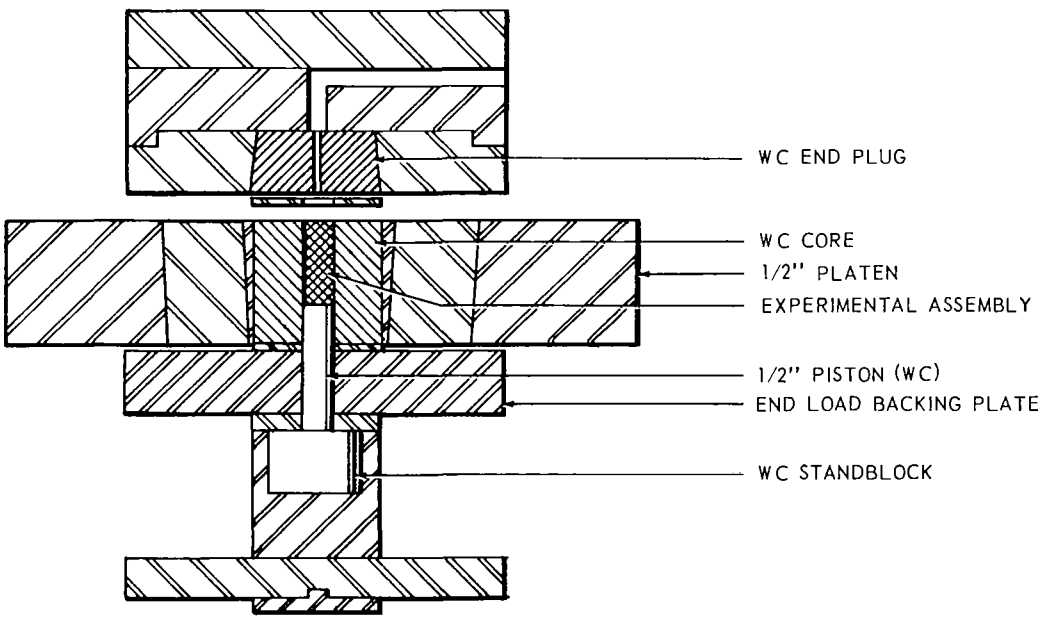

FIGURE 2. THE EXPERIMENTAL ARRANGEMENT FOR A SINGLE-STAGE OPERATION OF THE PRESS

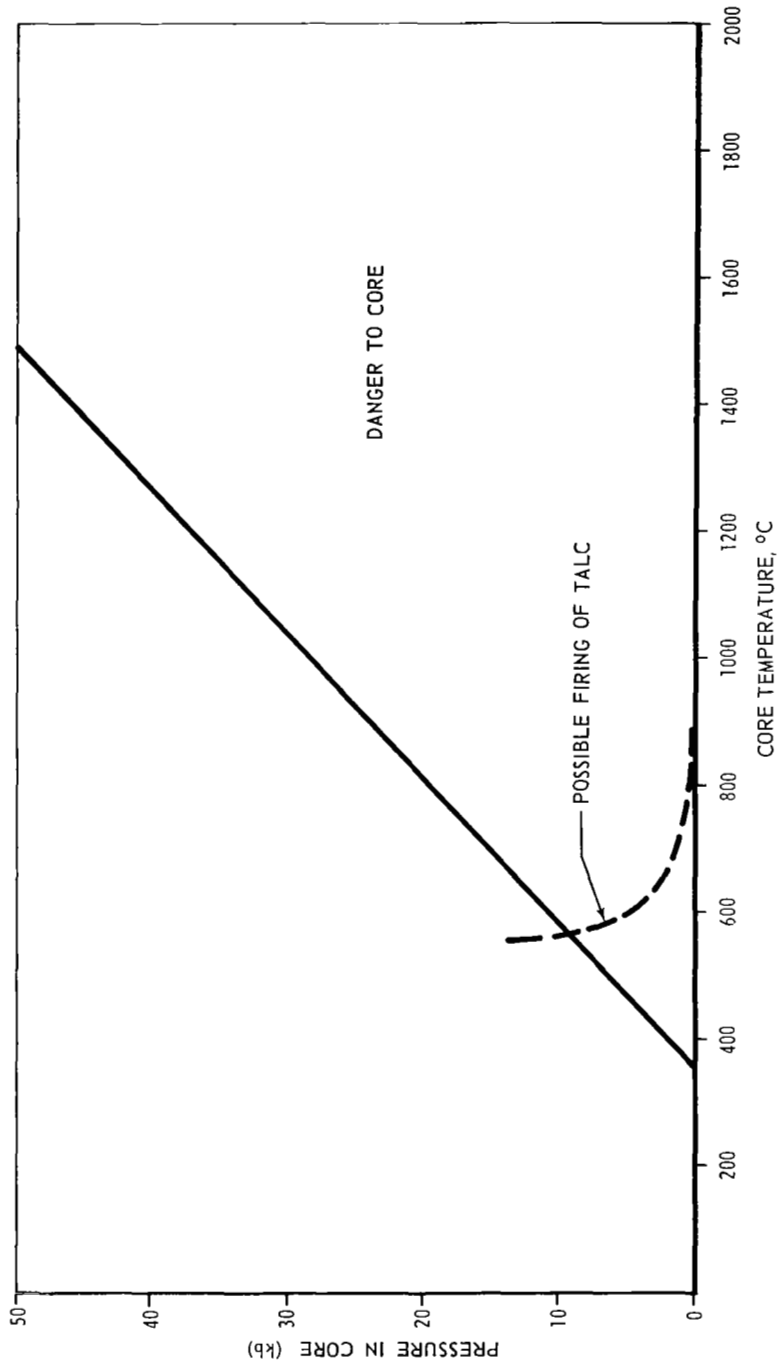

FIGURE 3. SAFE LOADING RANGE ON THE WC CORE (CALCULATED BY MAC PECKHAM OF NORTHROP)

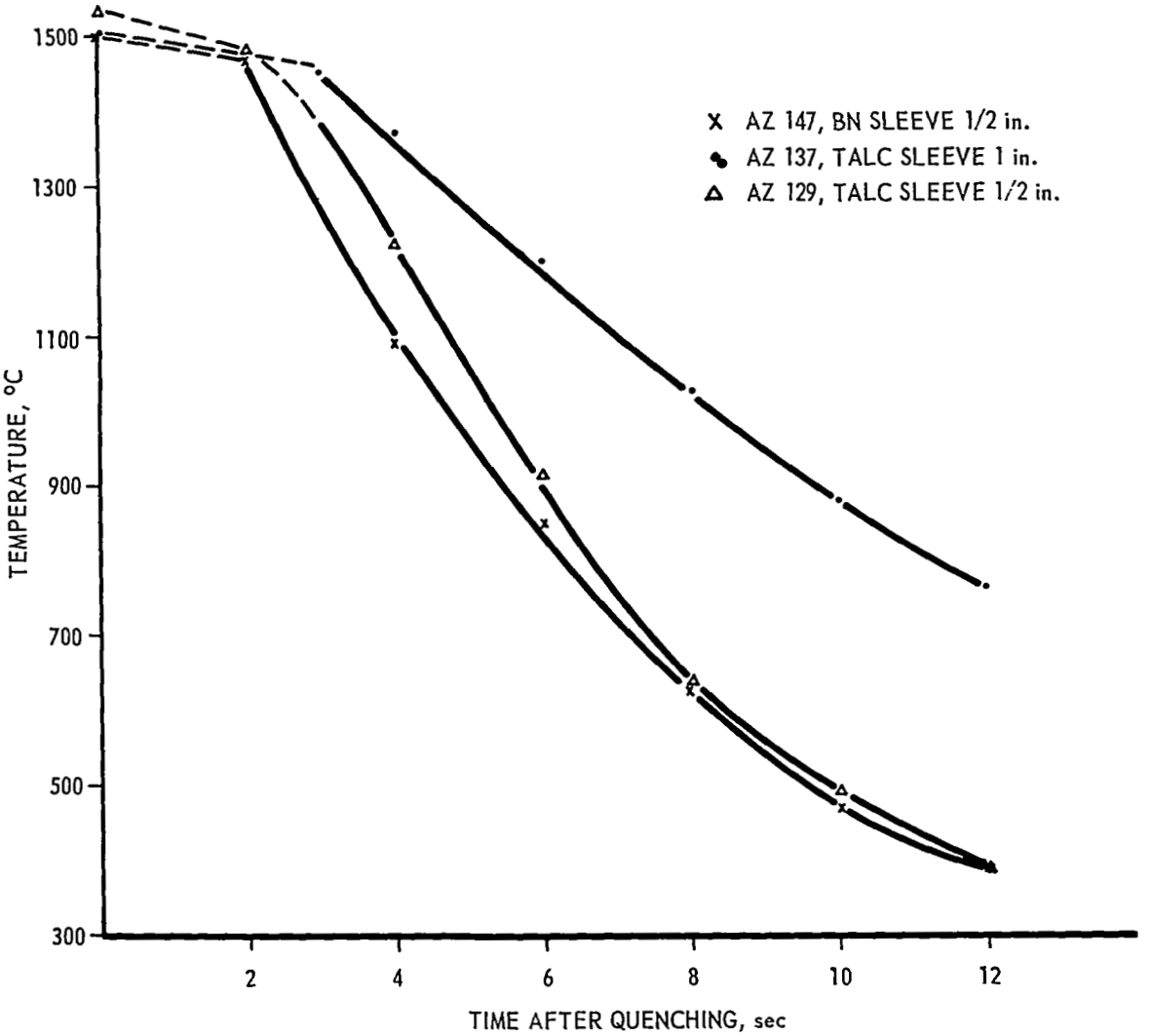

FIGURE 4. QUENCH RATES

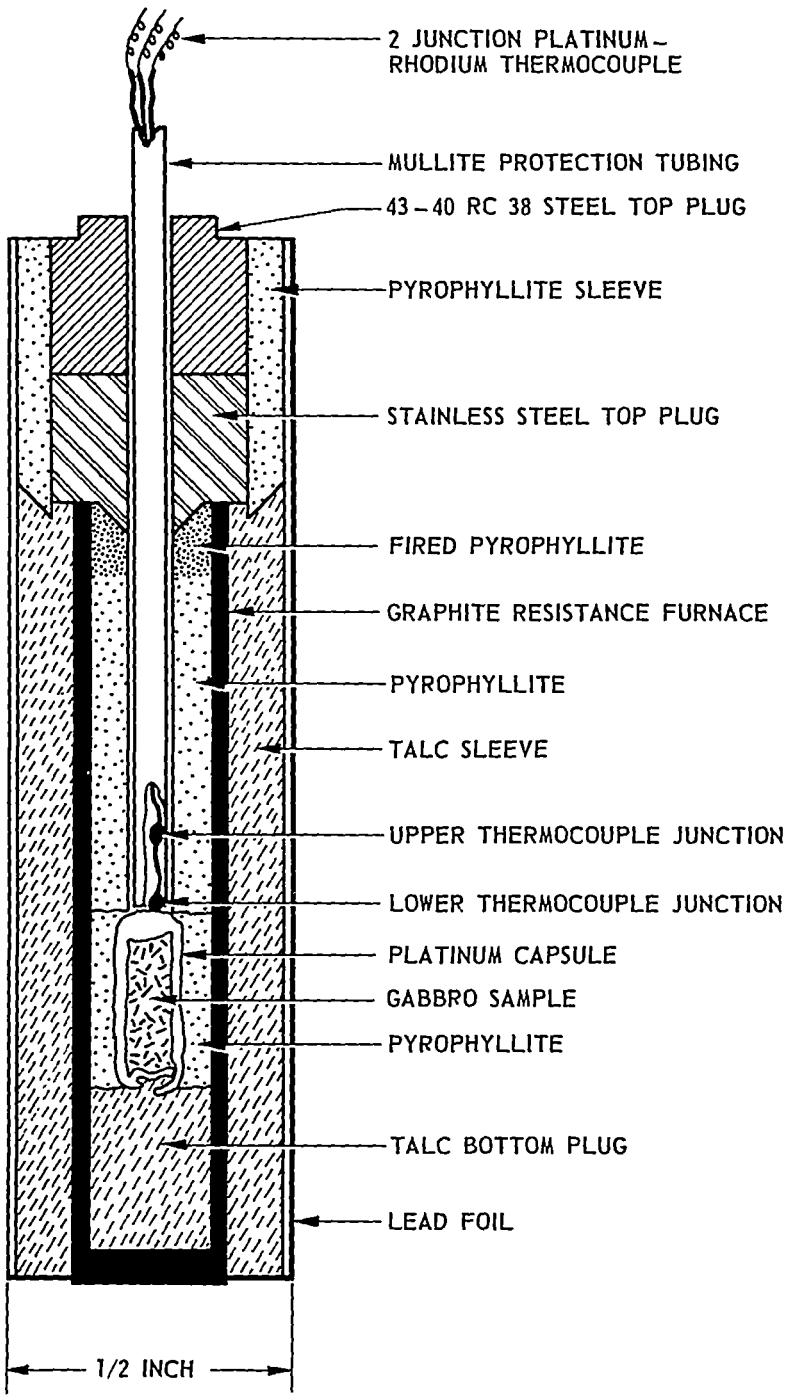

FIGURE 5. DTA ARRANGEMENT OF A RUN FOR HIGH PRESSURE MELTING

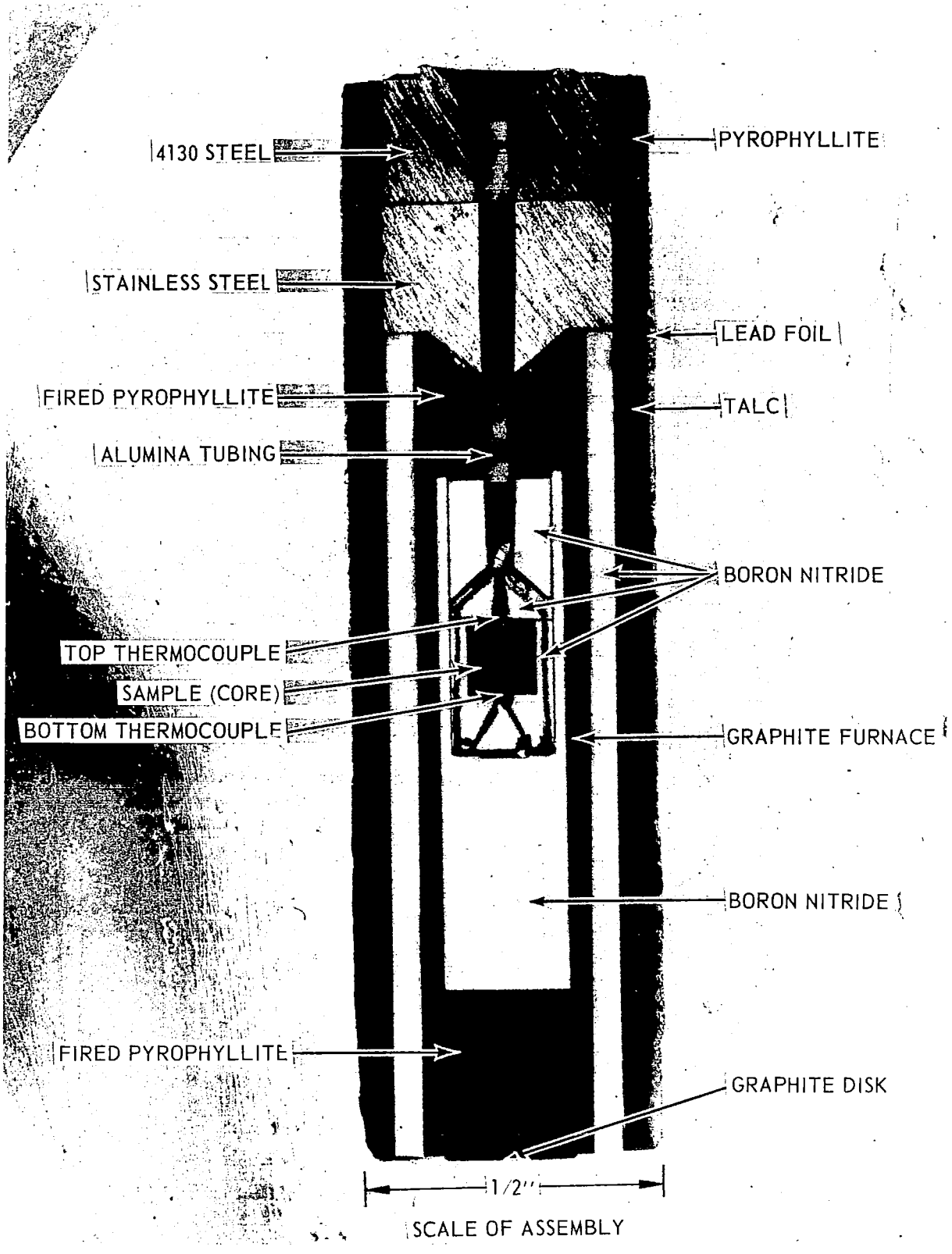

FIGURE 6. DOUBLE THERMOCOUPLE ARRANGEMENT OF A RUN FOR HIGH PRESSURE MELTING

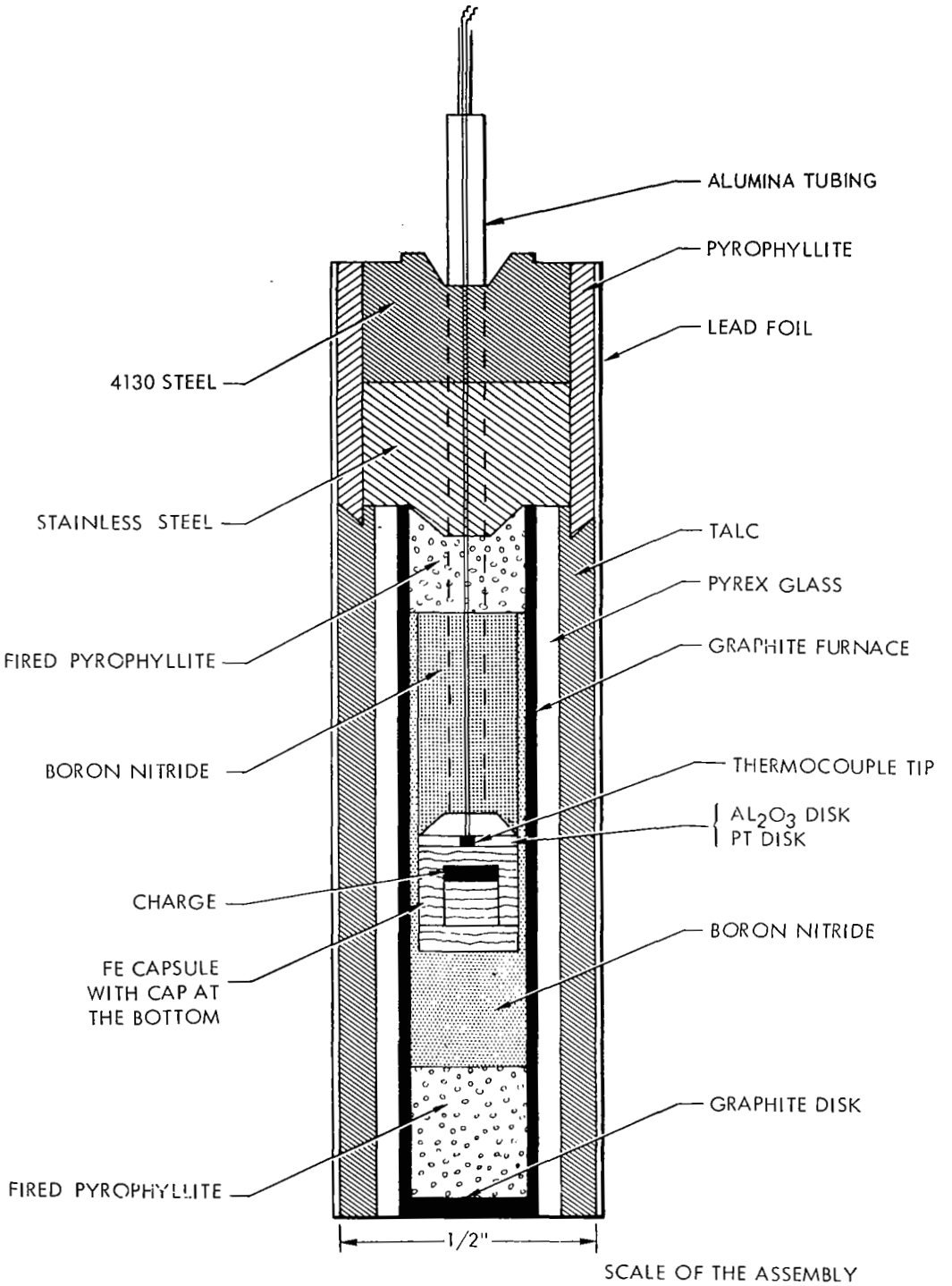

FIGURE 7. IRON CAPSULE ARRANGEMENT OF A RUN FOR HIGH PRESSURE MELTING

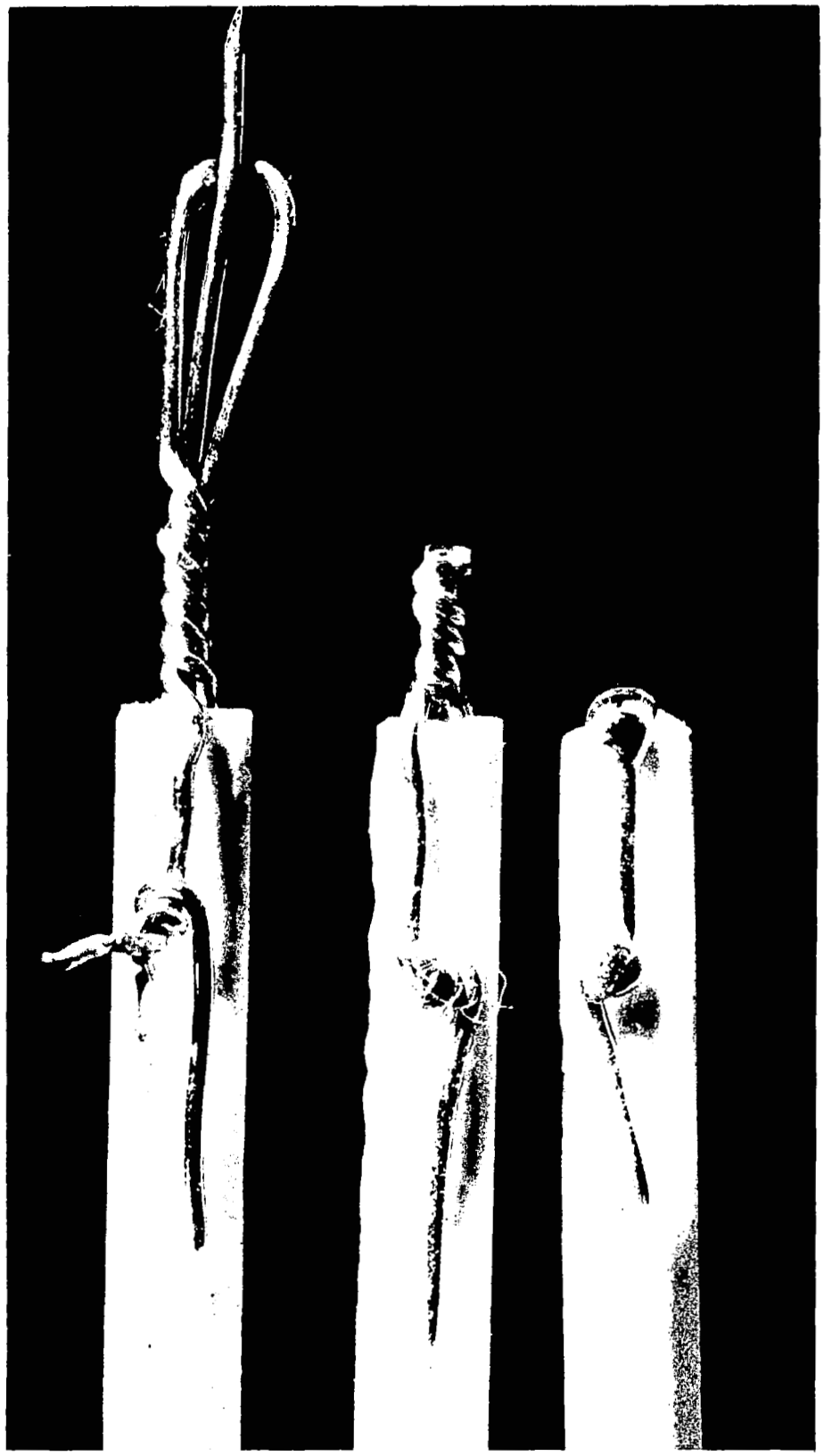

FIGURE 8. PREPARATION OF A DTA ARRANGEMENT.

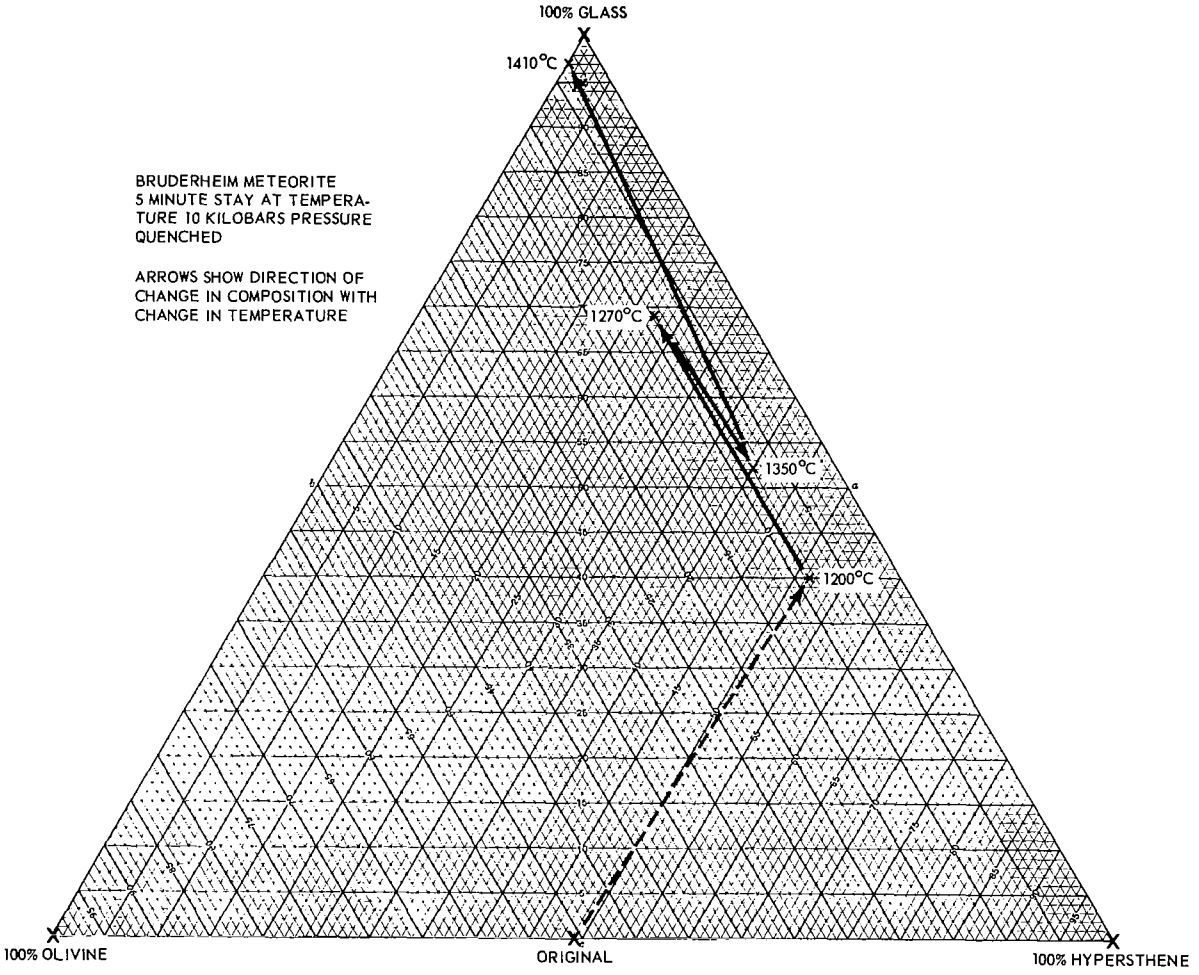

FIGURE 9 A MELTING PATTERN OF THE BRUDERHEIM METEORITE

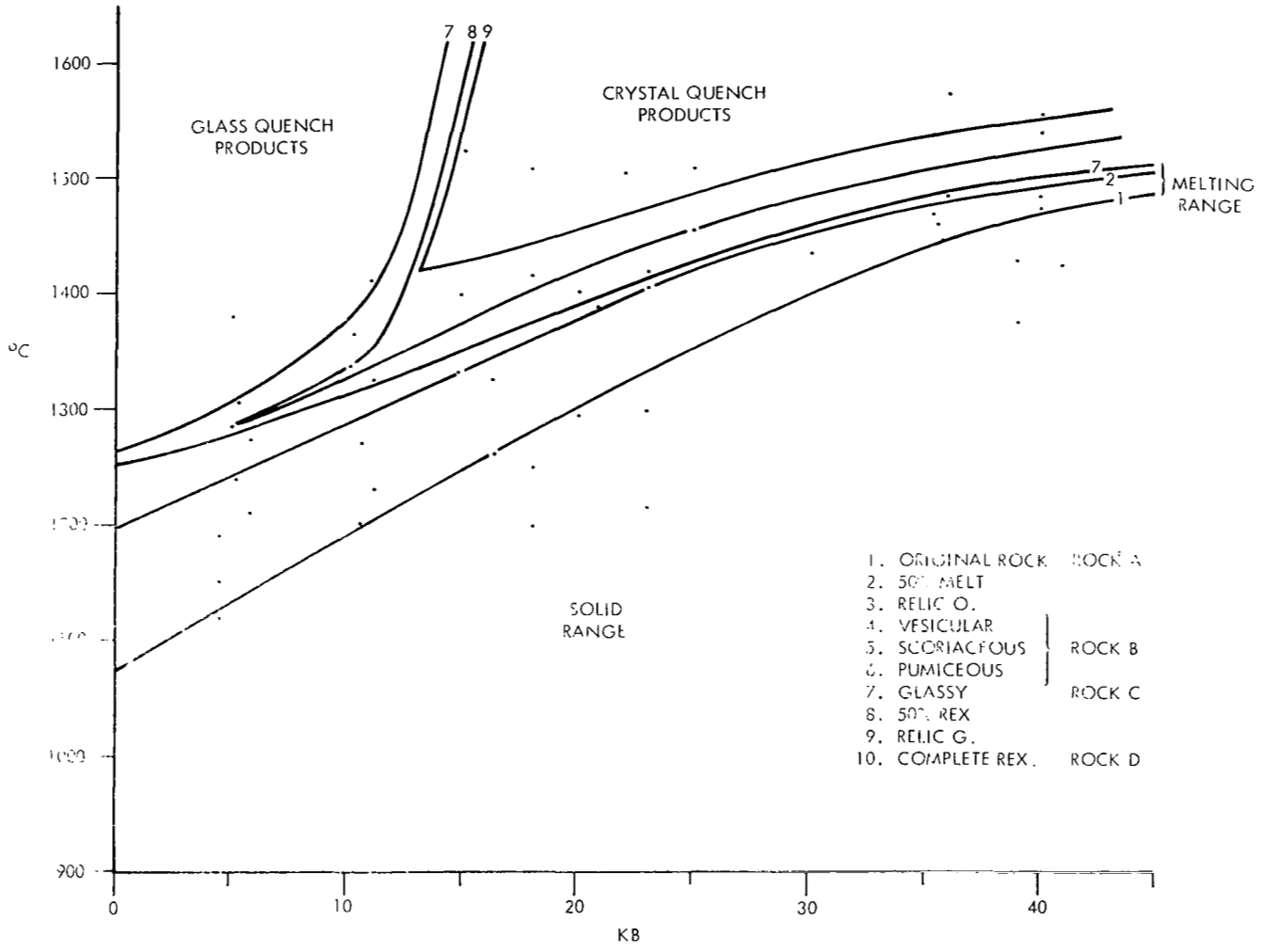

FIGURE 10. GENETIC DIAGRAM FOR THE BRUDERHEIM METEORITE. $T_{°C}$ vs P_{kb}, QUENCHED AFTER 5 MINUTES STAY AT TEMPERATURE

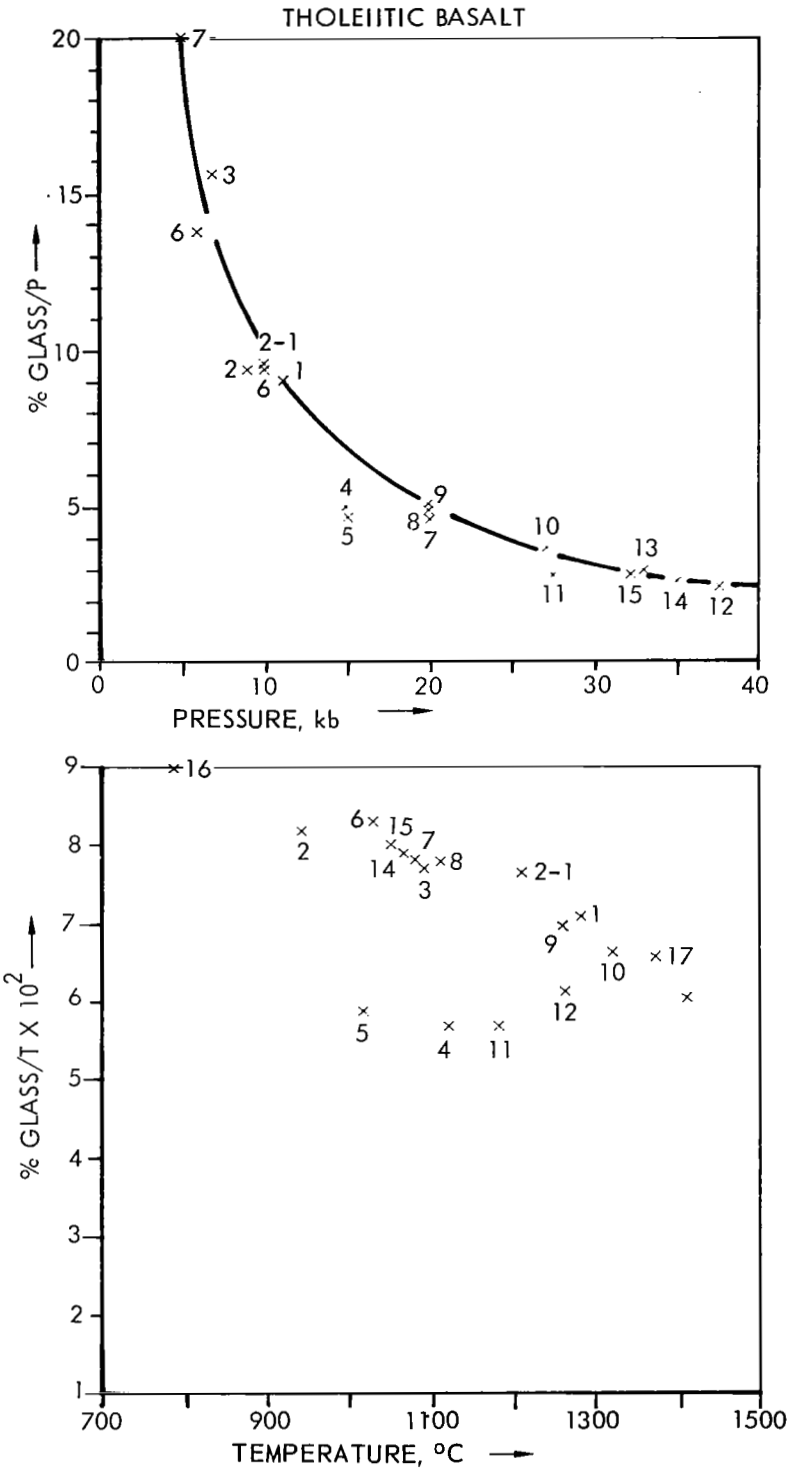

FIGURE 11 THOLEIITIC BASALT PRESSURE vs PERCENT GLASS DIVIDED BY CORRESPONDING PRESSURE, AND TEMPERATURE vs PERCENT GLASS DIVIDED BY CORRESPONDING TEMPERATURE

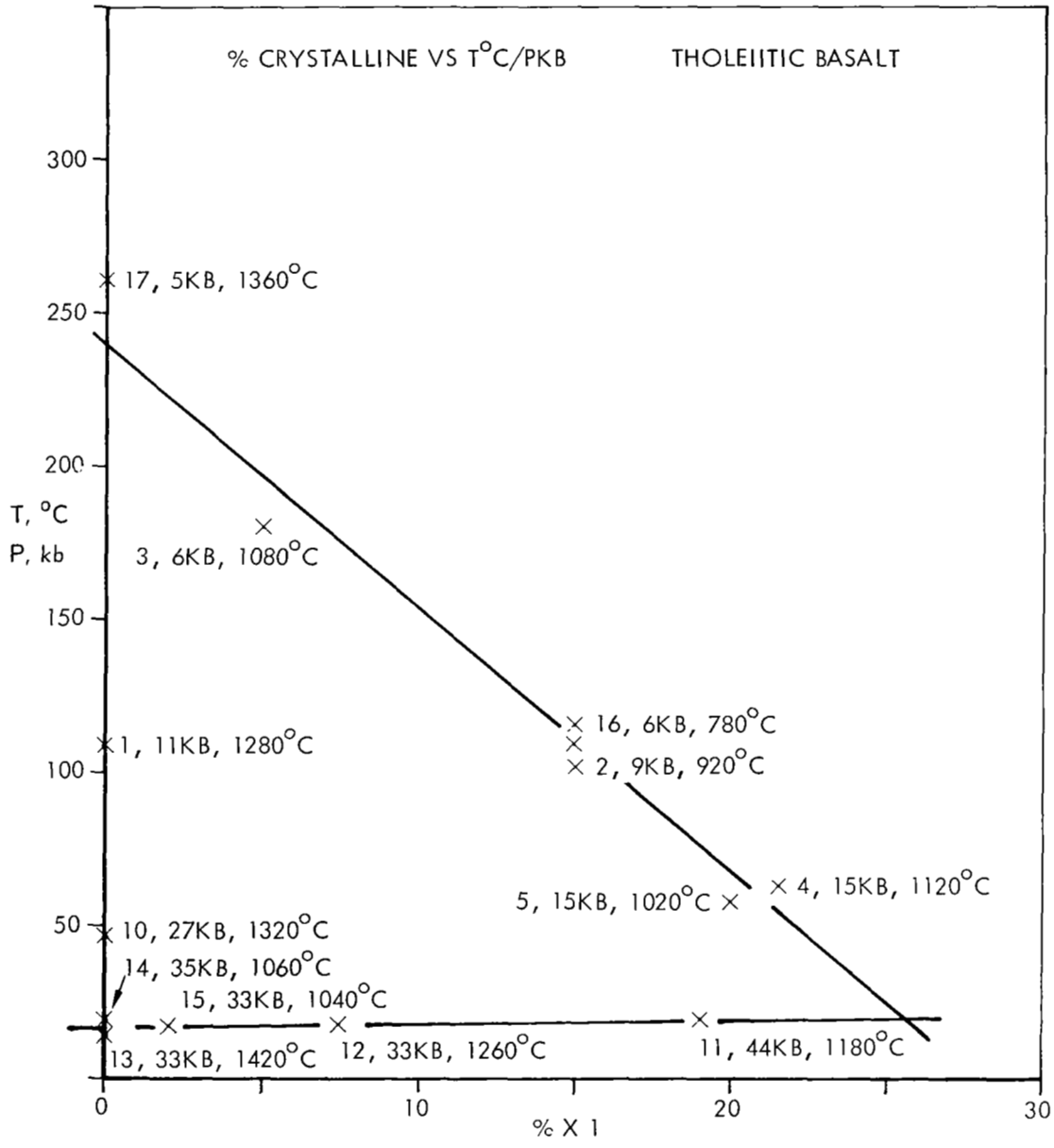

FIGURE 12 THOLEIITIC BASALT. PERCENT CRYSTALS vs TEMPERATURE DIVIDED BY PRESSURE

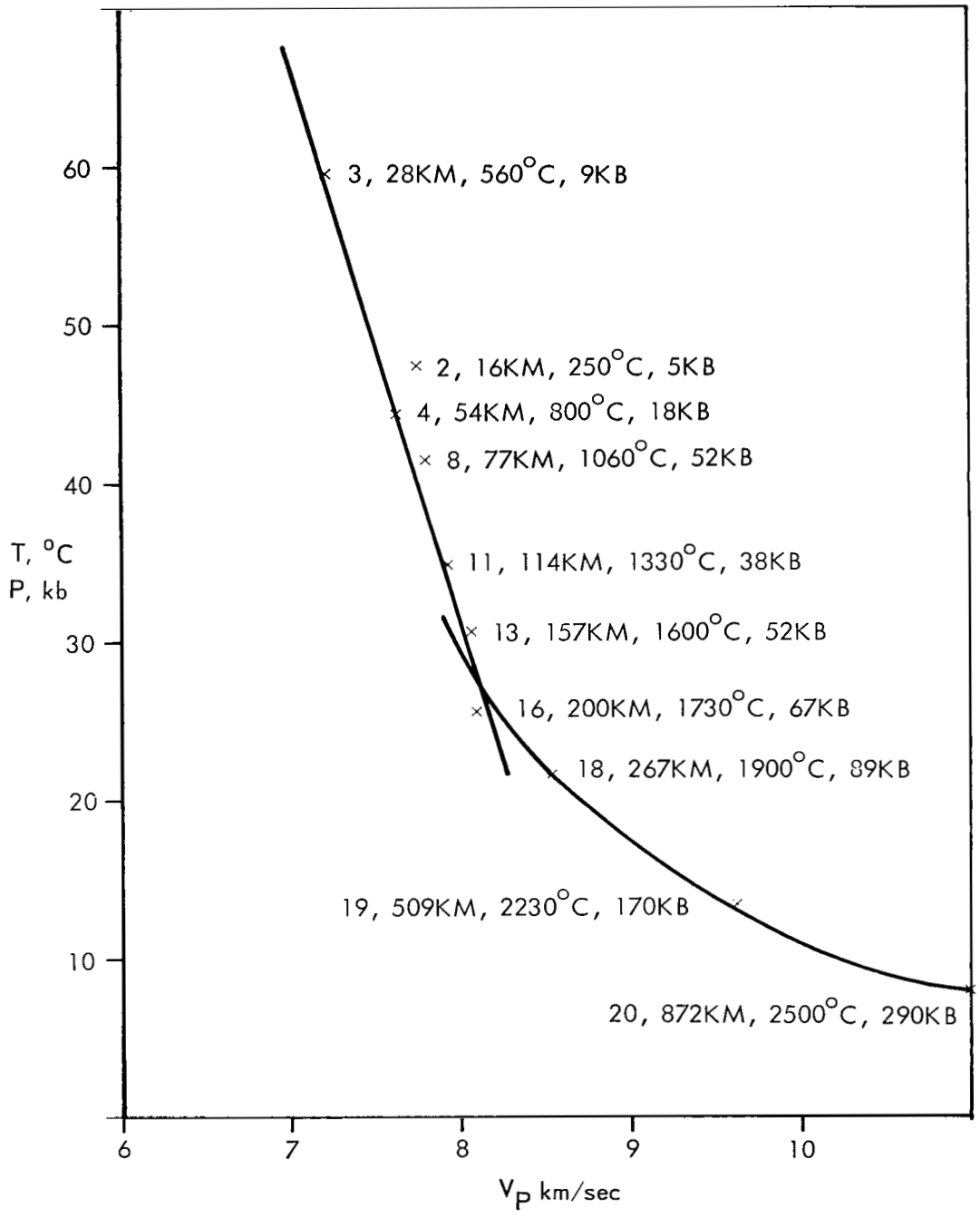

FIGURE 13. VELOCITY OF P WAVES vs TEMPERATURE DIVIDED BY PRESSURE ESTIMATED FOR CORRESPONDING POINTS IN THE DEPTH OF THE EARTH

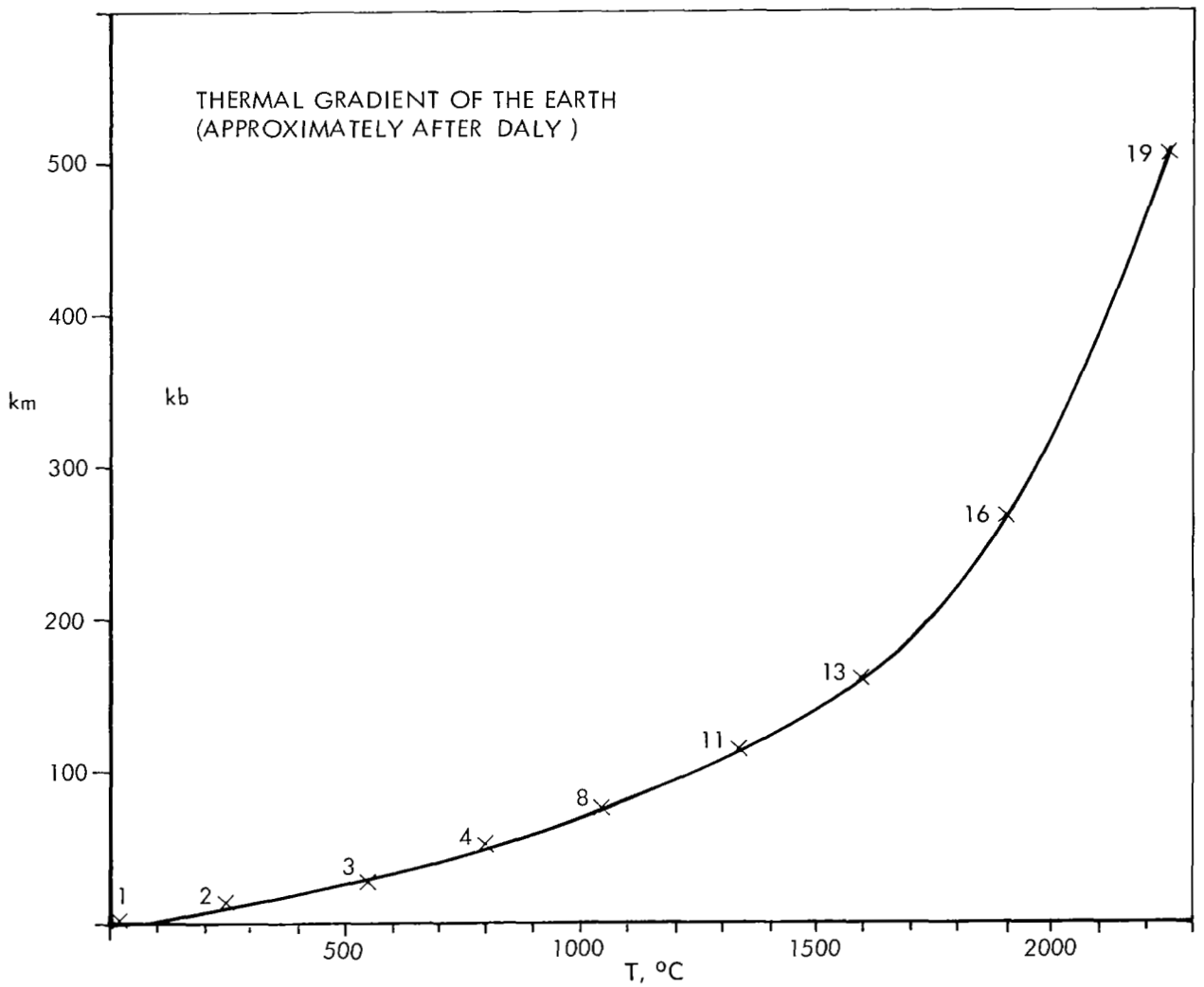

FIGURE 14. PRESSURE-TEMPERATURE ESTIMATES FOR THE EARTH (APPROXIMATELY AFTER DALY, 1943)

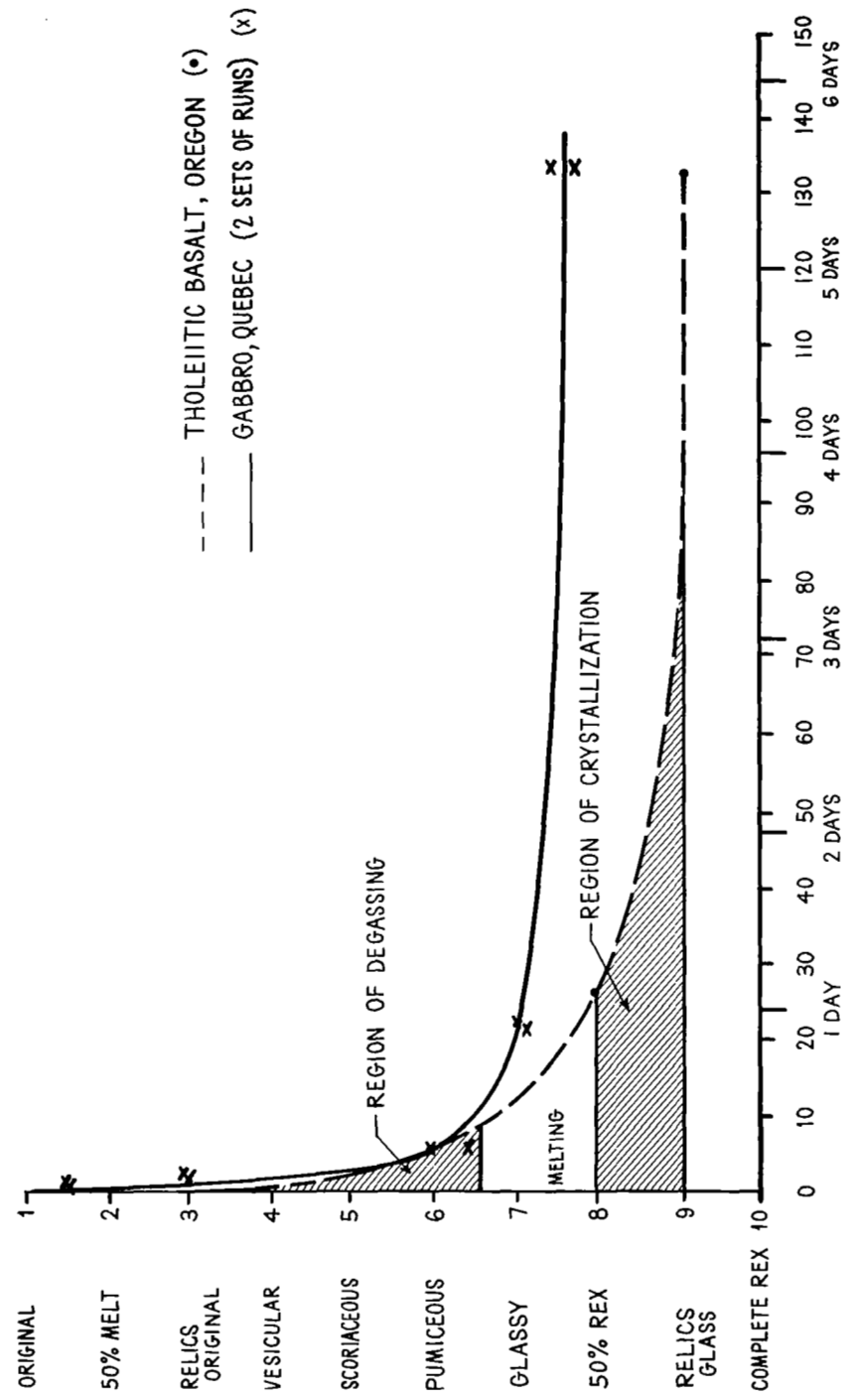

FIGURE 15 TIME DEPENDENCE OF GENETIC STATES, THOLEIITIC BASALT AND GABRO
(1000°C at 1 atm)

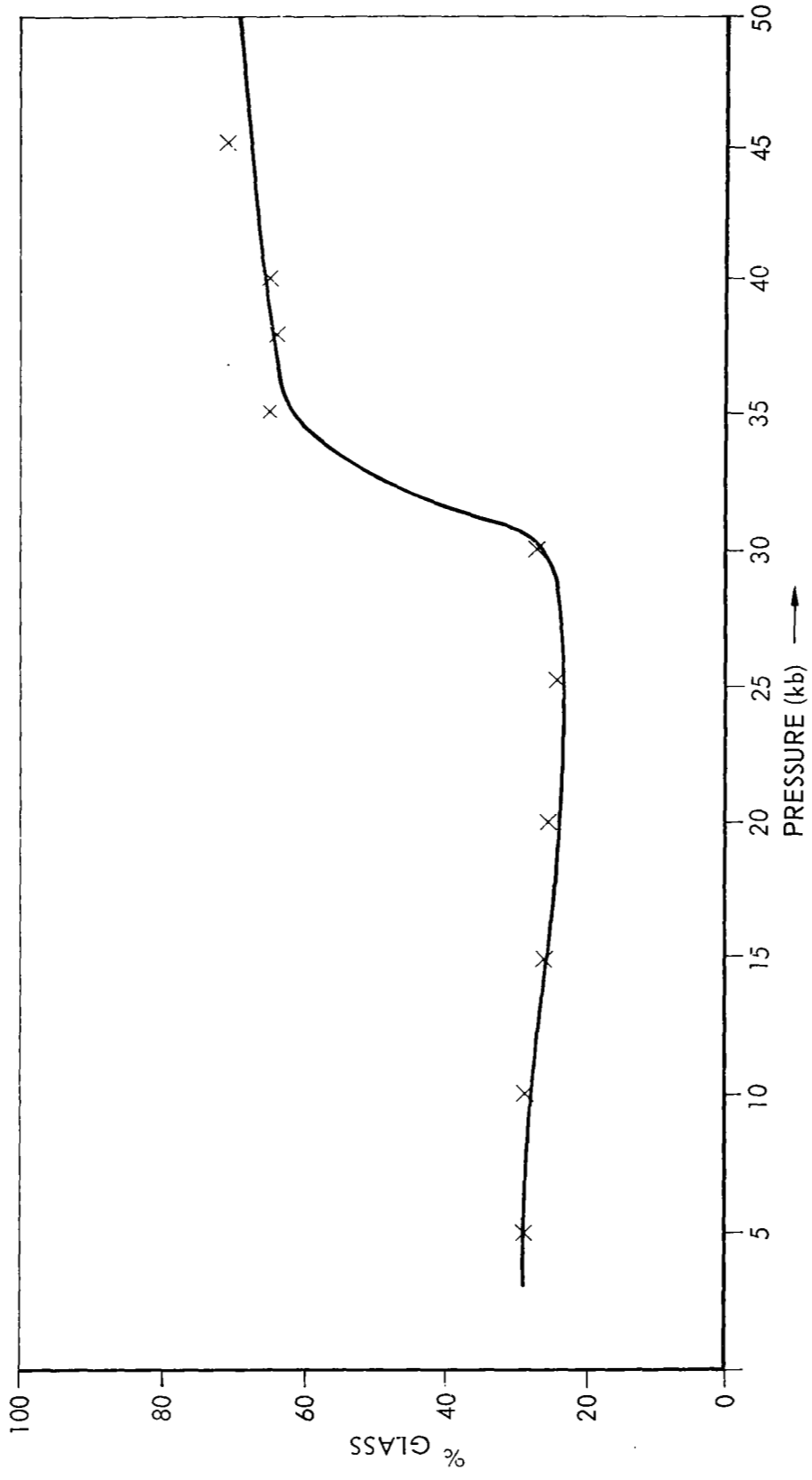

FIGURE 16. GRANODIORITE, PERCENT GLASS vs PRESSURE AT 1200°C

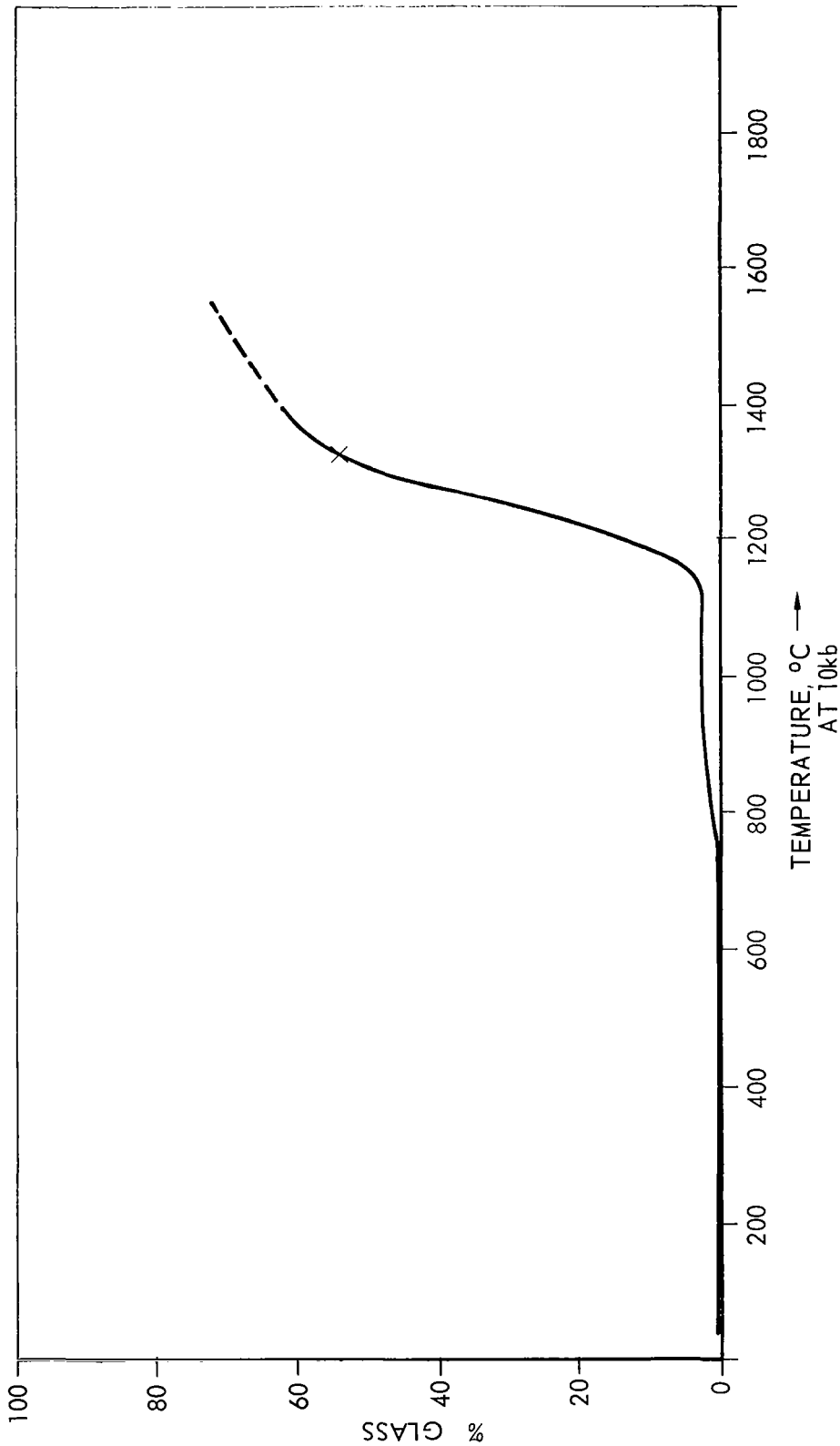

FIGURE 17. GRANODIORITE. PERCENT GLASS vs TEMPERATURE AT 10 KB

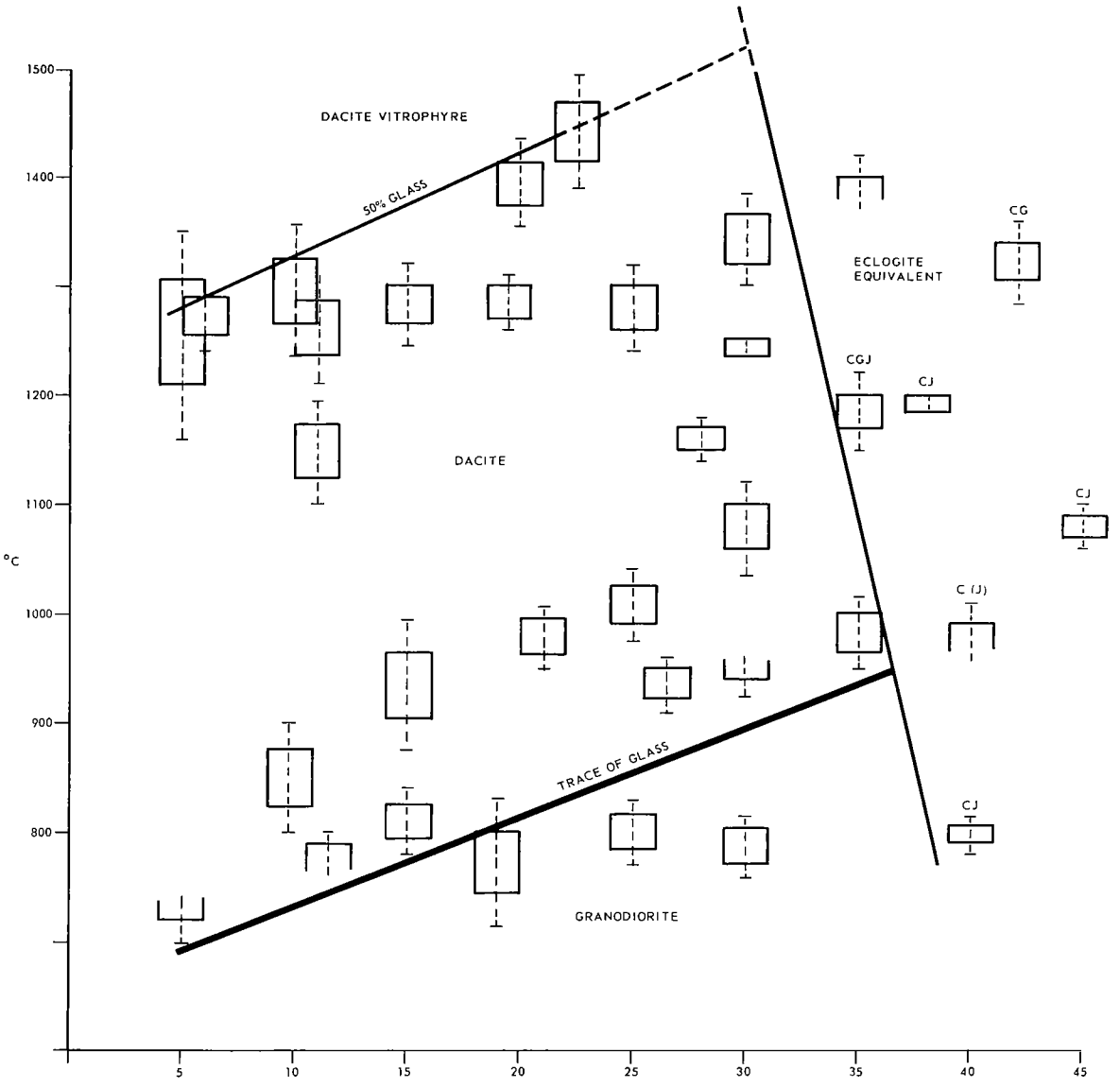

FIGURE 18 GENETIC DIAGRAM FOR A GRANODIORITE

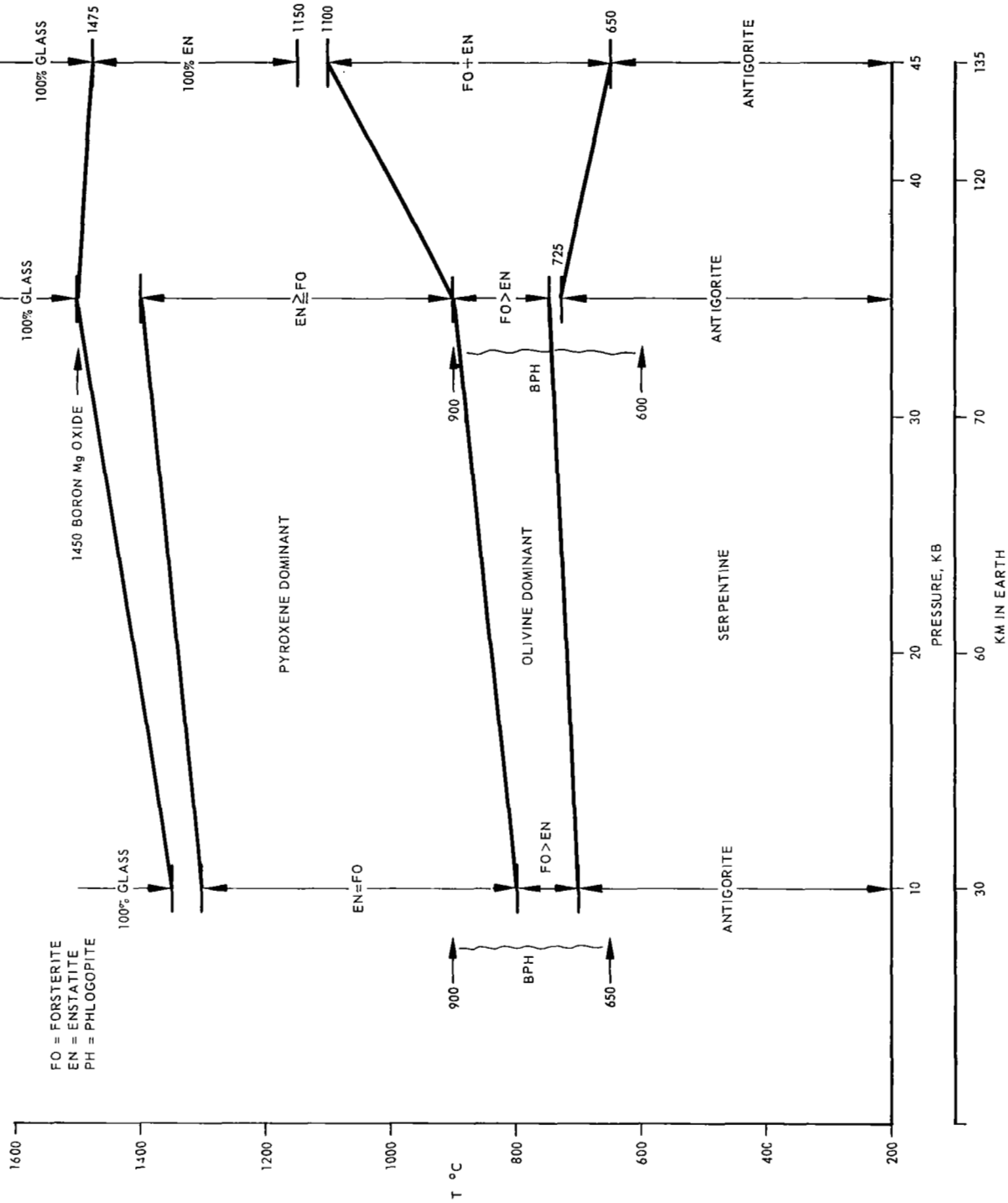

FIGURE 19. GENETIC DIAGRAM FOR A SERPENTINE

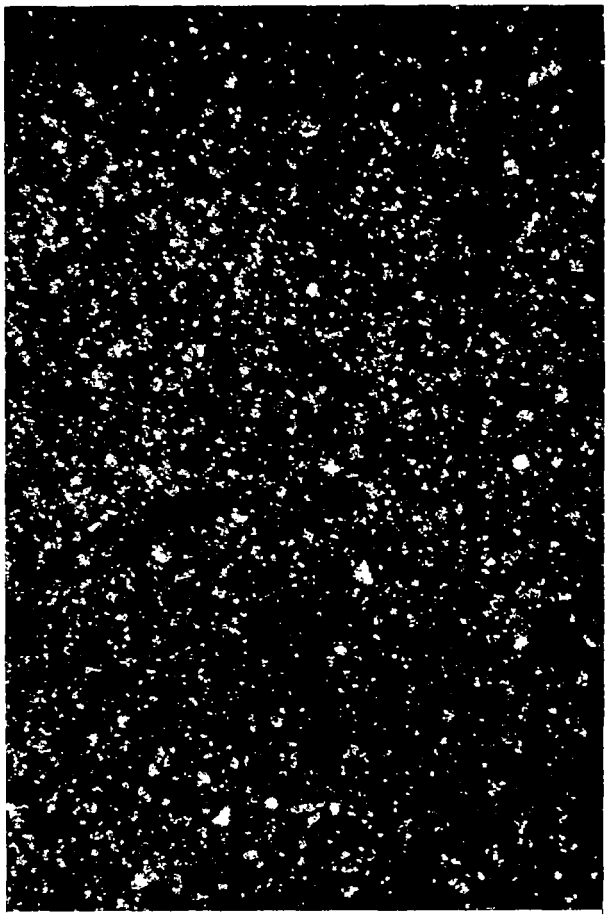

FIGURE 20 ESSENTIALLY INTACT FAYALITE CRYSTALS. POLARIZED LIGHT 35 mm = 16X

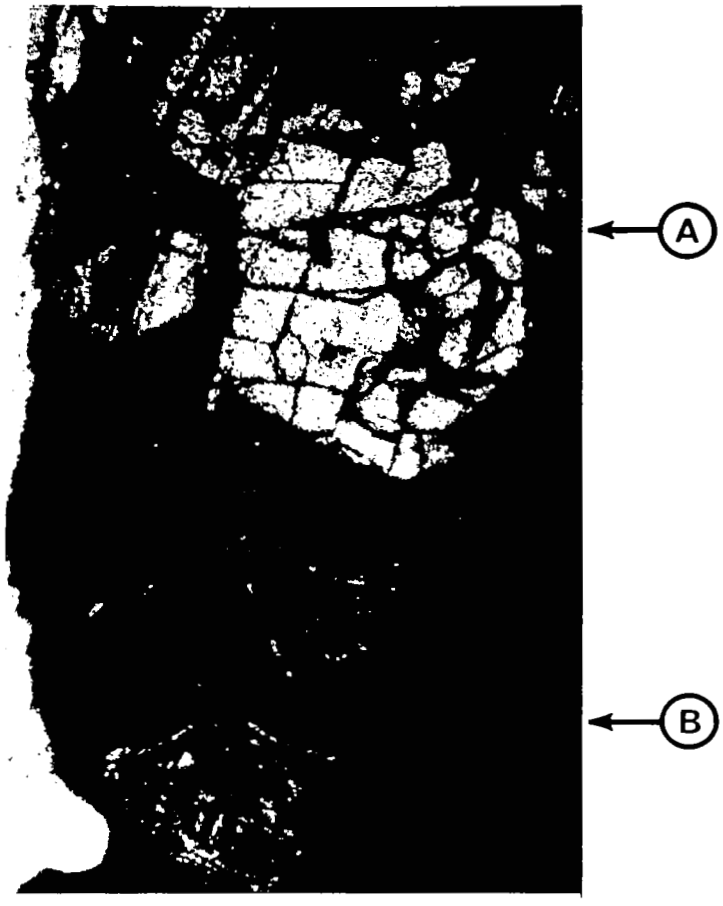

FIGURE 21 PARTIAL MELTING OF FAYALITE DUE PROBABLY TO THE PRESENCE OF TRACE AMOUNT OF H_2O. NOTE THE CONTRAST IN TEXTURES. ORDINARY LIGHT 35 mm = 16X

A. FAYALITE RECRYSTALLIZED IN THE SOLID STATE.
QUENCH CRYSTALS.

FIGURE 22 QUENCH TEXTURE OF FAYALITE. NOTE THE LONG QUENCH CRYSTALS RADIALLY SHOOTING INTO THE CENTER FROM THE WALL OF IRON CAPSULE LEAVING THE CENTRAL PORTION FILLED WITH DARK BROWN MATRIX. ORDINARY LIGHT. 35 mm = 10X

FIGURE 23 GRAPHIC TEXTURE OF QUENCH CRYSTALS. RUN MADE WITH C CAPSULE. ORDINARY LIGHT. 35 mm = 10X

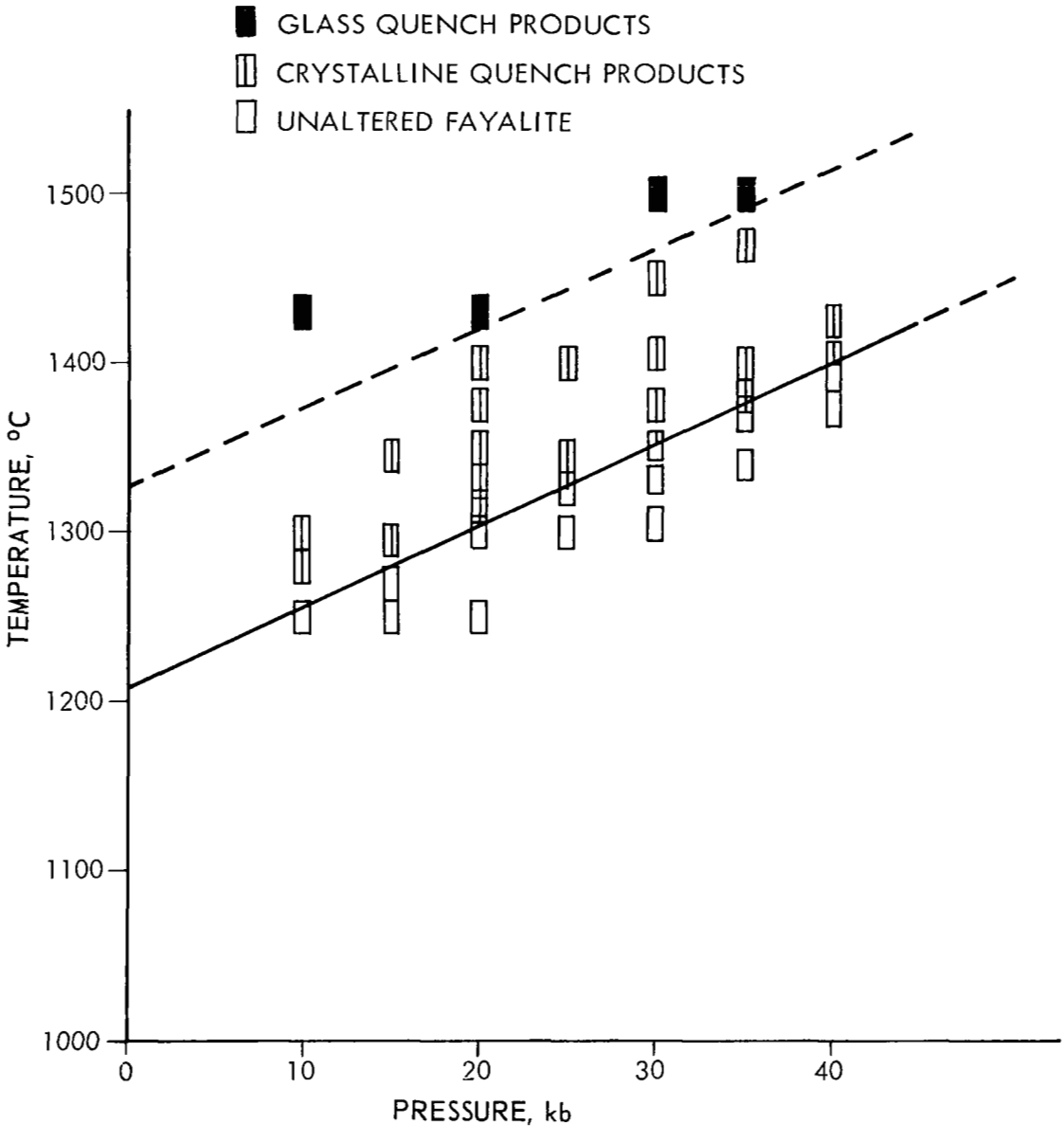

FIGURE 24 MELTING CURVES FOR FAYALITE

FIGURE 25 FAYALITE GLASS WITH SPHERULES OF BLACK OPAQUE MATERIAL IDENTIFIED TO BE DOMINANTLY IRON. ORDINARY LIGHT. 35 mm = 10X

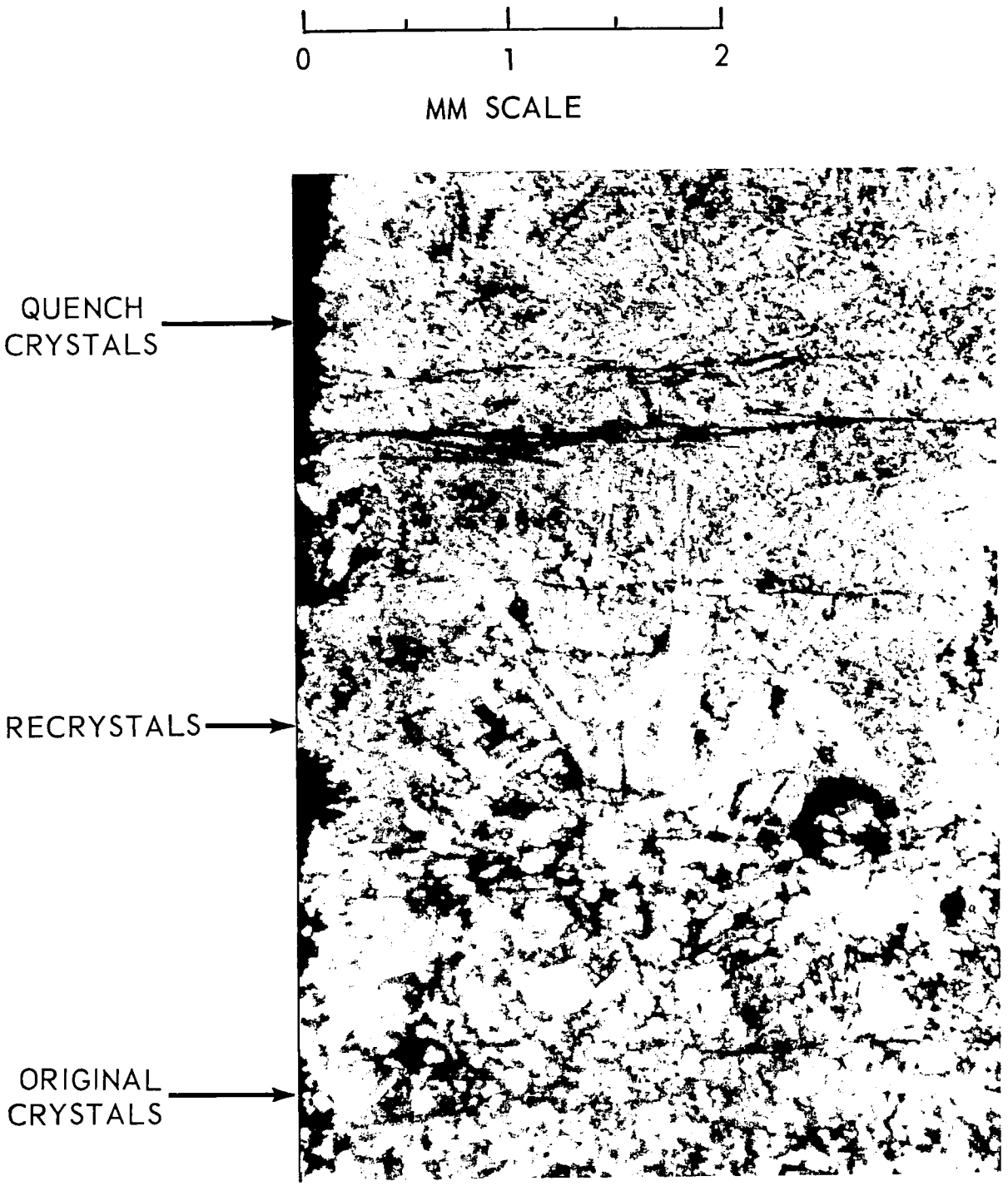

FIGURE 26 A TYPICAL TRANSITION IN GABBRO FROM ORIGINAL CRYSTALS, TO RECRYSTALS, TO QUENCH CRYSTALS (AZ129)

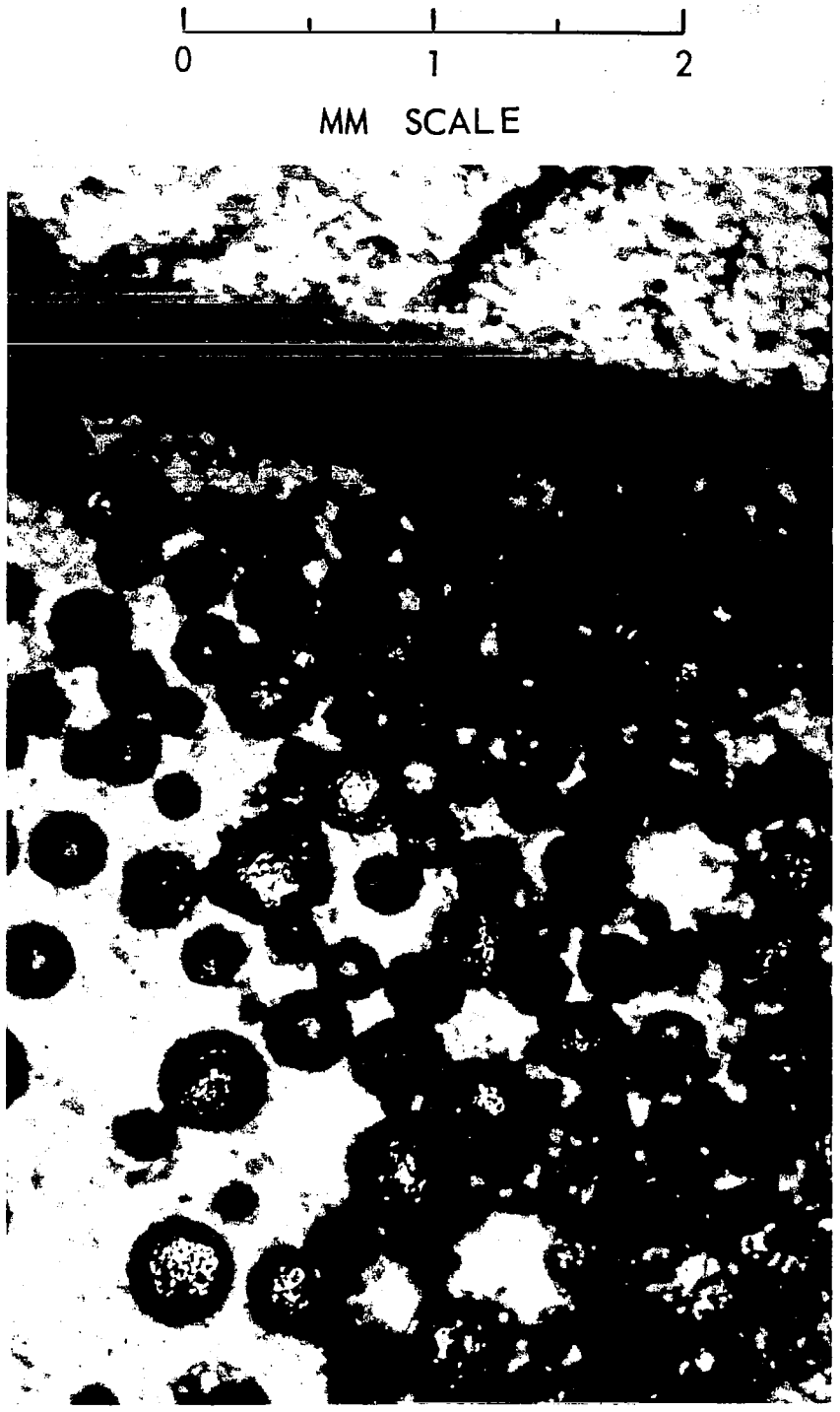

FIGURE 27 VESICLES IN GLASS MATRIX
(STARTING MATERIAL GABBRO)

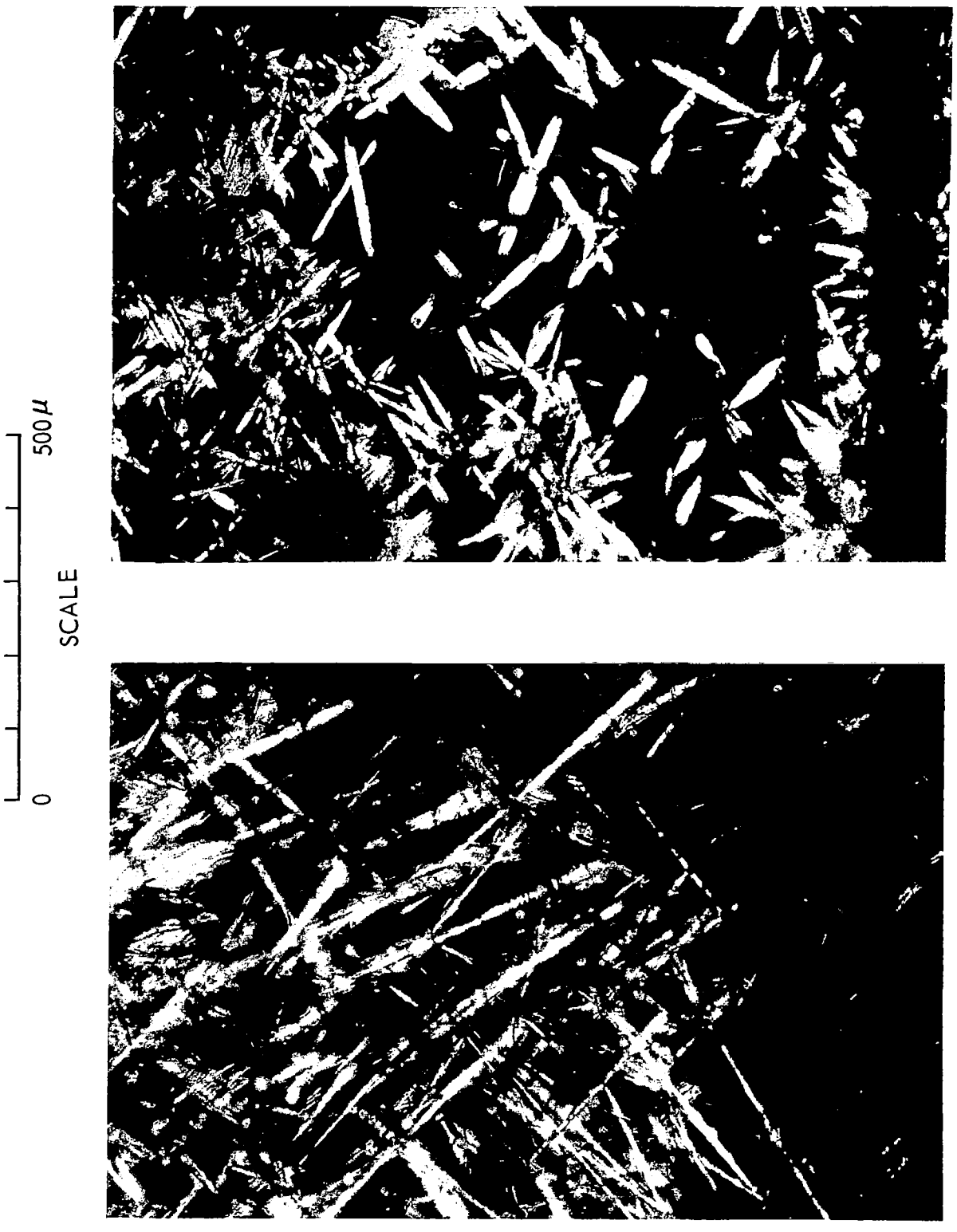

FIGURE 28 NEEDLE-LIKE QUENCH CRYSTALS (GABBRO)

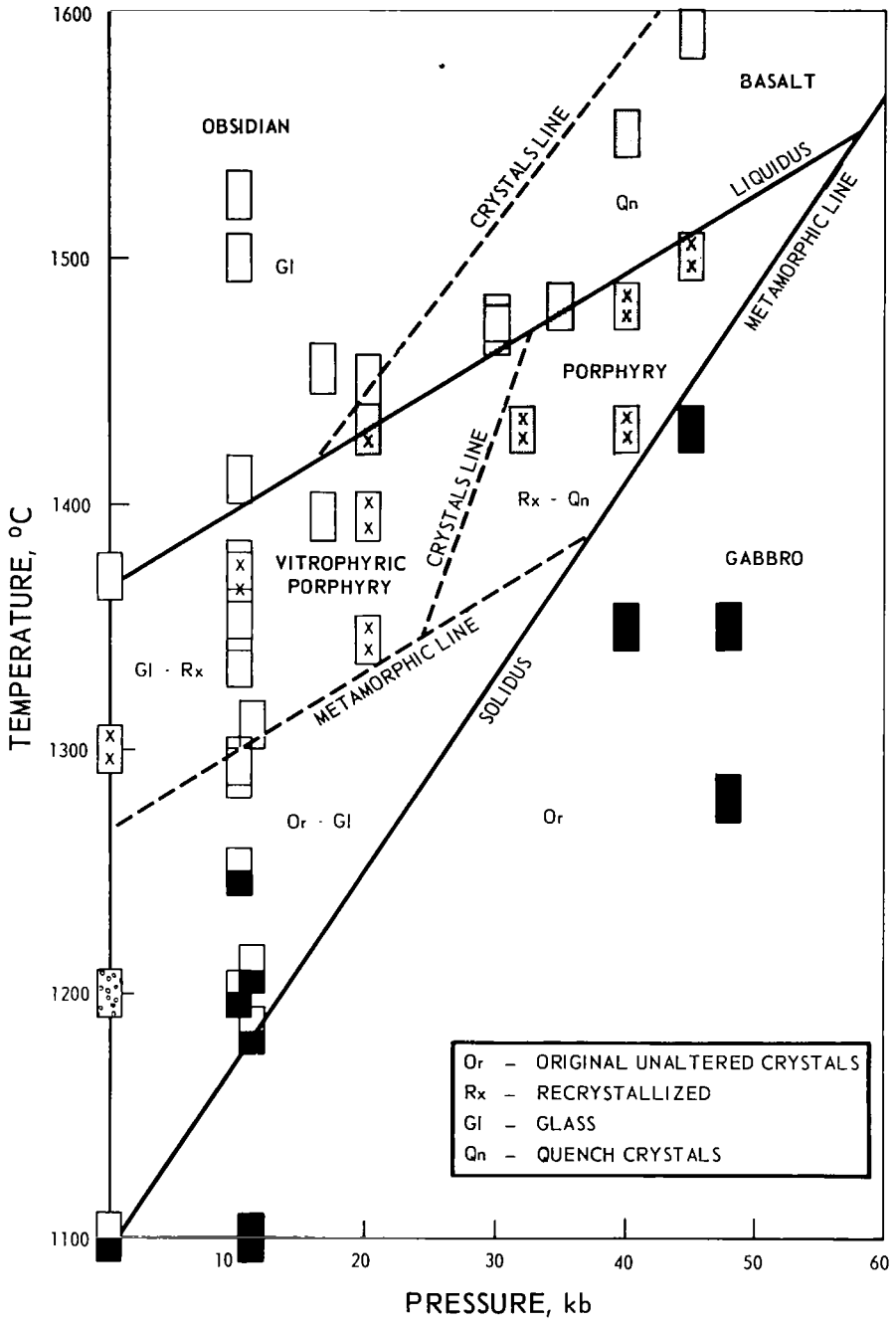

FIGURE 29 MELTING RANGE OF A GABBRO AT HIGH PRESSURES; SUPERIMPOSED IS A GENETIC DIAGRAM SHOWING SEVERAL PRESSURE-TEMPERATURE AREAS WHERE THE GABBRO USED AS AN INITIAL SAMPLE WOULD QUENCH INTO NEW ROCKS. PATTERNS: BLACK IS UNALTERED CRYSTALS; WHITE IS GLASS; DOTTED IS QUENCH CRYSTALS; XX IS RECRYSTALS

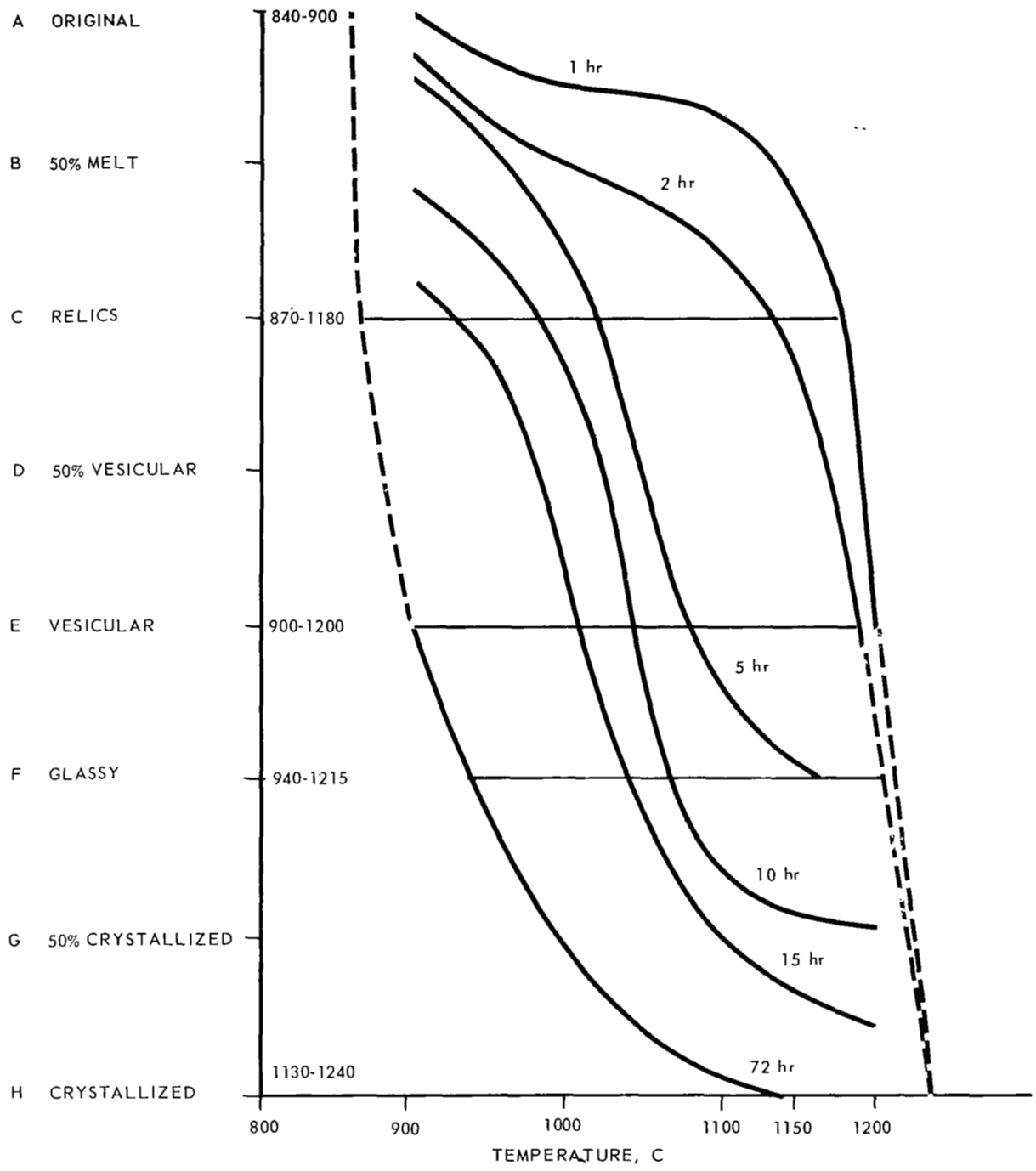

FIGURE 30. GENETIC DIAGRAM FOR HOKOOK BASALT

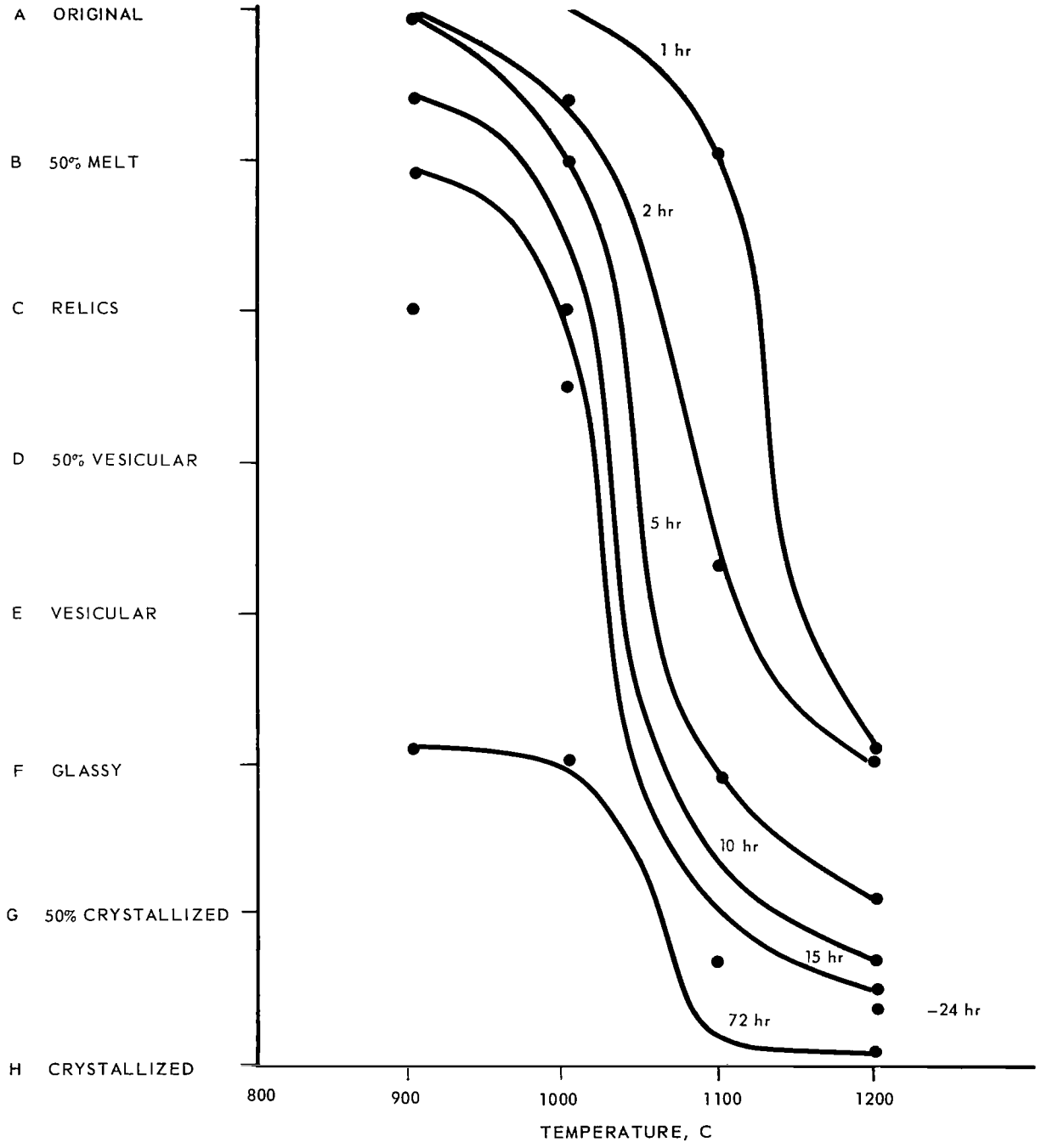

FIGURE 31 GENETIC DIAGRAM FOR GIVA'AT HAMOREH BASALT

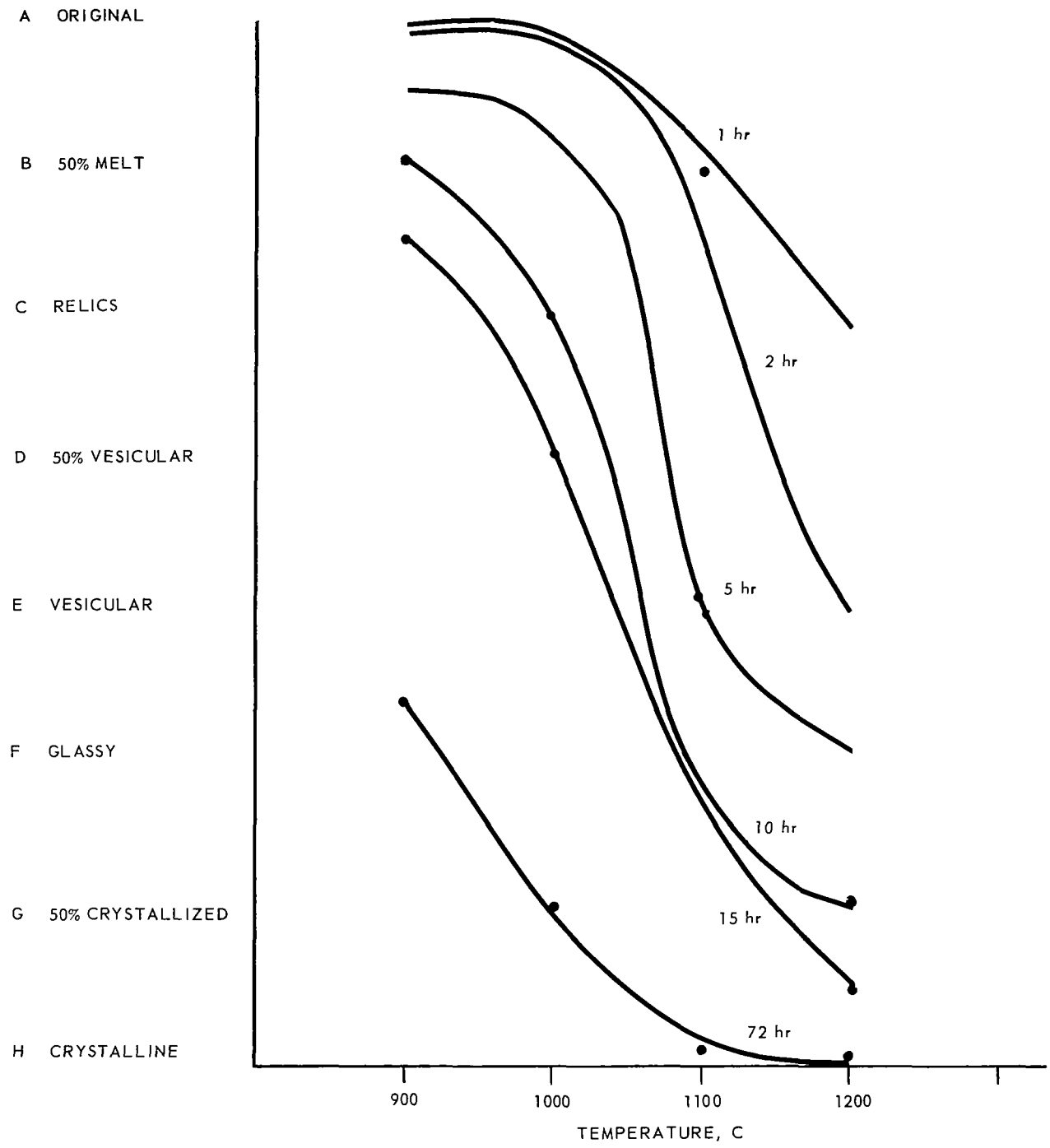

FIGURE 32. GENETIC DIAGRAM FOR HAZOR BASALT

(a) BASALT 1080 °C 1 1/2 HOURS BENDING BELOW THE MELTING

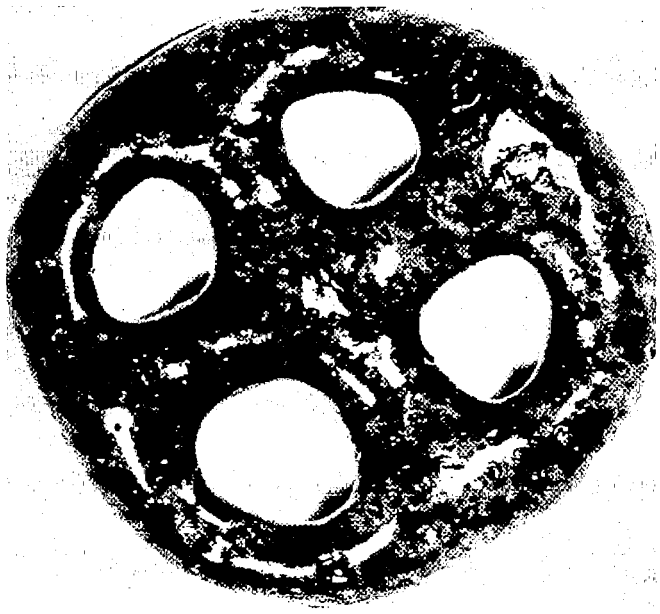

(b) OBSIDIAN DUST 1300 °C 1 1/2 HOURS MELT AND CAST

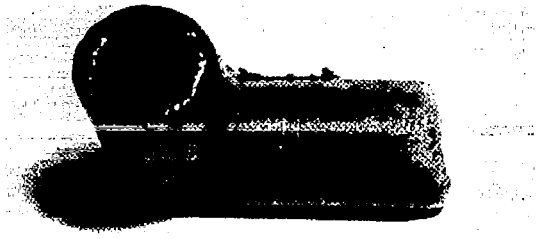

(c) OBSIDIAN DUST 1075 °C 12 HOURS MELT AND CAST

FIGURE 33. BENDING AND CASTING OF ROCKS

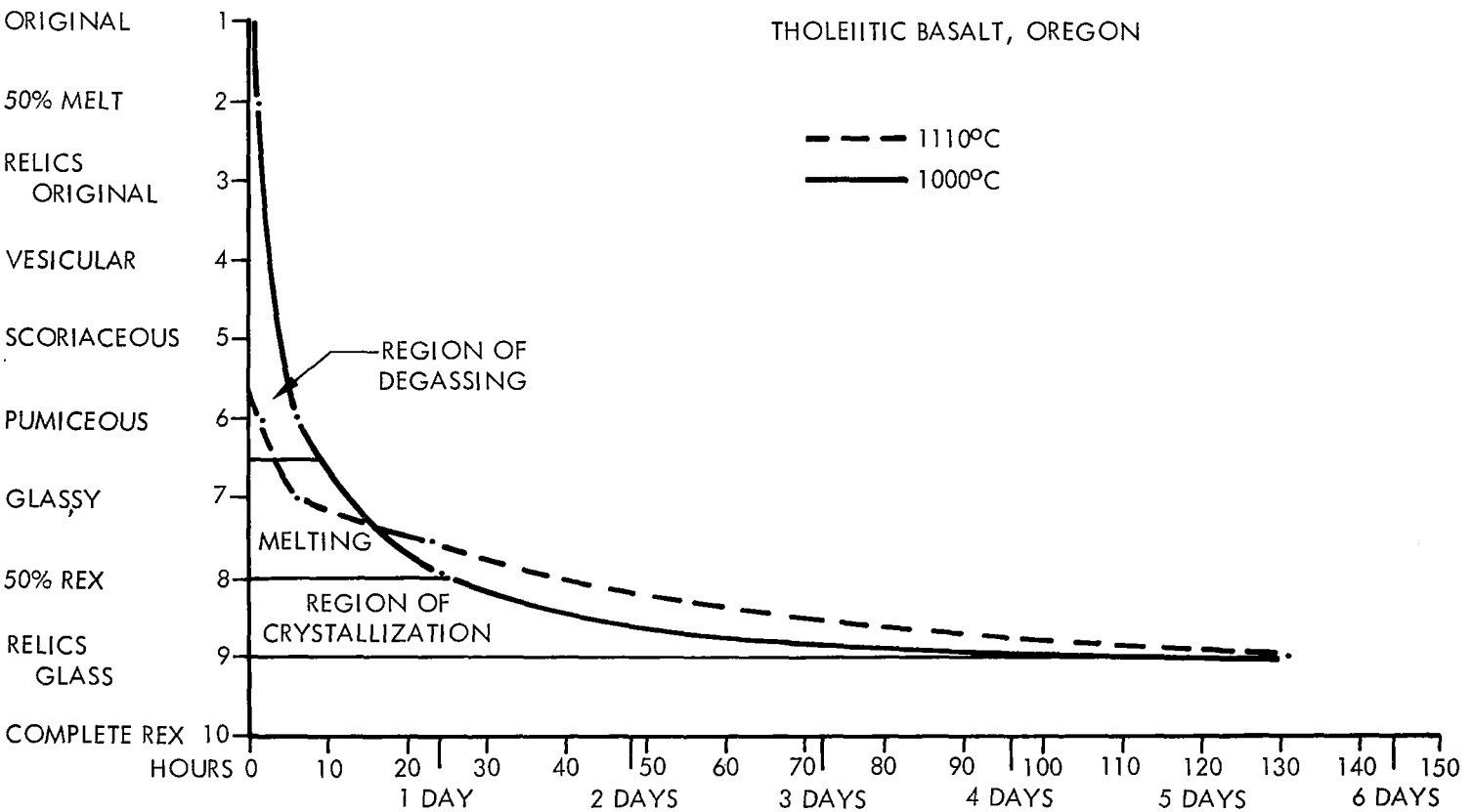

FIGURE 34 TIME DEPENDENCE OF GENETIC STATES, THOLEIITIC BASALT AT 1000°C AND 1100°C

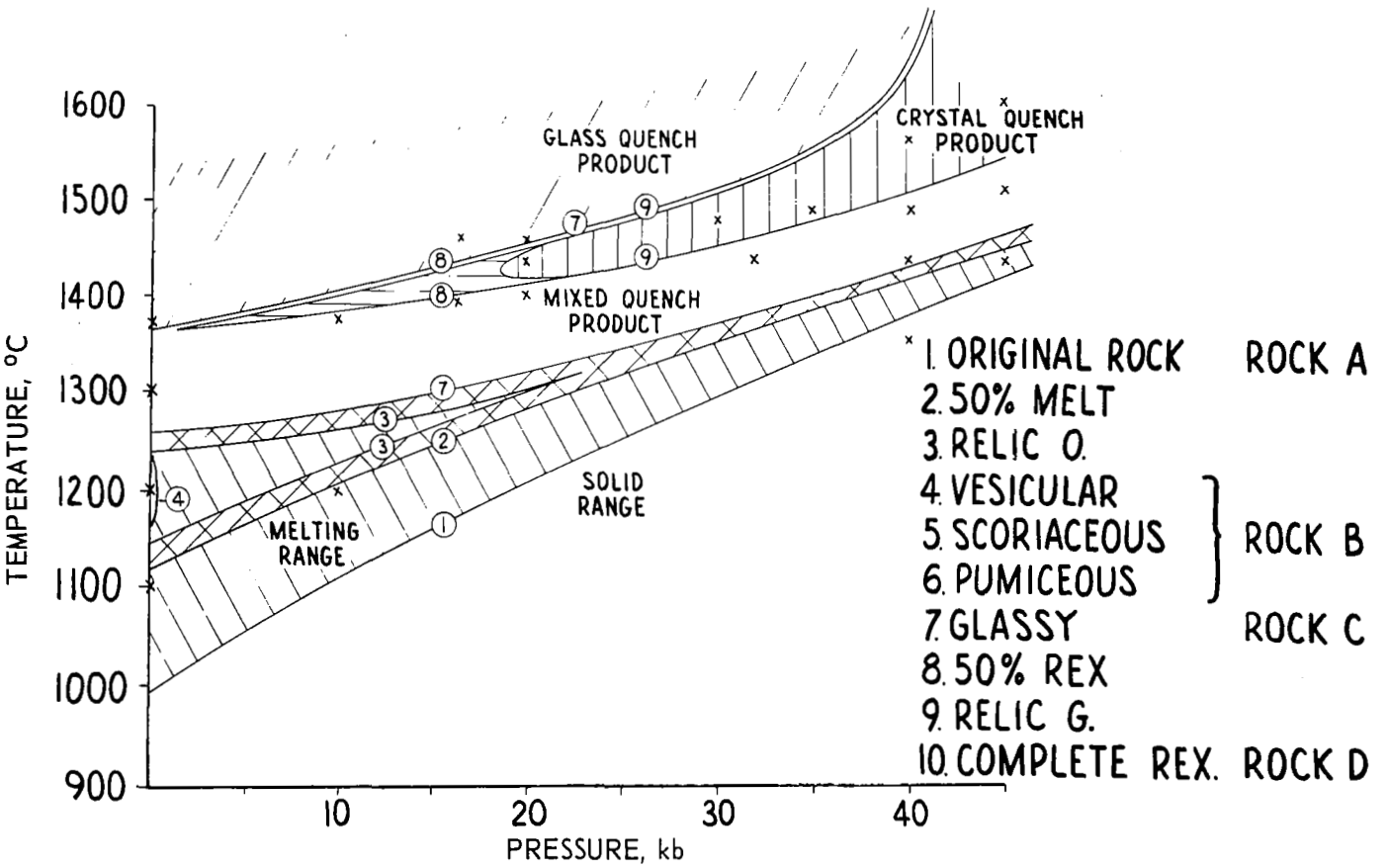

FIGURE 35 GENETIC DIAGRAM FOR A GABBRO

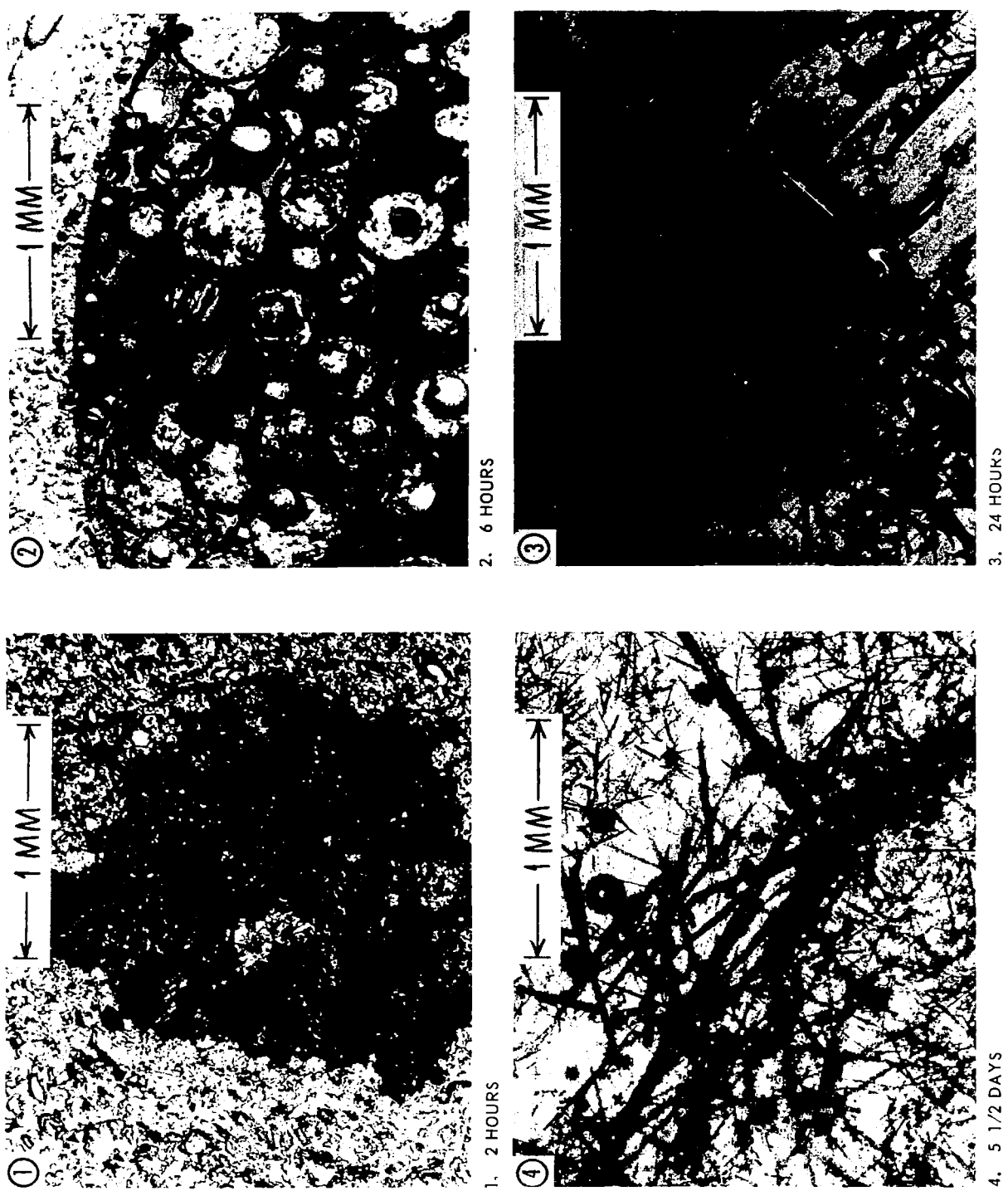

FIGURE 36 DEVELOPMENT OF GENETIC STATES IN BASALT (1000°C AT 1 atm)

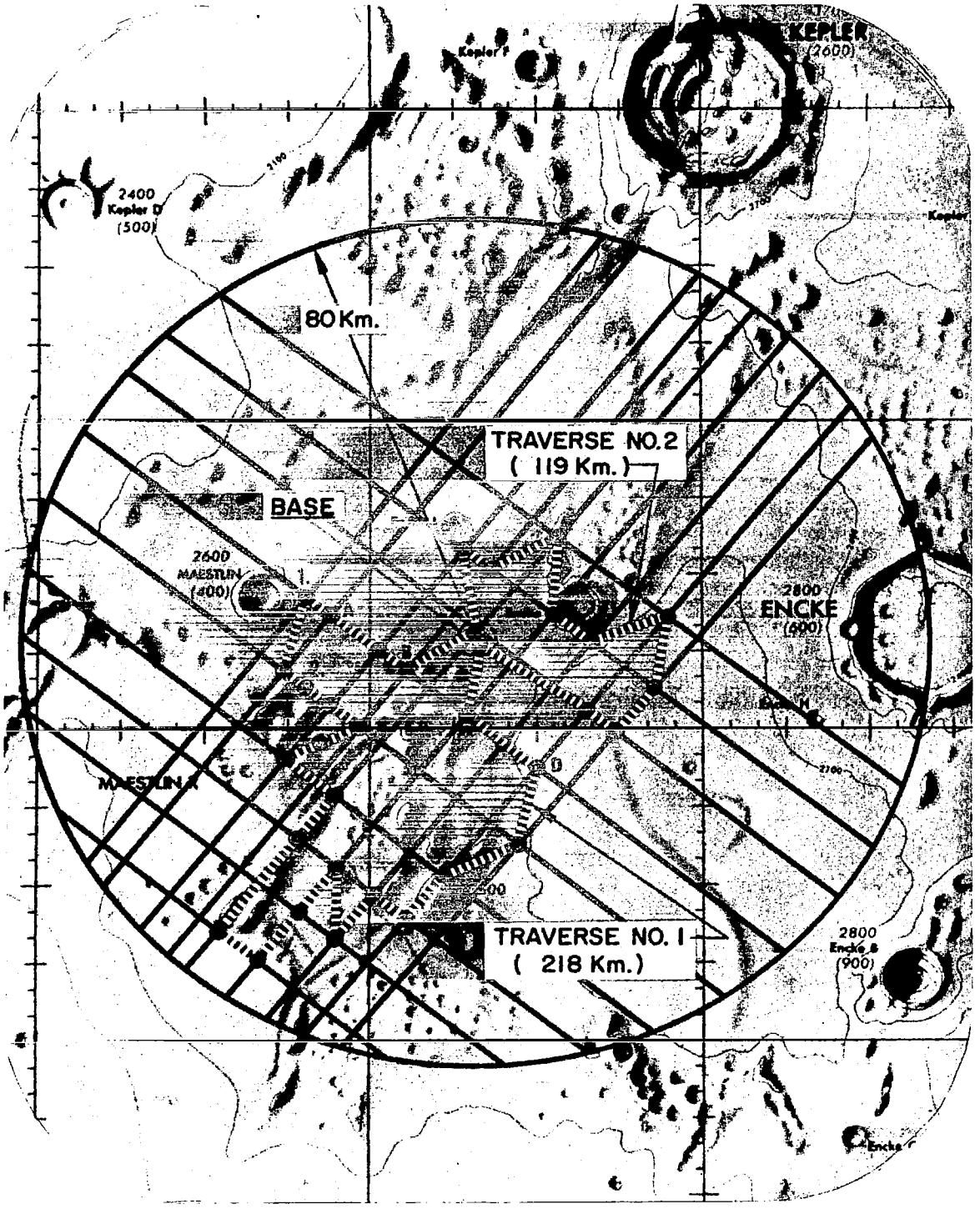

FIGURE 37 TYPICAL LUNAR TRAVERSE

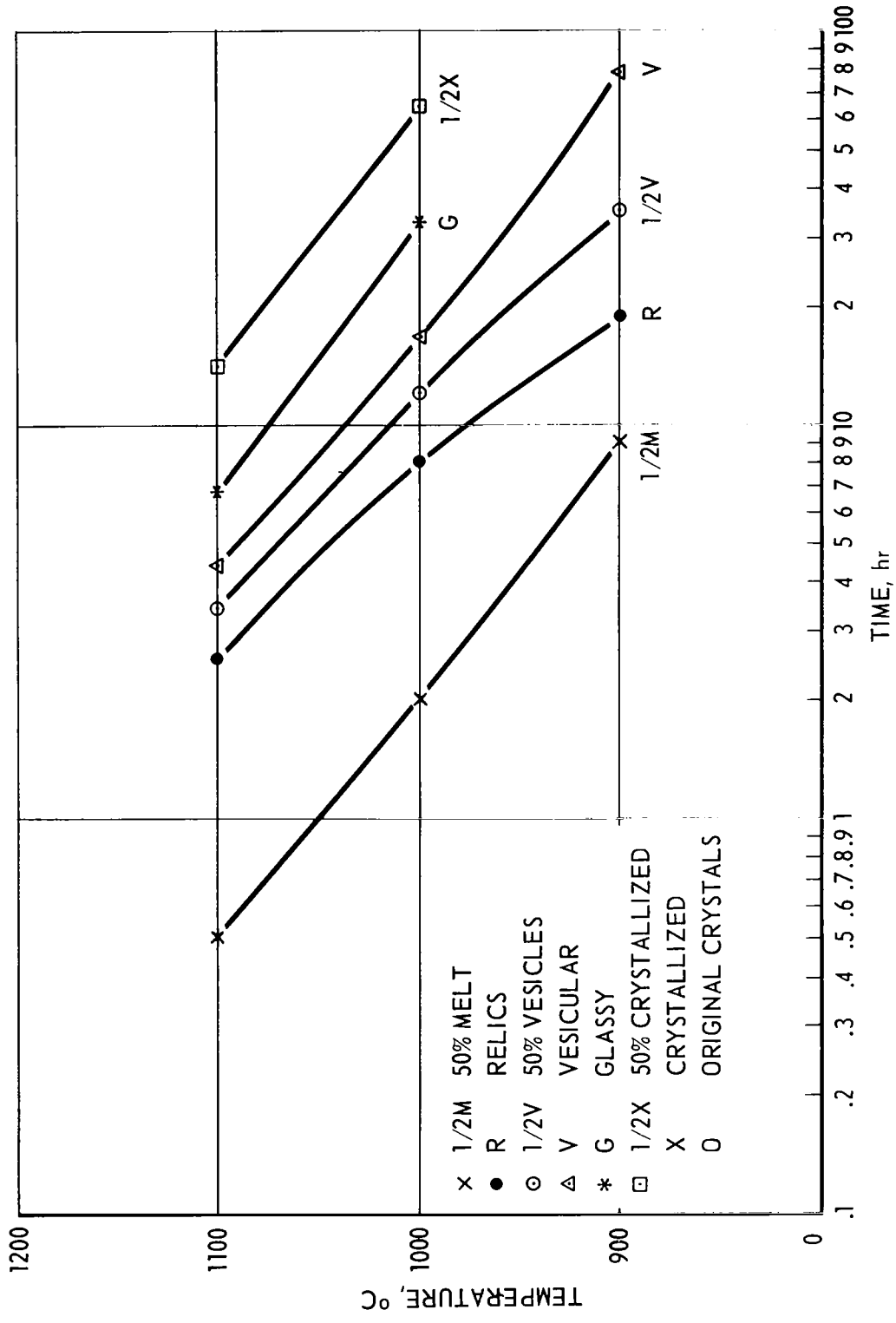

FIGURE 38 ANOTHER GENETIC DIAGRAM FOR HOKOOK BASALT (SEE FIGURE 30)

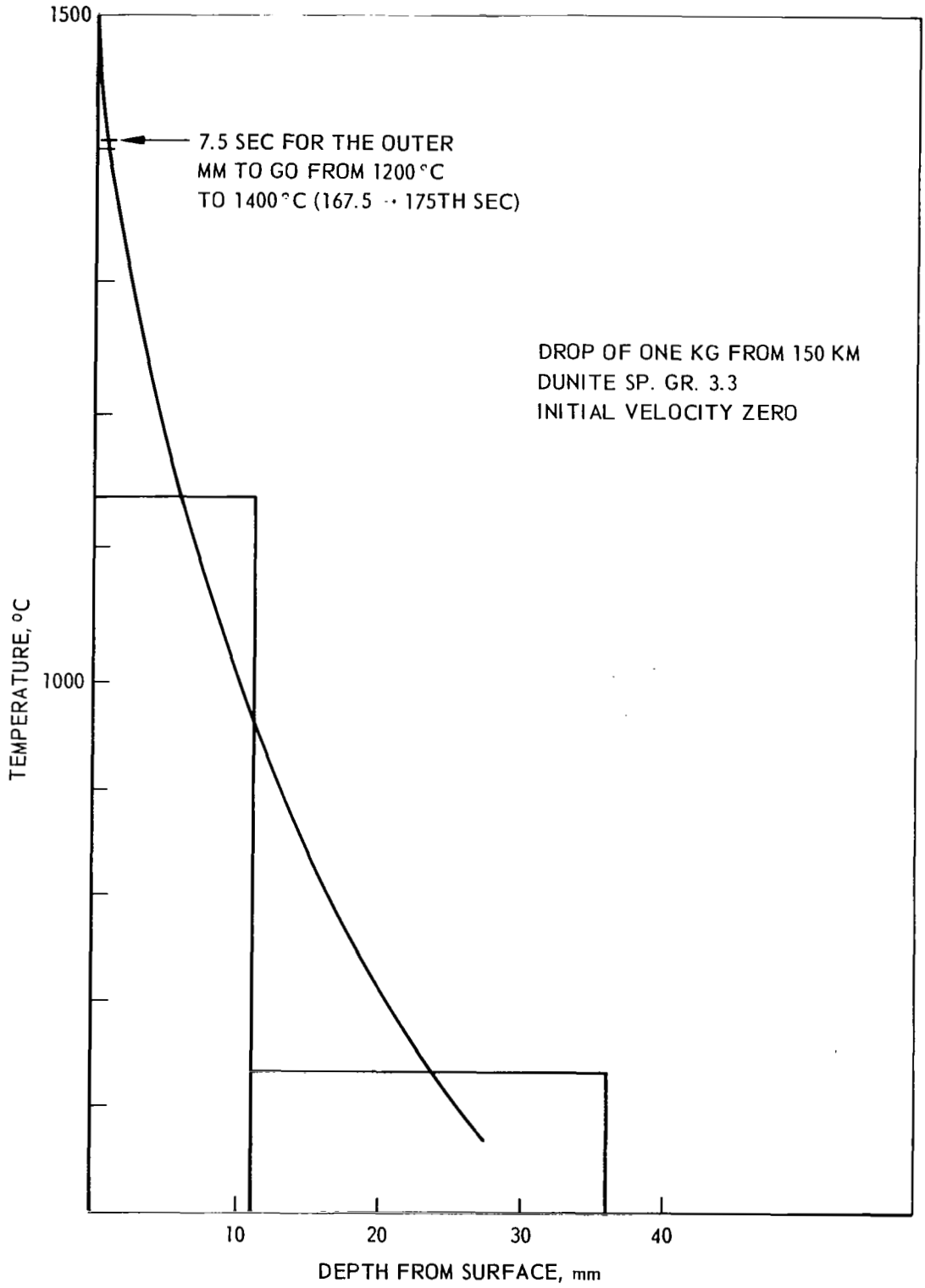

FIGURE 39 CALCULATED TEMPERATURE GRADIENT IN DUNITE ARTIFICIAL METEORITE

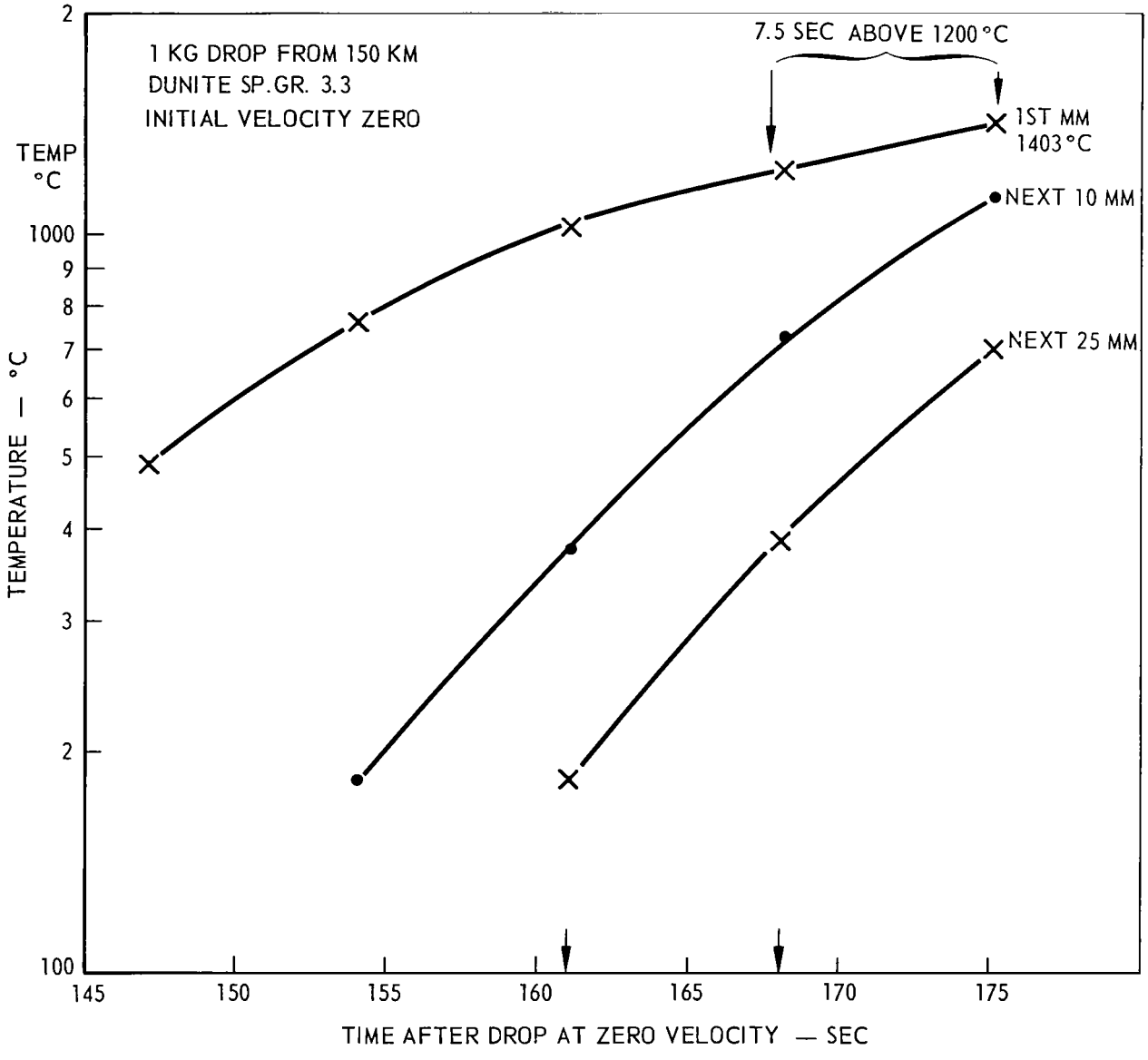

FIGURE 40 RATE OF HEATING OF DUNITE ARTIFICIAL METEORITE

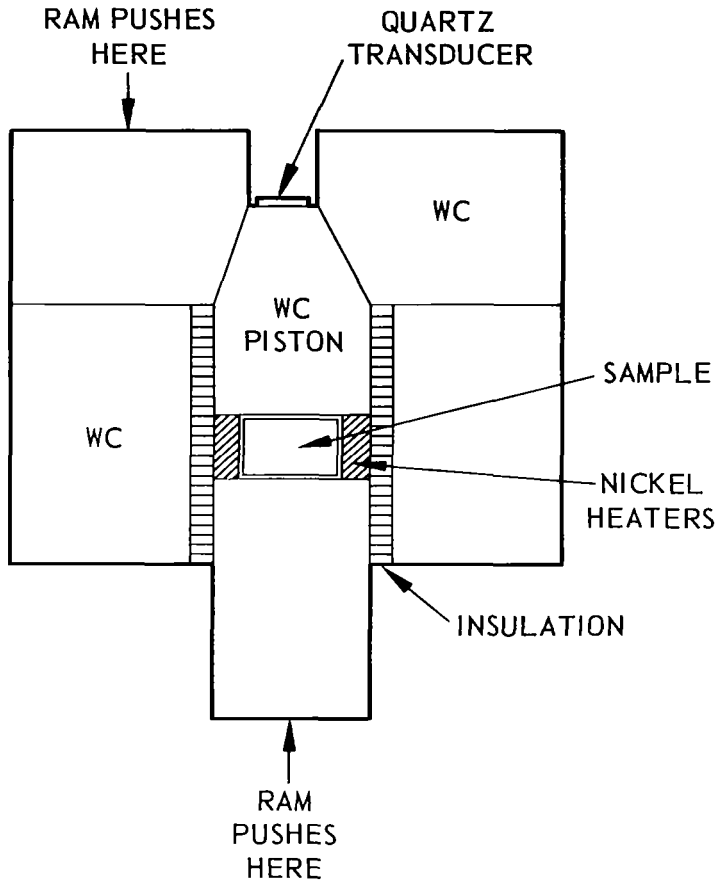

FIGURE 41 GEOMETRY OF THE LABORATORY CONFIGURATION USEFUL IN MELTING DETERMINATION IN SITU

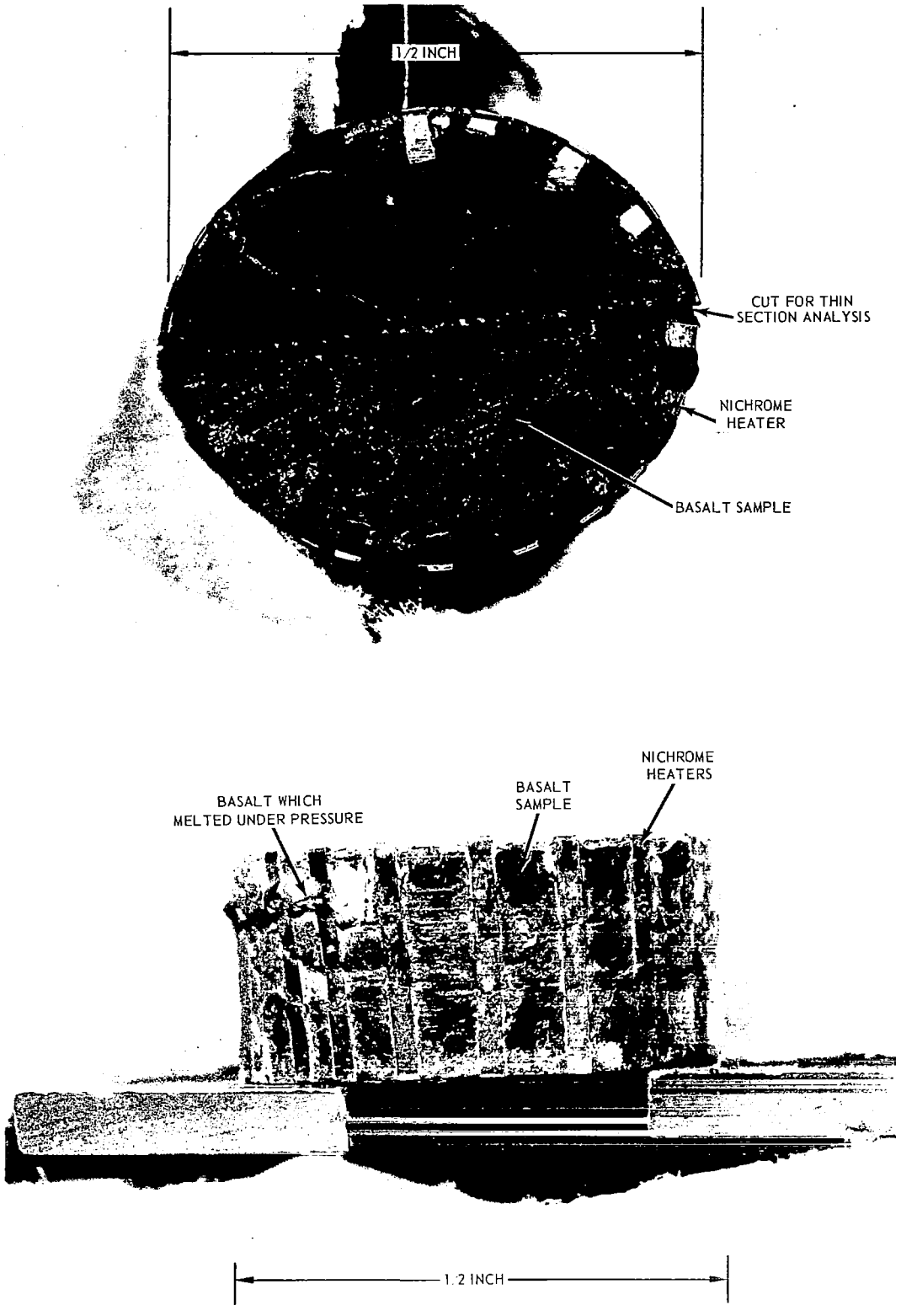

FIGURE 42 BASALT SAMPLE HEATER ARRANGEMENT USED BY DR. R.D. TOOLEY (NORTHROP) IN VELOCITY MEASUREMENTS UNDER HIGH PRESSURE AND TEMPERATURE

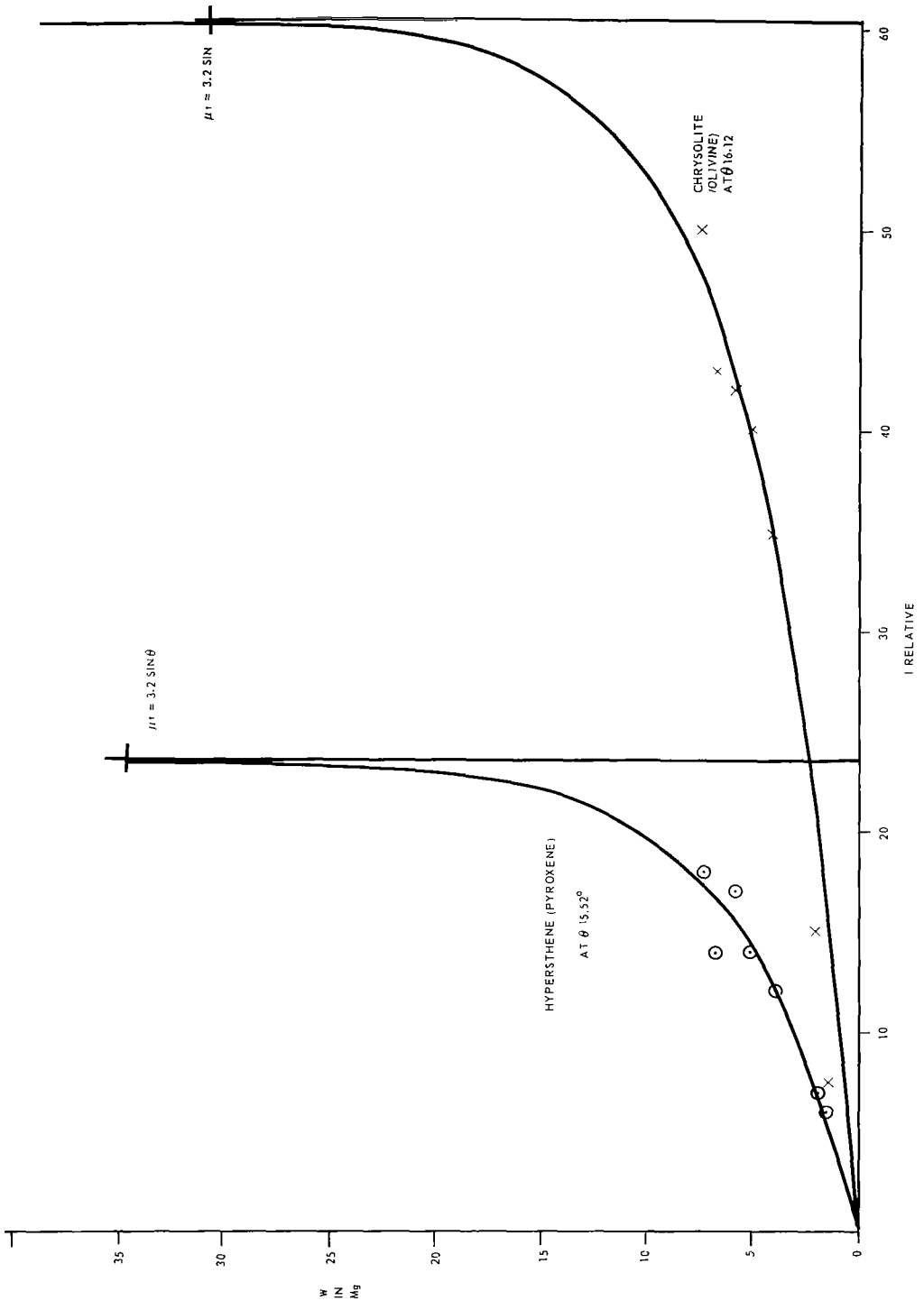

FIGURE 43. X-RAY INTENSITY vs SAMPLE WEIGHT

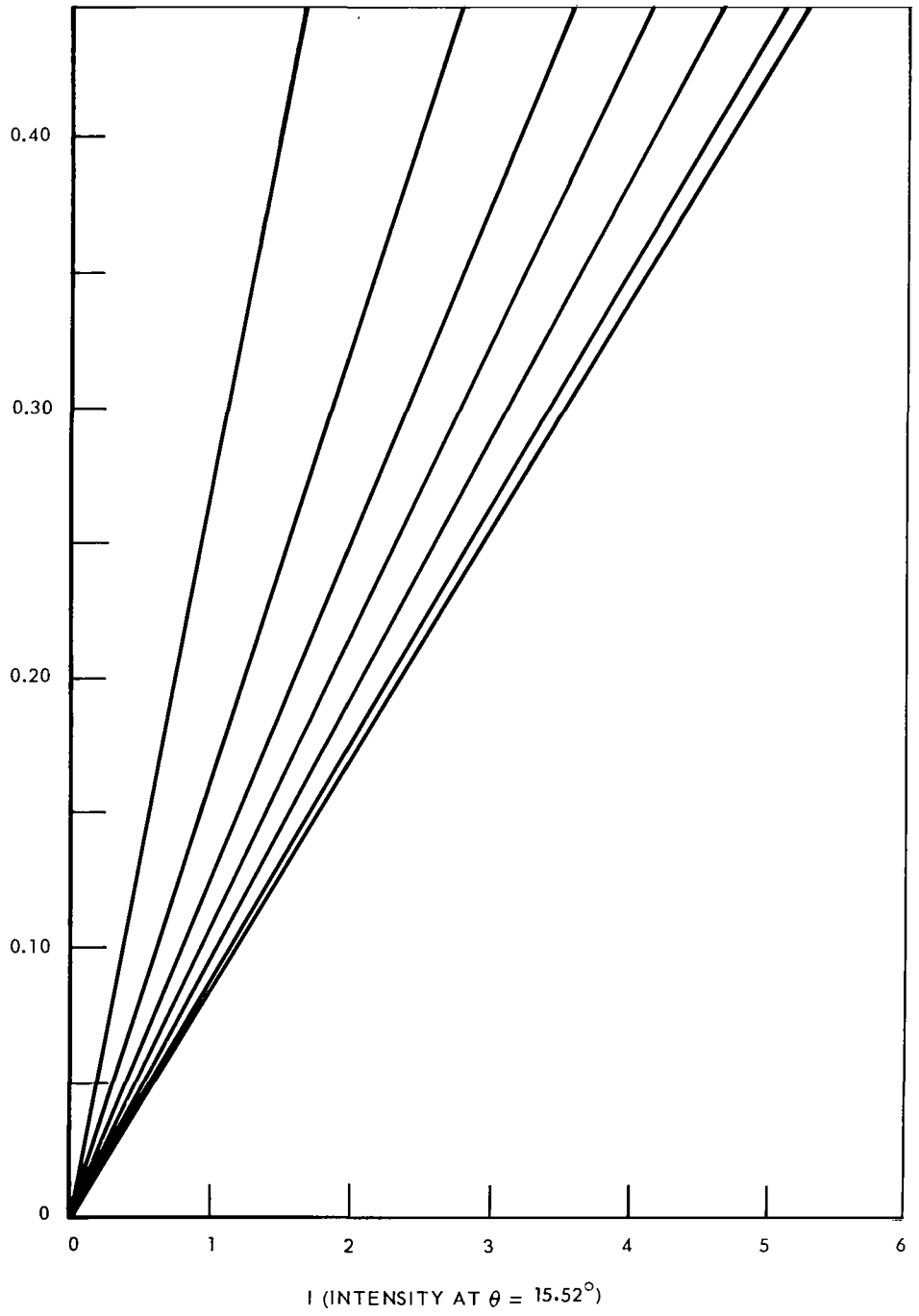

FIGURE 44. INTENSITY OF REFLECTION AT θ=15.52° FOR HYPERSTHENE IN THE BRUDERHEIM METEORITE AS A FUNCTION OF HYPERSTHENE FRACTIONAL WEIGHT IN THE TOTAL SAMPLE

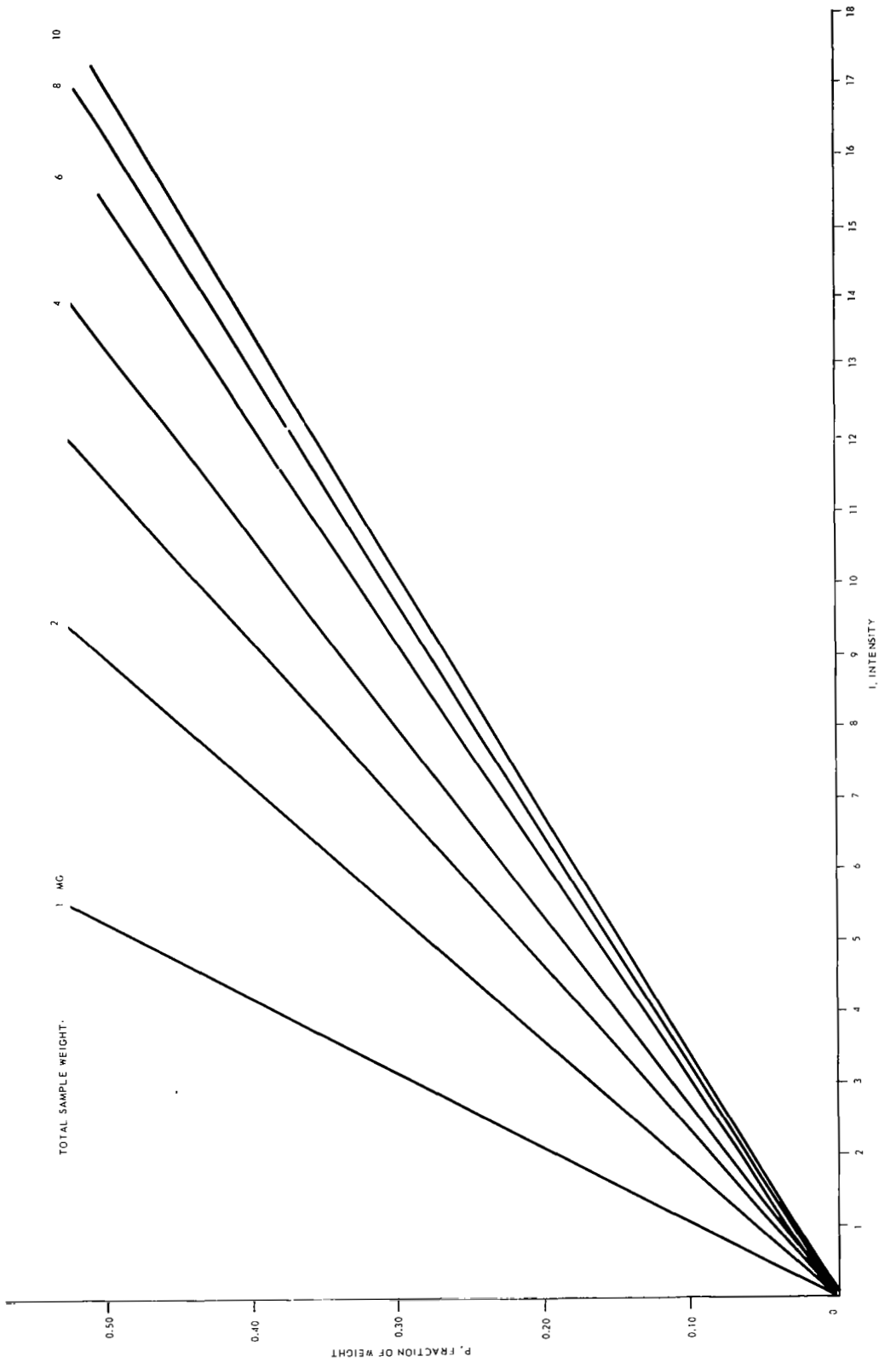

FIGURE 45 INTENSITY OF REFLECTION AT $\theta = 16.12^{\circ}$ FOR CRYSOLITE IN THE BRUDERHEIM METEORITE AS A FUNCTION OF CRYSOLITE FRACTIONAL WEIGHT IN THE TOTAL SAMPLE

NASA-Langley, 1968 —— 30 CR-1081